THE ASTROPHYSICAL JOURNAL

An International Review of Spectroscopy and Astronomical Physics

FOUNDED IN 1895 BY GEORGE E. HALE AND JAMES E. KEELER

VOLUME 89

JANUARY–JUNE, 1939

THE UNIVERSITY OF CHICAGO PRESS
CHICAGO, ILLINOIS

THE CAMBRIDGE UNIVERSITY PRESS, LONDON
THE MARUZEN COMPANY LIMITED, TOKYO
THE COMMERCIAL PRESS, LIMITED, SHANGHAI

PUBLISHED JANUARY, MARCH, APRIL, MAY,
JUNE 1939

COMPOSED AND PRINTED BY THE UNIVERSITY OF CHICAGO PRESS
CHICAGO, ILLINOIS, U.S.A.

CONTENTS

NUMBER 1

NUMBER 2

NUMBER 3

NUMBER 4

NUMBER 5

THE ASTROPHYSICAL JOURNAL

AN INTERNATIONAL REVIEW OF SPECTROSCOPY AND ASTRONOMICAL PHYSICS

VOLUME 89 JANUARY 1939 NUMBER 1

ATMOSPHERIC ABSORPTION OF INFRARED SOLAR RADIATION AT THE LOWELL OBSERVATORY. I

ARTHUR ADEL

ABSTRACT

Previous work has dealt with the complete opacity of the earth's atmosphere ($\lambda > 14\ \mu$) created in part by ν_2 of CO_2 and in the main by the rotation spectrum of the water-vapor molecule. In the present paper it is experimentally demonstrated that the influence of the rotation spectrum of water vapor extends down to $\lambda < 8\ \mu$. Provisional absorption coefficients are specified which describe the degree of opacity enforced by this spectrum between 8.34 and 13.40 μ. The absorption coefficient is then applied to the determination of the form of the solar energy curve in interplanetary space throughout this spectral interval. Satisfactory agreement obtains between this experimentally derived form and the black-body curve for 6000° or 7000° K.

THE CONTINUOUS ABSORPTION OF THE ROTATION SPECTRUM OF WATER VAPOR

Introduction.—Previous papers have discussed the positions, structures, and identifications of the absorption bands in the infrared atmospheric spectrum.[1] This spectrum profoundly affects incoming planetary or other long wave-length radiations by virtue of the complete atmospheric opacity at $\lambda > 14\ \mu$ and by reason of the lesser absorptions at $\lambda < 14\ \mu$. The present paper is the first of several to be concerned with this problem, namely, the degree of absorption suffered by incoming infrared radiations as a consequence of the infrared telluric absorption spectrum. In this report we shall confine ourselves to the effects of the rotation spectrum of the water-vapor molecule.

[1] Please see previous papers on the telluric spectrum by the author and his collaborators in this *Journal* and in the *Physical Review*.

The complete opacity occasioned at $\lambda > 14\ \mu$ by the amounts of water vapor and carbon dioxide normally present in the atmosphere has been known for some time.[2,1] More recently, observations at the Lowell Observatory have disclosed the continuation of the influence of the rotation spectrum of water vapor on the short wavelength side of $14\ \mu$. Thus, at $\lambda < 14\ \mu$ there exists a continuous absorption spectrum superimposed upon the selective absorptions heretofore described. Approximate absorption coefficients govern-

TABLE 1

ABSORPTION OF INFRARED RADIATION BY WATER VAPOR

$\lambda(\mu)$	Path Length (Cubic Centimeters of Liquid Water)	Intensity (Millimeters of Deflection)	$\lambda(\mu)$	Path Length (Cubic Centimeters of Liquid Water)	Intensity (Millimeters of Deflection)
13.40	4.36	2.5	10.84	3.14	34
	1.93	7.5		1.75	43
	1.46	9.5		1.36	44
12.83	3.93	7	10.10	3.08	51
	1.93	12		1.75	63
	1.45	14		1.33	64
12.22	3.58	13	9.25	2.93	80
	1.86	19		1.68	95
	1.41	21		1.31	97
11.55	3.36	22	8.34	2.79	115
	1.82	29		1.61	140
	1.39	31		1.29	148

ing the action of the rotation spectrum of water vapor at $\lambda < 14\ \mu$ have recently been computed by W. M. Elsasser,[3] whose work is based on the recent excellent analysis of this spectrum by H. M. Randall, D. M. Dennison, N. Ginsburg, and R. L. Weber.[4]

Observations.—The continuous infrared absorption spectrum of the earth's atmosphere at $\lambda < 14\ \mu$ is revealed by spectroradiometric measurement of the intensity of the infrared solar spectrum through several different quantities of atmospheric water vapor. The set of measures recorded in Table 1 was secured in this fashion.

[2] F. E. Fowle, *Smithsonian Miscellaneous Collections*, **68**, No. 8, 1917.

[3] *Ap. J.*, **87**, 497, 1938.

[4] *Phys. Rev.*, **52**, 160, 1937.

The first column lists the wave lengths at which the solar intensities were measured; the second column lists the several path lengths of water vapor through which the intensity of the corresponding wave length was measured; while the third column lists the intensities as recorded with a rock-salt-prism spectrometer. The path length of water vapor is given as an equivalent, that is, the number of centimeters of liquid water required to produce the actual amount of vapor present. The latter notion is taken from the numerous and splendid atmospheric researches by Fowle, whose method of de-

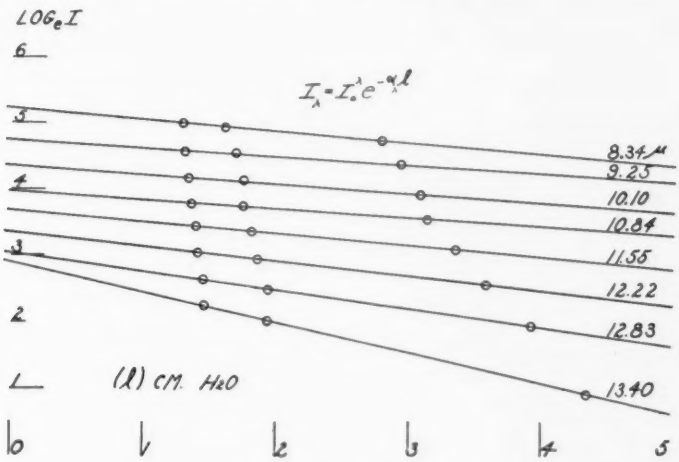

FIG. 1.—$\log_e I$ versus l

termining the atmospheric water-vapor content has been utilized in preparing the present work.

Reduction.—The obedience of these data to Lambert's law, $I^\nu = I_o^\nu e^{-\alpha_\nu l}$, is clearly displayed in the plot of Figure 1. The equivalent path length of liquid water (l) is plotted as abscissa, and the natural logarithm of I^ν is plotted as ordinate. The conformity of these data to Lambert's law implies that the continuous spectrum is akin to line absorption rather than to envelope absorption of a rotation-vibration band formed with moderate resolving-power and dispersion. We shall see later the reason for this behavior.

Discussion.—Two items of considerable importance are embodied in the plot of Figure 1. First, the negative slope of each line is the

corresponding absorption coefficient $a_{\tilde{\nu}}$. The curve of $a_{\tilde{\nu}}$ versus $\tilde{\nu}$ is contained in Figure 2 and is shown by the solid line. The absorption coefficient rises very steeply in the region of longer wave lengths and suffers an increase also as the great water band at 6.26 μ is approached. The theoretical curve for the absorption coefficient is in part discussed below.

It has long been known that radiation by the atmosphere to the ground at night occurs to a great extent in wave lengths longer than 14 μ by the emission of ν_2 by carbon dioxide and by the emission of the rotation spectrum of the water-vapor molecule. In a recent discussion W. M. Elsasser has correctly concluded that the emission

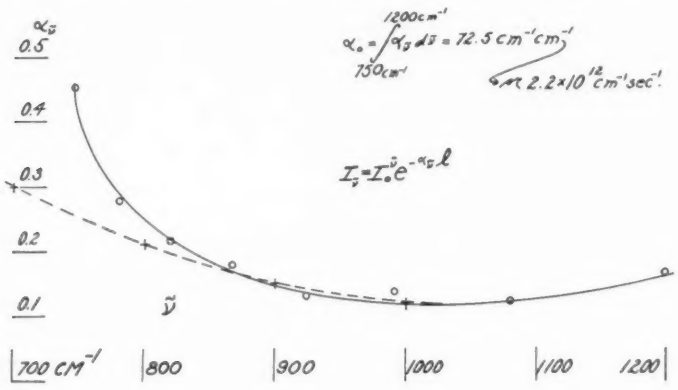

FIG. 2. $a_{\tilde{\nu}}$ versus $\tilde{\nu}$

of the rotation spectrum of water vapor should occur to a lesser extent at shorter wave lengths also.[3] Basing his work on the recent analysis of this spectrum by Randall *et al.*,[4] he showed that, with an amount of water vapor of the order of that normally present in the atmosphere, the influence of the combined wing absorptions of the rotation lines will extend to the shorter wave lengths in question. With the assumption of a half-width $\delta = 0.25$ cm^{-1}, he has deduced the following absorption coefficients, the path length being the equivalent number of centimeters of liquid water. These values were derived on the assumption of a constant atmospheric pressure of 760 mm. The proportionality which exists between the absorption in a band and the square root of the pressure implies that

Elsasser's values would be somewhat reduced by recognition of the exponential behavior of atmospheric pressure. They must be still further reduced for application to an observing station situated on a mountain or on a high plateau, as is the case with the Lowell Observatory.

$p = 760$ mm; $T = 300°$ K

$(\tilde{\nu})$ cm^{-1}	400	500	600	700	800	900	1000
$a_{\tilde{\nu}}$	3.50	0.90	0.46	0.30	0.21	0.15	0.12

It is also shown that for $\lambda < 20\ \mu$, $a_{\tilde{\nu}}$ is given to a good approximation by the formula

$$a_{\tilde{\nu}} = \frac{78{,}000 - 240\,t}{(\tilde{\nu} - 200)^2},$$

where t is the temperature in centigrade. In other words, the net effect of the integrated wing absorptions is that of the wing of a powerful line with center at 50 μ. This explains the adaptability of the data of Table 1 to Lambert's law, as noted earlier. The calculated absorption coefficient given above is shown for comparison with observation by the dotted line in Figure 2. The correction spoken of above has not been incorporated.

Insufficient information is at present available to warrant a detailed discussion of the departure of the theoretical curve from the observed one in Figure 2. Suffice it to say for the present that not only are the theoretical calculations of $a_{\tilde{\nu}}$ difficult from point of extreme accuracy but there is no attempt in this paper to produce a note of finality regarding the observed $a_{\tilde{\nu}}$. Further observations are in progress. It may not be amiss at this point to observe that the growth of the curve for $a_{\tilde{\nu}}$ can be enhanced or that the curve can be made to pass through a minimum (as at the short wave-length end of the observed curve) by the existence and superposed effects of a second absorption coefficient. Thus, it is perhaps possible that the large amount of water normally resident in the atmosphere extends the influence of the great water band at 6.26 μ to longer wave lengths than 8 μ. We would then have,

$$I^{\tilde{\nu}} = I_0^{\tilde{\nu}} e^{-(a_R + a_O)_{\tilde{\nu}} l},$$

where a_R refers to the pure rotation spectrum and where a_O refers to the great water band. In the event that the second absorption

coefficient is due to a substance other than water, the effective $a_{\tilde{\nu}} = (a_R + a_O)_{\tilde{\nu}}$ will vary with the relative amounts of the substances responsible for a_R and for a_O, although for any one prescribed relative amount of the two substances in the atmosphere Lambert's law will be obeyed. This is clearly seen by writing

$$I^{\tilde{\nu}} = I_0^{\tilde{\nu}} e^{-(a_R R + a_O O)_{\tilde{\nu}} M},$$

where R is the number of centimeters of liquid water per unit of air mass, O is the amount of the other substance per unit of air mass, and M is the number of air masses. This may be written

$$I^{\tilde{\nu}} = I_0^{\tilde{\nu}} e^{-\left(a_R + \frac{O}{R} a_O\right) l}$$

or $I_{\tilde{\nu}} = I_0^{\tilde{\nu}} e^{-a_{\tilde{\nu}} l}$, where $a_{\tilde{\nu}} = (a_R + (O/R)a_O)_{\tilde{\nu}}$. It is clear that $a_{\tilde{\nu}}$ will vary as O/R varies.

THE FORM OF THE SOLAR ENERGY-CURVE IN THE INFRARED

Introduction.—The second item of importance to be deduced from Figure 1 relates not to the terrestrial spectrum but to the solar spectrum, for each ordinate intercept provides the corresponding $I_0^{\tilde{\nu}}$ in interplanetary space. These extrapolated values for $I_0^{\tilde{\nu}}$ are, of course, for the dispersion of the 60° rock-salt prism employed in the investigation. Moreover, they do not recognize the differential extinction of infrared radiation within the prism. Reflection losses at the prism faces may be neglected by virtue of their essential constancy over the wave-length interval involved. We proceed now to derive the corrections for prismatic absorption and to reduce the spectrum to a normal one.

Analysis.—It is not difficult to determine the correction for prismatic absorption at minimum deviation. One readily derives the following formula for the fractional transmission

$$T = \frac{1}{h}\int_0^h e^{-a_{\tilde{\nu}} \frac{B}{h} x}\, dx = \frac{1 - e^{-a_{\tilde{\nu}} B}}{a_{\tilde{\nu}} B} = \frac{(1 - A_{\tilde{\nu}})^{B/l} - 1}{\log_e (1 - A_{\tilde{\nu}})^{B/l}},$$

where B is the length of base of the prism, h is the altitude of the prism, $(B/h)x$ is the width of the prism at the distance $h - x$ above

the base, and A_ν is the fraction of the incident radiation absorbed by thickness l. For $l = 1$ cm, A_ν is given by

$\lambda(\mu)$	10	12	13	14	15	16	17
A_λ	0.005	0.007	0.024	0.069	0.154	0.339	0.484

The normalization of the rock-salt prismatic solar spectrum may also be readily accomplished by the determination of $d\vartheta_\lambda/d\lambda$, where ϑ_λ is the deviation.

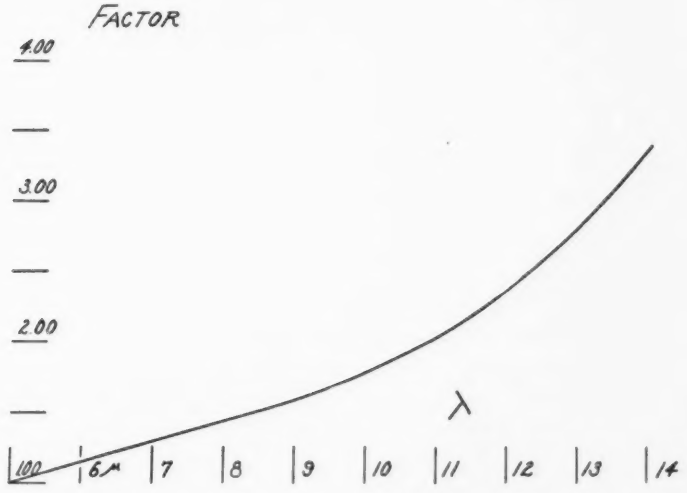

FIG. 3.—Factor of normalization and prismatic extinction

The corrections for absorption and normalization may be combined to form a single correction. This net corrective factor for the data of this paper is shown in curve form in Figure 3.

The thermocouple, made by Dr. C. O. Lampland, possessed a receiver coated with bismuth black by evaporation. No factor need therefore be introduced with respect to the response of the thermocouple over the spectral interval in question.

From Figure 3 are obtained the appropriate factors whose application to the extrapolated I_0^ν's of Figure 1 yield the I_0^ν's for solar radiation in interplanetary space. Table 2 sets forth the data pertinent to this calculation.

In plotting these data for comparison with a black-body curve at 6000° or 7000° K, greater accuracy will result if the black-body curve can be transformed to approximately linear dependence

TABLE 2

SUN'S ENERGY-CURVE IN THE INFRARED

$\lambda(\mu)$	I_0^λ(Mm)	Factor	Product (Mm)
8.34	190	1.48	281
9.25	115	1.62	186
10.10	78	1.79	139.4
10.84	53	1.97	104.4
11.55	40	2.18	87.2
12.22	28.5	2.43	69.3
12.83	20.7	2.71	56.2
13.40	18.0	2.99	53.8

upon $\tilde{\nu}$. This may be accomplished in the following manner. We have

$$I_0^\nu = C_1\nu^3(e^{h\nu/kT} - 1)^{-1} .$$

If $h\nu/kT = x$, then

$$I_0^\nu \propto \frac{x^3}{e^x - 1} .$$

In the present application x is small, and we may expand to get

$$I_0^\nu \propto \frac{x^2}{x + 2} ,$$

where $x \ll 2$. Thus, a near linear relationship exists between $\sqrt{I_0^{\tilde{\nu}}}$ and $\tilde{\nu}$. In Figure 4 the heavy full line is a plot of $\sqrt{I_0^{\tilde{\nu}}}$ against $\tilde{\nu}$ for 6000° or 7000° K. The observed points are given by the circles.

There has been no attempt to measure absolute intensities in this paper, and the agreement of Figure 4 implies only that the *form* of the solar energy-curve in the infrared is similar to that of a black body radiating at a temperature in the neighborhood of 6000° or 7000° K. It is to be expected that the form of the solar energy-curve at long wave lengths may well correspond to a temperature in excess

of 6000° K because of the greater depths at which the infrared radiations presumably originate. The relative intensities of blackbody emission at 6000° and 7000° K between 8 and 14 μ are

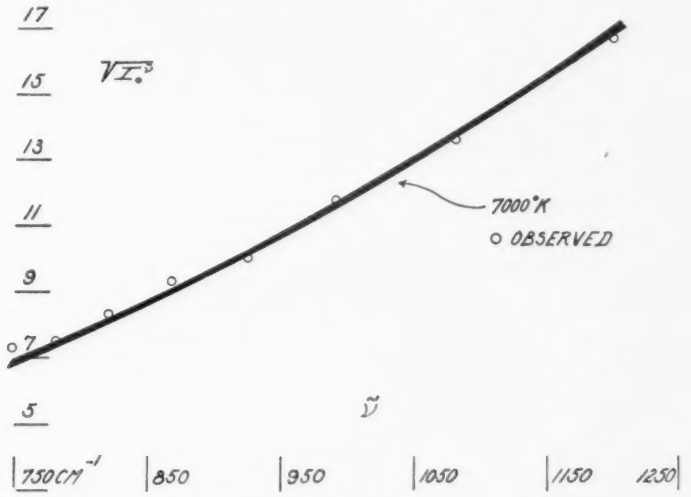

FIG. 4.—The form of the sun's energy-curve in the infrared

very nearly the same, and the present work therefore does not enable one to discriminate between temperatures in this neighborhood.

Here, as in the work on a_ν, further observations are desirable and are being sought.

LOWELL OBSERVATORY
FLAGSTAFF, ARIZONA

THE RELATION BETWEEN ABSOLUTE MAGNITUDE AND REDUCED PROPER MOTION, AND THE MEAN ERRORS IN THE SPECTROSCOPIC ABSOLUTE MAGNITUDES, FOR STARS OF SPECTRAL CLASSES G AND K*

GUSTAF STRÖMBERG

ABSTRACT

A study has been made of the corrections to be applied to the spectroscopic absolute magnitudes (M_s) for the case in which the stars are to be grouped on a neutral or impartial basis of grouping. The stars studied are of spectral types Go–G7 and G8–K2. They have been grouped both on the basis of M_s itself and on the basis of $H = m + 5 \log \mu$, a quantity which is correlated with the absolute magnitude (M). In this study the spectroscopic distinction between giants and dwarfs has not been utilized, and some of the regression effects studied by Russell and Miss Moore are thus partly obliterated. Mean values and dispersions in the absolute magnitude have been derived for the two methods of grouping with the aid of Schlesinger's list of trigonometric paral'axes. The systematic errors are found to be small, and the two methods of grouping give practically the same results. The dispersion in M_s has been found in most cases to have been underestimated. The mean error of the individual value of M_s has been found to be between 0.5 and 0.6 mags.

Formulae are derived for the computation of mean absolute magnitudes from trigonometric parallaxes, for the derivation of the dispersion in M, and for the determination of mean errors in the individual values of M_s.

The existence of giants and dwarfs is clearly shown when the grouping is made on the basis of H. There are distinct discontinuities in the functional relationship between M and H, the presence of which is obviously independent of the relative proportions of stars of different apparent magnitudes and proper motions used in the investigation.

INTRODUCTION

In a recent publication[1] Russell and Miss Moore have studied the systematic effects produced by the accidental errors in the spectroscopic absolute magnitudes. Such effects must appear when a comparison is made between the mean absolute magnitudes for stars grouped on the basis of the spectroscopically determined absolute magnitudes and the mean absolute magnitudes for stars grouped on any other basis. This regression effect can best be studied for homogeneous groups of stars, which have all been reduced by the same set of reduction-curves.

Before undertaking an independent study of the regression effect,

* *Contributions from the Mount Wilson Observatory, Carnegie Institution of Washington*, No. 603.

[1] *Mt. W. Contr.*, No. 589; *Ap. J.*, **87**, 389, 1938.

it was thought desirable to determine the systematic errors and the mean errors in the spectroscopic absolute magnitudes which are applicable to the tabular spectroscopic data when the stars are grouped on an "impartial" or "neutral" basis that ignores the spectroscopic difference between giants and dwarfs. Some of the regression effects studied by Russell and Miss Moore for the giants and dwarfs taken separately are then partly obliterated, since there is an overlap of giants and dwarfs in some of the groups. The systematic effect found in the present study is very small, and the mean error of M_s determined here refers to the published system of M_s when no clear distinction is made between giants and dwarfs.

In this preliminary investigation only stars of spectral types Go–K2 have been studied. The mean spectroscopic absolute magnitudes of the stars have been compared with absolute magnitudes determined from their trigonometric parallaxes both for a grouping according to spectroscopic absolute magnitude and according to reduced proper motion. It has been assumed that the parallaxes in Schlesinger's *General Catalogue of Stellar Parallaxes* (2d ed., 1935) do not require any systematic correction and that the probable errors in this catalogue are substantially correct.

Since the reduced proper motions, $H = m + 5 \log \mu$, are used as the means of securing an impartial method of grouping, the results also give the general relationship between H and the absolute magnitude, M.

METHOD

The stars used are those of types Go to K2, inclusive, as given in *Mt. Wilson Contr.* No. 511, for which trigonometric parallaxes appear in the second edition of Schlesinger's *Catalogue*. These stars were divided into two groups, Go–G7 and G8–K2, the first being regarded as characteristic for the G stars, and the latter for the Ko stars. Within each of these spectral divisions groups of different absolute magnitudes were formed, first according to a neutral basis of grouping and then according to the spectroscopic absolute magnitude itself. For each of these subgroups the mean absolute magnitude, the dispersion in these magnitudes, and the mean errors in the individual absolute-magnitude determinations were derived

from the trigonometric parallaxes by methods which will now be described.

The following notations have been used:

M = the true absolute magnitude
M_s = the spectroscopic absolute magnitude as given in *Mt. Wilson Contr.* No. 511
m = the apparent magnitude as given in the *Henry Draper Catalogue*. For the case of close double stars the individual magnitudes are derived from the combined magnitude. (Several improvements in the data given in *Mt. Wilson Contr.* No. 511, to which our attention was called by Professor Russell, have been incorporated)
π = the true parallax
π_t = the trigonometric parallax as given in Schlesinger's *Catalogue*
π_s = the spectroscopic parallax derived from $M_s - m$
ϵ = the true error in π_t
r_t = the probable error in π_t
T = accidental error in M_s
S = systematic error in M_s
θ = mean error in $M_s + S$
q_s = dispersion in M_s
q = dispersion in M as derived from π_t
p = weighting factors of one type or another

As the basis for the neutral grouping, I have used $H = m + 5 \log \mu = M + 5 \log t - 8.378$, where μ is the total proper motion in seconds of arc per year and t is the tangential motion in kilometers per second. There must clearly be a correlation between H and M, and this correlation is, of course, independent of the errors in M_s and π_t.

For each star we have the relation

$$\pi = \pi_t + \epsilon = 0.1 \cdot 10^{0.2(M-m)} . \qquad (1)$$

In general we can expect a correlation between M and m, the intrinsically brighter stars in a group being on the average also ap-

parently brighter. To separate M from m, we multiply each side of equation (1) by $10^{0.2m}$ and obtain

$$\left.\begin{aligned} \epsilon_0 &= 0.1I - \pi_0 , \\ \epsilon_0 &= \epsilon \cdot 10^{0.2m} , \\ \pi_0 &= \pi_t \, 10^{0.2m} , \\ I &= 10^{0.2M} . \end{aligned}\right\} \qquad (2)$$

where

The "reduced" trigonometric parallaxes and their "reduced" errors are π_0 and ϵ_0, respectively.

For a number of stars *grouped according to H* we may assume that either one of the following conditions is approximately fulfilled:

$$\Sigma p\epsilon = 0 , \qquad (3)$$

$$\Sigma p\epsilon^2 = \text{min.} \qquad (4)$$

The weight p is assumed to be proportional to $1/r_t^2$.

Although the condition

$$\Sigma p\epsilon_0 = \overline{10^{0.2m}} \, \Sigma p\epsilon = 0$$

is statistically permissible, it will, in general, give unnecessarily large accidental errors, since we give the apparently fainter stars greater weight than the brighter ones. In fact, we then disregard entirely the high weights of the near-by stars in the determination of $\overline{I}$ and $\overline{M}$.

Let us introduce new weights p_0 proportional to $p10^{-0.4m}$.

We have then

$$p_0 \sim p10^{-0.4m} \sim \frac{1}{r_0^2} ,$$

where $r_0 = r_t 10^{0.2m}$ is the reduced probable error. It is clear that p_0 is the correct weight to be used for the reduced parallaxes, since in this case $\Sigma p_0\epsilon_0^2 = \Sigma p\epsilon^2$ and the individual errors are thus kept as small as possible.

The condition

$$\Sigma p_0\epsilon_0 = 10^{-0.2m} \, \Sigma p\epsilon = 0$$

not only gives the apparently brighter stars too large a weight but also reintroduces m and M under the same summation sign, and a knowledge of the coefficient of correlation between m and M would be necessary for the derivation of $\bar{I}$, at least if there is an appreciable dispersion in either m or M.

The best method of determining $\bar{I}$ must be based on the condition

$$\Sigma p\epsilon^2 = \Sigma p_0\epsilon_0^2 = \text{min.} \tag{5}$$

We have then

$$\Sigma p_0\epsilon_0^2 = 0.01\Sigma p_0 I^2 + \Sigma p_0\pi_0^2 - 0.2\Sigma p_0 I\pi_0 . \tag{6}$$

But

$$\begin{aligned}\Sigma p_0 I^2 &= \Sigma(I^2 - \overline{I^2})(p_0 - \overline{p_0}) + \overline{I^2}\Sigma p_0 , \\ &= n\kappa\sigma'\sigma'' + (\bar{I}^2 + \sigma_1^2)\Sigma p_0 .\end{aligned}$$

Here

κ = coefficient of correlation between I^2 and p_0
σ_1 = dispersion in I
σ' = dispersion in I^2
σ'' = dispersion in p_0
n = number of stars

Furthermore,

$$\begin{aligned}\Sigma p_0 I\pi_0 &= \Sigma\,(I - \bar{I})(p_0\pi_0 - \overline{p_0\pi_0}) + \bar{I}\Sigma p_0\pi_0 , \\ &= n\kappa'\sigma_1\sigma''' + \bar{I}\Sigma p_0\pi_0 ,\end{aligned}$$

where σ''' is the dispersion in $p_0\pi_0$ and κ' is the coefficient of correlation between I and $p_0\pi_0$.

Substituting into the equation (6) and differentiating with respect to $\bar{I}$, we find

$$\bar{I} = \frac{10\Sigma p_0\pi_0}{\Sigma p_0} . \tag{7}$$

We assume that in the smaller groups the distribution of M about the mean value $\overline{M}$ can be represented by the normal error-curve,

$$F(M)dM = \frac{1}{\sqrt{2\pi q}}\, e^{-(M-\overline{M})^2/q^2}\, dM .$$

Denoting $M - \overline{M}$ by Δ, we find[2]

$$\left.\begin{aligned} \overline{10^{0.2\Delta}} &= e^{0.02q^2/\mathrm{Mod}^2} = C\,, \\ \overline{10^{0.4\Delta}} &= e^{0.08q^2/\mathrm{Mod}^2} = C^4\,, \\ C^2 &= 1 + \frac{\sigma_1^2}{\overline{I}^2}\,, \\ \overline{M} &= 5\log\overline{I} - 5\log C\,, \\ q^2 &= 50\ \mathrm{Mod}\log C = 21.71\log C\,. \end{aligned}\right\} \tag{8}$$

The dispersion σ_1 in I can be determined from the sum of the squares of the residuals in the equations of condition $\sqrt{p_0}\,\overline{I} - 10\sqrt{p_0}\,\pi_0 = 0$, reduced by the effect of the errors in the measured parallaxes. The following formula is convenient:

$$\sigma_1^2 = \frac{100\Sigma p_0(\pi_0 - A)^2}{\Sigma p_0} - 100\left(A - \frac{\overline{I}}{10}\right)^2 - \frac{100n\eta_0^2}{\Sigma p_0}\,. \tag{9}$$

Here A is an arbitrary provisional value of $\overline{\pi_0}$, and η_0 is the mean error in a determination of π_0 having unit weight. The value of η_0 was derived from the probable errors in π_t as given by Schlesinger.

To find the probable errors in the individual spectroscopic absolute magnitudes, we put

$$M = M_s + S + T\,. \tag{10}$$

Hence from equation (1)

$$\pi = \pi_t + \epsilon = \pi_s\sigma\tau\,, \tag{11}$$

where

$$\begin{aligned} \pi_s &= 0.1\cdot 10^{0.2(M_s - m)}\,, \\ \sigma &= 10^{0.2S}\,, \\ \tau &= 10^{0.2T}\,. \end{aligned}$$

[2] *Mt. W. Contr.*, No. 558; *Ap. J.*, **84**, 563, 1936.

The factor σ is regarded as constant for the group. M_s and T, and hence also π_s and τ, are correlated quantities.

We have

$$\pi_s = \frac{\pi_l + \epsilon}{\sigma\tau},$$

$$\pi_s - \pi_l = \pi_l\left(\frac{1}{\sigma\tau} - 1\right) + \frac{\epsilon}{\sigma\tau} = \nu,$$

$$\Sigma p\nu = \left(\overline{\frac{1}{\sigma\tau} - 1}\right)\Sigma p\pi_\tau .$$

We assume here that $\Sigma p\epsilon = 0$. Denoting the mean error in an individual M_s by θ and replacing in the formulae (8) Δ by T, q by θ, and C by A, we get

$$\left(\overline{\frac{1}{\tau}}\right) = \overline{10^{-0.2T}} = \overline{10^{0.2T}} = e^{0.02\theta^2/\mathrm{Mod}^2} = A,$$

$$\left(\overline{\frac{1}{\tau^2}}\right) = \overline{10^{-0.4T}} = \overline{10^{0.4T}} = e^{0.08\theta^2/\mathrm{Mod}^2} = A^4 .$$

Hence

$$\Sigma p\nu = \left(\frac{A}{\sigma} - 1\right)\Sigma p\pi_l ,$$

or

$$\frac{A}{\sigma} - 1 = \frac{\Sigma p\nu}{\Sigma p\pi_l} = F_1 . \tag{12}$$

Furthermore,

$$\Sigma p\nu^2 = \left(\overline{\frac{1}{\sigma^2\tau^2} + 1 - \frac{2}{\sigma\tau}}\right)\Sigma p\pi_l^2 + \left(\overline{\frac{1}{\sigma^2\tau^2}}\right)\Sigma p\epsilon^2 + 2\left(\overline{\frac{1}{\sigma^2\tau^2} - \frac{1}{\sigma\tau}}\right)\Sigma p\pi_l\epsilon ,$$

$$= \left(\frac{A^4}{\sigma^2} + 1 - \frac{2A}{\sigma}\right)\Sigma p\pi_l^2 + \frac{A^4}{\sigma^2}\Sigma p\epsilon^2 - 2\left(\frac{A^4}{\sigma^2} - \frac{A}{\sigma}\right)\Sigma p\epsilon^2 .$$

We denote by η the mean error in a determination of π_l having unit weight.

We find then

$$\frac{A^4}{\sigma^2} + 1 - \frac{2A}{\sigma} = \frac{\Sigma p\nu^2 - n\eta^2}{\Sigma p\pi_l^2 - n\eta^2} = F_2 . \tag{13}$$

The formulae now become

$$\left.\begin{aligned} A^2 &= \frac{1 + F_2 + 2F_1}{(1 + F_1)^2}, \\ \sigma &= \frac{A}{1 + F_1}, \qquad S = 5 \log \sigma, \\ \theta^2 &= 50 \text{ Mod} \log A = 21.71 \log A. \end{aligned}\right\} \tag{14}$$

The probable error (r_s) in a spectroscopic parallax can be found from the equation

$$\frac{r_s}{\pi_s} = \frac{0.6745\theta}{5 \text{ Mod}} = 0.3106\theta. \tag{15}$$

If both F_1 and F_2 are small, equations (14) can be replaced by the approximate expression

$$\theta^2 = 25 \text{ Mod}^2 F_2 = 4.715 \frac{\Sigma p v^2 - n\eta^2}{\Sigma p \pi_r^2 - n\eta^2}. \tag{16}$$

This equation was first given in *Mt. Wilson Contr.* No. 199; *Ap. J.*, **53**, 26, 1921.

It should be noted that we have here assumed $\Sigma p\epsilon = 0$. This means that the weighting system is based solely on the accuracy of the trigonometric parallaxes and that no attention is given to the accuracy of the spectroscopic parallaxes. The result is that the apparently fainter stars are given higher weight than in the method based on equations (7) and (8). The value of the systematic correction to the absolute-magnitude system derived in this way is less accurate than the previous one, but the method seems to be the best for determining the probable errors in the individual values of M_s, since the effective number of individual values is greatly increased. An alternative method is to put $S = \overline{M} - \overline{M}_s$, where $\overline{M}$ is determined by equation (8) and $\overline{M}_s$ is weighted according to the size of p_0. A can then be determined from equation (13) written in the form

$$A^4 - 2A\sigma + \sigma^2(1 - F_2) = 0, \tag{17}$$

which can be solved by approximations.

TABLE 1

GROUPING ACCORDING TO H

H	No.	$\overline{H}$	$\overline{M}$	Mean Error	q	$\overline{M}_s$	q_s	$\overline{M}-\overline{M}_s$	θ
	Spectral Type Go–G7								
≤ − 4.0..	20	−6.3	−2.2	±1.0	.....	−2.04	1.25	−0.2	±0.03
−3.9 to − 3.0..	25	−3.4	−0.60	0.43	1.28	−0.25	0.87	− .35	.89
−2.9 to − 2.0..	29	−2.3	−0.15	0.30	0.60	+0.21	0.74	− .36	.66
−1.9 to − 1.0..	28	−1.2	+0.10	0.27	0.79	+0.35	0.31	− .25	.33
−0.9 to − 0.1..	24	−0.4	+0.86	0.30	0.88	+0.74	0.34	+ .12	.79
0.0 to + 0.9..	18	+0.5	+1.00	0.34	.....	+0.82	0.55	+ .18	.....
+1.0 to + 1.9..	18	+1.7	+2.58	0.42	1.46	+2.85	1.46	− .27	.40
+2.0 to + 2.9..	27	+2.4	+3.35	0.24	1.04	+3.76	1.09	− .41	.53
+3.0 to + 3.9..	34	+3.3	+2.78	0.25	1.26	+3.24	1.32	− .46	.61
+4.0 to + 4.9..	58	+4.5	+4.16	0.12	0.77	+4.27	0.34	− .11	.60
+5.0 to + 5.9..	52	+5.4	+4.90	0.10	0.61	+4.75	0.48	+ .15	.39
+6.0 to + 6.9..	54	+6.6	+5.02	0.09	0.40	+4.67	0.29	+ .35	.23
+7.0 to + 7.9..	17	+7.2	+5.59	0.18	0.49	+5.05	0.36	+ .54	.24
+8.0 to +12.2..	16	+9.2	+6.20	±0.18	0.59	+5.60	0.70	+0.60	±0.51
−3.9 to + 0.9..	124	−1.8	−0.03	±0.15	0.98	+0.24	0.70	−0.27	±0.63
+1.0 to + 3.9..	79	+2.5	+2.90	.16	1.22	3.23	1.37	− .33	.52
≥4.0.....	197	+5.3	+4.62	±0.07	0.85	+4.54	0.51	+0.08	±0.54
	Spectral Type G8–K2								
≤ − 4.5..	14	−5.8	−2.3	±0.9	.....	−1.27	1.00	−1.0	.....
−4.4 to − 3.0..	20	−3.7	+0.13	.30	.....	+0.01	0.34	+0.12	
−2.9 to − 2.0..	21	−2.4	+0.08	.37	0.67	+0.34	0.52	−0.26	±0.57
−1.9 to − 1.0..	25	−1.3	+0.17	.30	0.97	+0.45	0.38	−0.28	
−0.9 to − 0.3..	33	−0.7	+1.02	.21	0.80	+0.66	0.51	+0.36	.46
−0.2 to + 0.3..	31	+0.1	+0.75	.25	0.64	+0.60	0.28	+0.15	
+0.4 to + 0.9..	27	+0.6	+1.17	.18	.....	+0.82	0.55	+0.35	
+1.0 to + 1.6..	23	+1.2	+0.73	.22	.....	+0.88	0.49	−0.15	.26
+1.7 to + 2.4..	12	+2.0	+0.95	.52	1.40	+0.85	1.24	+0.10	
+2.5 to + 2.9..	17	+2.6	+1.67	.43	1.25	+1.91	1.19	−0.24	.51
+3.0 to + 3.9..	12	+3.3	+3.84	.49	1.41	+3.87	2.08	−0.03	
+4.0 to + 4.9..	21	+4.6	+5.37	.15	0.57	+5.37	0.90	0.00	.39
+5.0 to + 5.9..	22	+5.4	+5.12	.25	1.04	+5.58	0.52	−0.46	
+6.0 to + 6.9..	30	+6.3	+5.77	.10	0.40	+5.54	0.19	+0.23	
+7.0 to + 7.8..	11	+7.2	+5.45	.30	0.61	+5.82	0.25	−0.37	±0.50
≤+7.9.....	7	+8.2	+6.00	±0.16	.....	+5.57	0.15	+0.43	
−4.4 to + 0.3..	130	−1.4	+0.55	±0.12	0.77	+0.46	0.45	+0.09	±0.53
+0.4 to + 2.4..	62	+1.3	0.97	.16	.81	0.85	.83	+ .12	
≤+4.0.....	91	+5.3	+5.43	±0.09	0.69	+5.47	0.70	−0.04	±0.46

APPLICATION

As before mentioned, the method here outlined was applied to stars in the spectral intervals Go–G7 and G8–K2. The stars in the first group are, in the following, referred to as G stars; and the stars in the second group as Ko stars. In the present study all the stars in these intervals having measured values of M_s and π_t were taken together and grouped, first according to H and then according to M_s. The results are shown in Tables 1 and 2. $\overline{M}$ and q are derived by using the equations (7), (8), and (9). $\overline{M}_s$ is defined as $\Sigma p_0 M_s / \Sigma p_0$; q_s is defined by the equation $q_s^2 = \Sigma p_0 (M_s - \overline{M}_s)^2 / \Sigma p_0$; and θ is determined by the use of equations (12), (13), and (14). Obviously, q_s and θ cannot be determined for the individual groups in the case when the grouping is based on M_s itself.

It is seen from Table 1 that the dispersions q derived from π_t are in most cases somewhat larger than the dispersions q_s in the measured spectroscopic absolute magnitudes. The mean error θ in an individual determination of M_s is on the average between 0.5 and 0.6, except for the supergiants.

In general, θ is appreciably smaller than q, which shows that the spectroscopic measurements are of value even within the groups of giants and dwarfs.

The results given in Table 1 are shown in graphical form in Figures 1 and 2, in which the values of $\overline{M}$ and $\overline{M}_s$ are plotted against $\overline{H}$ as abscissae. The continuous curve is an approximate representation of the values of $\overline{M}$ as derived from π_t. The agreement between $\overline{M}$ and $\overline{M}_s$ is very good, except for the stars of smallest H among the Ko stars and for the stars of largest H for the G stars.

In these figures straight lines representing constant values of t, the linear tangential motions, have also been drawn. These lines obviously must form angles of 45° with the H-axis.

A very important feature of the curves representing $\overline{M}$ as a function of $\overline{H}$ is that they can be represented by straight lines separated by portions with greater slope. The transitions occur for the G stars around $M = +2.5$, and for the Ko stars around $M = -1.0$ and $M = +3.0$. These discontinuities clearly represent the transition from giants to dwarfs and from supergiants to giants. The shape of

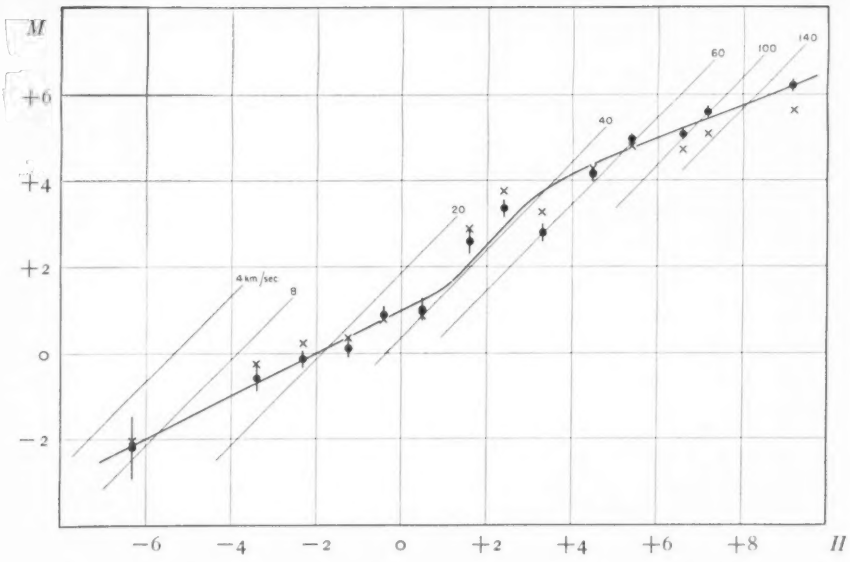

FIG. 1.—Relation between $\overline{M}$ and $\overline{H}$ for Go–G7 stars. The mean absolute magnitudes are derived from trigonometric parallaxes, the stars being grouped according to $H = m + 5 \log \mu$. Values of $\overline{M}$ are plotted as dots, the vertical lines representing their mean errors. Crosses indicate the corresponding mean values of M_S. The sloping straight lines are loci for stars having the same linear tangential motion.

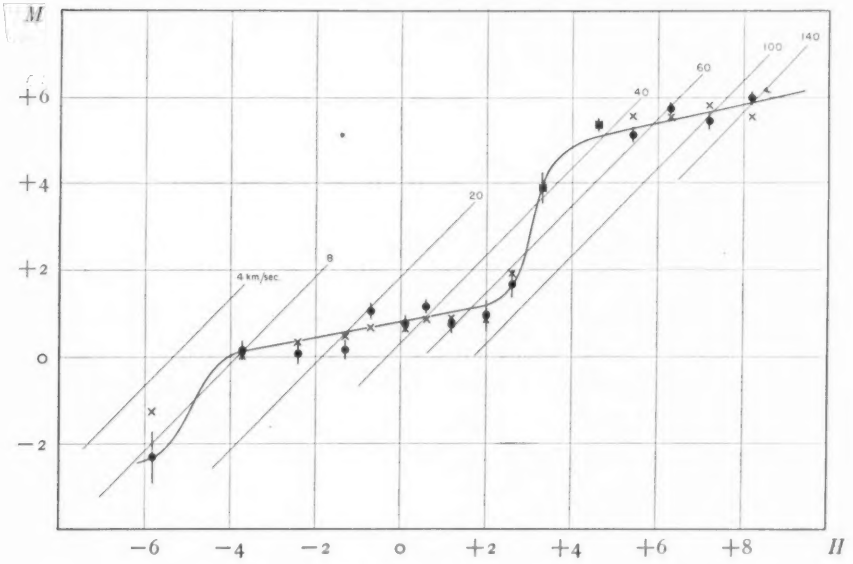

FIG. 2.—Relation between $\overline{M}$ and $\overline{H}$ for G8–K2 stars. Otherwise similar to Fig. 1

the curves is independent of the relative proportion of stars having different values of H in the observational material. The existence

TABLE 2

GROUPING ACCORDING TO M_s

M_s	No.	$\overline{M}$	Mean Error	$\overline{M}_s$	q	$\overline{M} - \overline{M}_s$
	Spectral Type Go–G7					
≤ -2.0	11	−3.2	±1.8	−2.67	2.0	−0.5
−1.9 to −1.0	10	−1.6	1.0	−1.48		− .1
−0.9 to 0.0	10	−0.69	0.64	−0.14	.....	− .55
+0.1 to +0.5	45	−0.15	0.22	+0.27	0.66	− .42
+0.6 to +0.9	61	+0.51	0.19	+0.71	0.79	− .20
+1.0 to +1.9	22	+1.31	0.21	+1.09	.....	+ .22
+2.0 to +2.8	10	+2.15	0.55	+2.53	.....	− .38
+3.2 to +3.9	21	+3.02	0.21	+3.72	0.77	− .70
+4.0 to +4.5	107	+4.11	0.07	+4.27	0.63	− .16
+4.6 to +4.9	79	+4.65	0.09	+4.73	0.62	− .08
+5.0 to +5.3	32	+5.30	0.10	+5.18	0.37	+ .12
+5.4 to +6.3	11	+6.07	±0.10	+5.66	0.26	+0.41
+3.2 to +6.3	250	+4.10	±0.06	+4.34	0.97	−0.24
	Spectral Type G8–K2					
≤ -1.4	8	−4.1	±2.1	−2.01	.....	−2.1
−1.0 to −0.1	10	−1.49	0.82	−0.31	.....	−1.18
0.0 to +0.4	69	+0.31	0.19	+0.28	0.78	+0.03
+0.5 to +0.8	98	+0.85	0.12	+0.62	.29	+0.23
+0.9 to +1.9	24	+1.26	0.21	+1.03	.....	+0.23
+2.0 to +2.5	16	+2.02	0.24	+2.16	.56	−0.14
+4.0 to +4.9	10	+3.73	0.19	+4.41	.46	−0.68
+5.0 to +5.3	21	+5.00	0.16	+5.20	.55	−0.20
+5.4 to +5.5	20	+5.56	0.16	+5.44	.53	+0.12
+5.6 to +5.7	20	+5.56	0.21	+5.61	.81	−0.05
+5.8 to +5.9	20	+5.73	0.07	+5.88	.18	−0.15
+6.0 to +6.5	9	+6.21	±0.10	+6.10	0.20	+0.11
+4.0 to 6.5	100	+4.96	±0.06	+5.21	0.96	−0.25

of these discontinuities is *a direct proof of the division of the stars of later types into giants and dwarfs.* Such a proof is important, since some astronomers have felt that this division may be illusory, having

been introduced by the selection of parallax stars on the basis of apparent brightness and large proper motions.

The straight-line portions of the curves $\overline{M} = f(H)$ are inclined to the H-axis by angles which depend only on the dispersions in M and t, or rather on the ratio of these dispersions. To prove this we start from the equation

$$H = M + 5 \log t - C . \tag{18}$$

We denote $5 \log t$ by t_1, and $H + C$ by u, and find

$$M + t_1 = u .$$

Denoting the distribution function of M by $F_1(M)dM$, and that of t_1 by $F_2(t_1)dt_1$, we find that the probability $F(M, u)dMdu$ of a certain combination of M and u is given by the equation

$$F(M, u)dMdu = F_1(M)F_2(u - M)dMdu . \tag{19}$$

It is here assumed that there is no correlation between M and t_1. Denoting by $\overline{M}_u$ the mean value of M for a small range in u, we find

$$\overline{M}_u = \frac{\int_{-\infty}^{+\infty} MF(M, u)dM}{\int_{-\infty}^{+\infty} F(M, u)dM} . \tag{20}$$

In the first approximation we can well neglect the correlation between M and t. Assuming error-curves for the distributions of M and t_1, with the dispersions σ_1 and σ_2, we find from (27), after replacing u by $H + C$,

$$\overline{M}_H = \frac{H + C - \bar{t}}{1 + \frac{\sigma_2^2}{\sigma_1^2}} + \frac{\overline{M}}{1 + \frac{\sigma_1^2}{\sigma_2^2}} . \tag{21}$$

This equation can be written

$$\overline{M}_H = \overline{H} \tan \alpha + \text{const.} ,$$

$$\tan \alpha = \frac{1}{1 + \frac{\sigma_2^2}{\sigma_1^2}} . \tag{22}$$

$\overline{M}_H$ denotes here the mean value of M for a small range in H. $\overline{M}$, on the other hand, is the mean value of M for the total range in H. From equation (22) it follows that if σ_1 is small compared with σ_2,

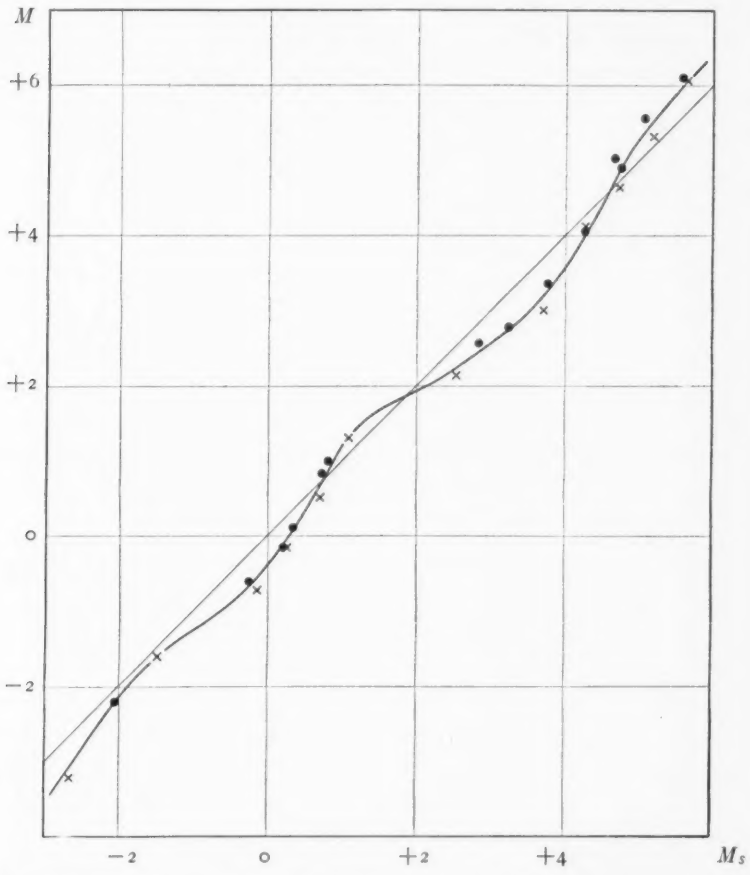

FIG. 3.—Relation between true (M) and spectroscopic (M_S) absolute magnitudes for Go–G7 stars. Dots represent mean values for a grouping of stars according to H; crosses, means for a grouping according to M_S. The curve indicates the relationship found; the straight line corresponds to identity between M and M_S.

α approaches the value zero, and that if σ_1 is large compared with σ_2, α approaches 45°. The former case corresponds to a small spread, and the latter to a large spread in M compared with that in $l_1 = 5 \log l$.

The small dispersion among the normal giants as indicated by the spectroscopic absolute magnitude is clearly shown by the present data, both from the small range in M and from the values of q for a large range in H. The writer[3] has previously tried to establish this

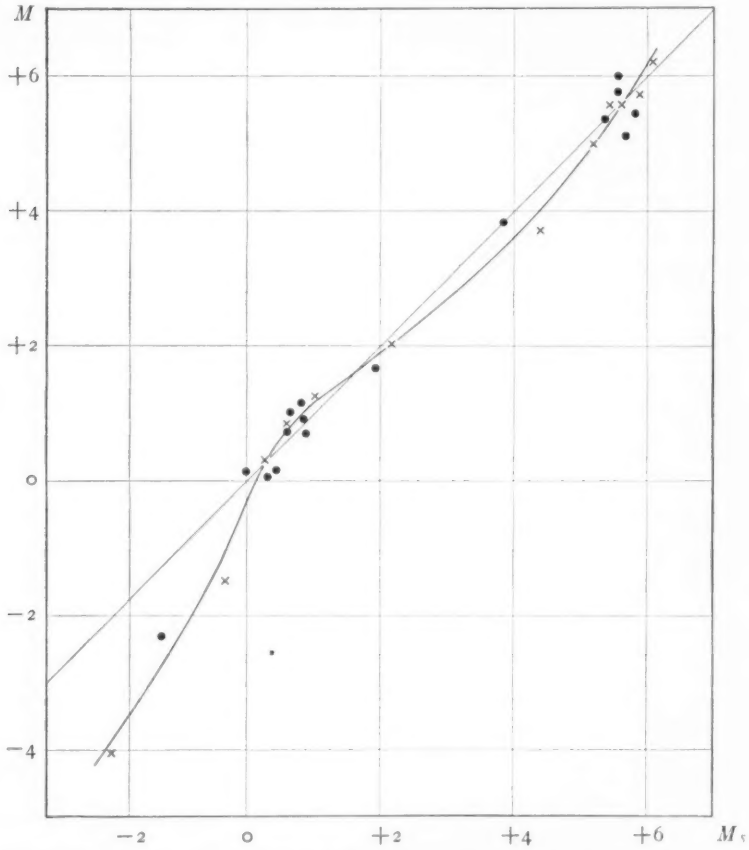

FIG. 4.—Relation between M and M_s for G8–K2 stars. Otherwise similar to Fig. 3

small dispersion by studies of proper motion, and it is here confirmed by a study of the trigonometric parallaxes. Obviously a grouping according to H affects the dispersion in M and M_s in the same way, whereas the dispersion in a group of giants, defined by certain limits in M_s, tends to reduce the spread in M_s relative to that in M.

[3] *Mt. W. Contr.*, No. 442; *Ap. J.*, **75**, 115, 1932.

Whether the groups of stars in the transition regions are mixtures of giants and dwarfs or are partly made up of stars of intermediate brightness requires a special study.

The data in Tables 1 and 2 are shown in a different way in Figures 3 and 4. Here $\overline{M}_s$ and $\overline{M}$ are plotted against each other for a grouping both according to H and according to M_s. The difference in $\overline{M}$ for the two methods of grouping is surprisingly small; only in one case (K0 stars for M about $+3.8$) does the difference amount to half a magnitude. The curves shown in Figures 3 and 4 represent, within the limits of accuracy, both the partial and the impartial methods of grouping.

The present study shows, as Russell and Miss Moore[1] have also found, that the systematic errors in the spectroscopic absolute magnitudes of the G and K stars are rather small. The greatest deviations occur for the supergiants, but for these stars the uncertainties are necessarily very large. The mean errors of the individual determinations are in general between 0.5 and 0.6 mag., in agreement with previous estimates. On the face of it, this result seems to be in contradiction to that of Russell and Miss Moore, who have found a mean error in the spectroscopic parallaxes of 38 per cent, corresponding to a mean error of 0.82 mag. in M_s. Professor Russell has pointed out to the writer that the last result applies to the absolute magnitudes after they have been corrected for the regression effect and that somewhat different scales of absolute magnitudes have then been used. For this reason the results can both be correct, but they refer to different quantities.

CARNEGIE INSTITUTION OF WASHINGTON
MOUNT WILSON OBSERVATORY
October 1938

AN OPTICAL STUDY OF SOLAR CORONA PHOTOGRAPHS OF JUNE 8, 1937

BRIAN O'BRIEN, H. S. STEWART, JR., AND C. J. ARONSON

ABSTRACT

By using isophote contours of eclipse negatives made by Stevens, it is shown that the diffuse luminosity observed by him is actually part of the corona and is not of atmospheric origin. The contours are nearly circular and differ greatly from the visual appearance of streamers in the corona. It is shown that the corona has nearly spherical symmetry and that the streamers are only slight, though abrupt, transitions in brightness superimposed on the main luminosity. Their visual prominence is due only to a well-known property of the eye. This is further demonstrated by a laboratory experiment in which true brightness contours are compared with visual appearance.

The eclipse photographs of June 8, 1937, secured by Major A. W. Stevens on the Hayden Planetarium–Grace Expedition to Peru, exhibited an unusual amount of diffuse luminosity surrounding the sun. This has been reported briefly by Stevens, and a full description will be published by him shortly.[1] In order to determine whether this diffuse luminosity was a real part of the solar corona or was due to some spurious optical effect, extensive tests of the photographic equipment were undertaken by him in collaboration with the Eastman Kodak Research Laboratory. The conclusion was reached that no camera or film defects could have produced the observed image surrounding the sun. While there, the negatives were also mounted against a dark background and illuminated from the front, so that they could be viewed and photographed by reflected light to bring out more clearly the fainter portions of the image. It remained to determine whether any atmospheric or other phenomena external to the cameras could have been responsible, and at Major Stevens' request we undertook this investigation.

The diffuse and quite uniform luminosity surrounding the usual coronal streamer image was observed on negatives made with three cameras. Two of these used 9-inch aero base film and carried 24-inch and $8\frac{1}{4}$-inch focal-length Bausch and Lomb lenses, respectively. The third used 35-mm motion-picture film and carried a Bausch and Lomb Raytar lens of 6-inch focal length. These will be described

[1] Stevens, unpublished.

more fully by Stevens. For our detailed measurements we used negatives made with the cameras of 24-inch and 6-inch focal length.

Rayleigh scattering[2] in the earth's atmosphere by particles very small compared to a wave length could not produce a limited region of luminosity around a celestial source. Large-particle scattering with particles of random size and random distribution, however, would result in a diffuse blur of light around each point of a source; and since the light source chiefly effective during totality is the very bright inner corona, each point of this narrow luminous ring would be surrounded by a diffuse glow. Evidently under these conditions the center of the moon would have a brightness more than twice that at a point only one solar radius out from the sun's limb, if there were no luminosity at all due to the corona at this point. Since this was contrary to the observed optical densities on all the coronal photographs, it was agreed that atmospheric scattering of this type could not alone produce the effect.

This reasoning is acceptable for a distribution of scattering particles of random size in the atmosphere; but for particles of constant size or a narrow range of sizes, a series of luminous rings will appear surrounding each point on the source. If the radius of the first bright ring subtends an angle θ at the observer, then

$$\sin \theta = 1.65 \frac{\lambda}{2a}, \tag{1}$$

where λ is the wave length of the light and a the radius of the particle.[3] This produces one type of ring around the sun or moon when viewed through thin clouds or haze, and is usually termed a "corona." We shall refer to this as an "atmospheric corona," to distinguish it from the "solar corona." Such an atmospheric corona can be formed by any kind of particles, such as dust, water droplets, or ice crystals, and is not dependent in its important features upon the shape of the particles, provided only that these are not too elongated. Atmospheric coronas are not to be confused with halos, the latter being refraction and reflection phenomena associated with ice crystals of a definite shape and orientation. An atmospheric co-

[2] Rayleigh, *Collected Works*, 1, 87; 2, 397. [3] *Traité d'optique*, 1, 310.

rona consists of a series of concentric rings; but the first or inner ring is much brighter than the outer rings, which are seldom seen.

If the distribution of the uniform-size particles forming an atmospheric corona is completely at random, there will be a diffuse luminosity surrounding each point on the source but lying within the first ring surrounding that point. This central diffuse luminosity is usually referred to as the "aura." Atmospheric coronas commonly observed exhibit a pronounced aura; but if the space distribution of the particles approaches regularity, the aura dims or vanishes alto-

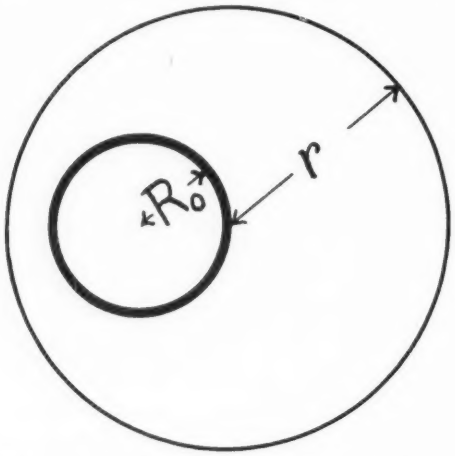

FIG. 1.—Position of aura due to scatter about one point of the corona

gether, leaving only the rings. This condition is uncommon in meteorological phenomena but might possibly be approached on occasion—as, for example, in a cloud of electrically charged particles, the mutual repulsion of the particles serving to maintain some approach to regularity in space distribution. The condition must therefore be considered.

It will be evident from Figure 1 that under such conditions there will be, surrounding any point A on the bright inner coronal ring, a ring of radius r subtending an angle θ at the observer's position, as given by equation (1) above. The family of such rings surrounding each point on the bright inner corona will produce a luminous annular region concentric with the lunar disk, and of inner and outer

radii, R_1 and R_2, as shown in Figure 2. Since there will be an extreme spread of about 2 to 1 in the photographically effective wave lengths, or an effective spread of about $1\frac{1}{2}$ to 1 in wave length (panchromatic film and no filter), the rings will not be sharp as drawn, the inner and outer radii R_1 and R_2 being ill defined. A finite range of particle size or particle shape will cause a further departure from the ideal sharp rings, and a photograph of a total eclipse under these conditions

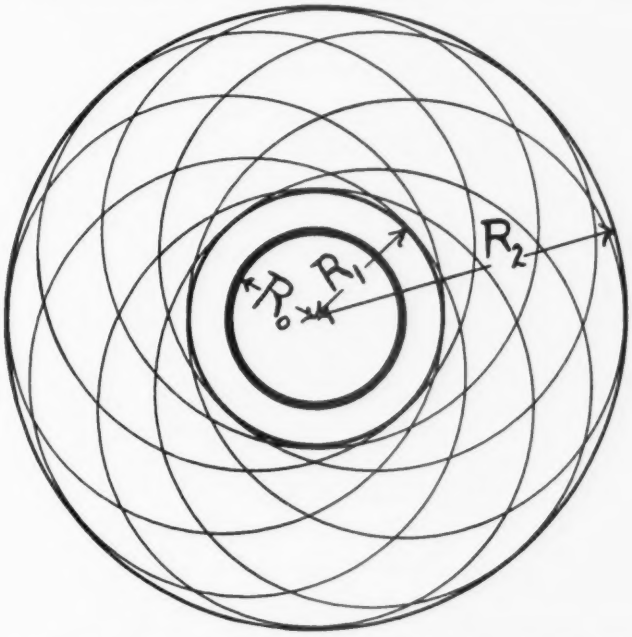

FIG. 2.—Combination of auras about all points of the corona at mid-totality

should show a diffuse luminosity surrounding the corona, such as the one noted by Stevens. If any gap existed between the inner radius R_1 of the annulus and the radius of the moon R_0, it would be obscured upon the photographs by the image of the solar corona.

On discussing this suggestion with Major Stevens, there appeared to be no evidence to rule out the existence of a thin cloud of such particles above the 25,000-foot level from which the photographs were made. While there were no clouds visible above the airplane, Major Stevens agreed that, if thin, an extended cloud might have gone unnoticed. The existence of a dust cloud seems unlikely be-

cause of the position of the observers off the west coast of Peru in a prevailing west wind from the Pacific Ocean. The air temperature at 25,000 feet was $-18°$ C, so that the existence of a cloud of water droplets above the airplane seems unlikely, although Simpson[4] has shown that supercooled droplets may exist in clouds far below the freezing-point. It seems more probable that, if any cloud existed, it was composed of ice crystals, although, as discussed above, this distinction is not material to the production of an atmospheric corona. Such an atmospheric corona would appear in a direct photograph, as would a diffuse structureless portion of the solar corona.

The same optical effect might have been produced by condensed moisture on the surface of the camera lenses used to photograph the eclipse. If one simply breathes upon a glass surface and views through the glass surface a distant point source, a broad luminous ring will be seen, its inner radius subtending an angle of several degrees. The condensed droplets upon the glass are quite regular in size and are distributed with some approach to regularity, so that the central aura is faint or absent. The experiment is more striking when carried out with glass which is ground and polished than with fusion-finished surfaces such as window glass.

The eclipse cameras were mounted with their lenses some inches within the open window of the airplane, so the air stream past the lenses was not particularly rapid. If the photographer's breath happened to strike the lens surface just before an exposure was made, some condensation might well be expected, since the lens surfaces were well below the freezing-point. However, the fact that many photographs made with three different cameras all show the same effect would seem to rule out this possibility as a source of the diffuse glow observed about the eclipsed sun.

Distinguishing between an atmospheric corona and a true solar phenomenon would be difficult, or impossible, if photographs made at one time only were available. It occurred to one of us, however, that the series of negatives made throughout totality might be used to distinguish between the two phenomena. In Figure 3 suppose that the moon is advancing from left to right across the solar disk and that the time is just after second contact. A greater width of the

[4] *J. R. Met. Soc.*, **38**, 291, 1912.

bright inner coronal ring will be exposed at A than at B. Consequently, the diffraction ring of radius r about A will be much brighter than the ring of the same radius about B. The diffraction about the points C and D will be intermediate in brightness between those about A and B, respectively. There will thus be a shift to the right in the position of the contour lines of equal brightness, or isophotes, for an atmospheric corona, as compared to the isophotes

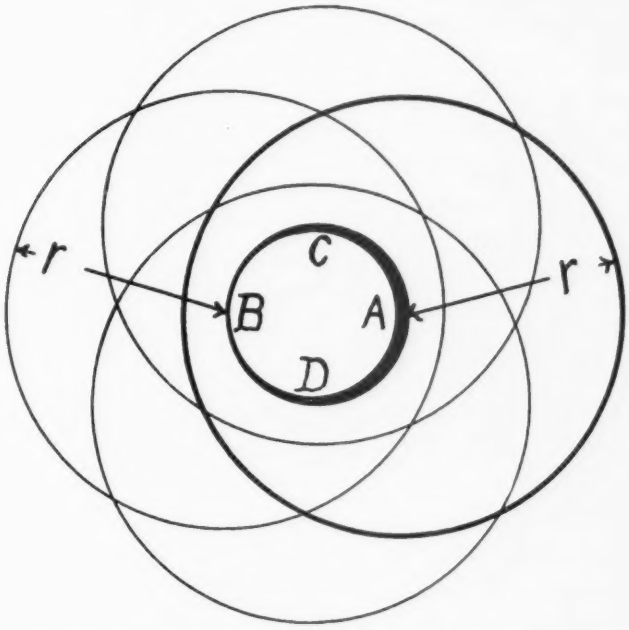

FIG. 3.—Combination of auras about all points of the corona at second contact

for the condition of mid-totality shown in Figure 2, or the condition of third contact, which will be the mirror image, right for left, of Figure 3. The magnitude of this shift of the isophotes from second to third contact will depend upon the radial distribution of brightness in the innermost regions of the solar corona, as well as the angular diameters of sun and moon. As the effective ring source of light (innermost solar corona) becomes narrower, the shift in the center of gravity of luminosity, owing to an atmospheric corona, increases.

There do not appear to be good data upon the radial distribution of brightness in the innermost corona, but De Saussure[5] finds again that Turner's expression giving the brightness as proportional to the inverse sixth power of the distance from the center of the sun holds fairly well from 3′ to 16′ from the sun's limb, in agreement with earlier measures; and there is ample qualitative evidence that an even steeper law of brightness distribution holds as one approaches within a minute or less of the sun's limb. If the diffuse luminosity is due to an atmospheric effect, a shift of the order of magnitude of the sun's radius or more might be expected to occur between second and third contact. If this luminosity is actually due to the solar corona, there will, of course, be no shift unless rapid coronal motions, so far not observed, can occur.

The labor involved in determining a series of isodensity contour lines upon a photographic plate is very great when the usual method of point-for-point measurement of optical density is employed. The use of a recording microdensitometer reduces the labor somewhat but still leaves the task of constructing the contour lines from a long series of microdensitometer traces.

We have recently developed a technique for the rapid contouring of wedge spectra by the use of multiple reproductions upon a photographic material of very high gamma. Such a procedure has been used by others,[6] but difficulties have been experienced in securing high precision, owing to slight irregularities both in development and in the photographic materials used for the reproductions. We have given special attention to the elimination of these irregularities. Briefly, the method consists of making contact or projection prints upon Eastman Kodalith film (ordinary, not orthochromatic). These are developed in a high-contrast developer, Eastman Formula D-85, with carefully controlled temperature and time, and with special precautions to secure very complete agitation and to avoid the use of oxidized developer. With care, a gamma of 6 or 7 may be obtained, yet with a high degree of uniformity over large areas of film. After processing, a second, contact print produces a duplicate negative

[5] *Arch. des sci.*, **18**, 282, 1936.

[6] Goldberg, *Rept. Intl. Cong. Phot.*, August 26, 1910, p. 140; Luther, *Brit. J. Phot.*, September 2, 1910, p. 57.

PLATE I

FIG. 4

FIG. 5

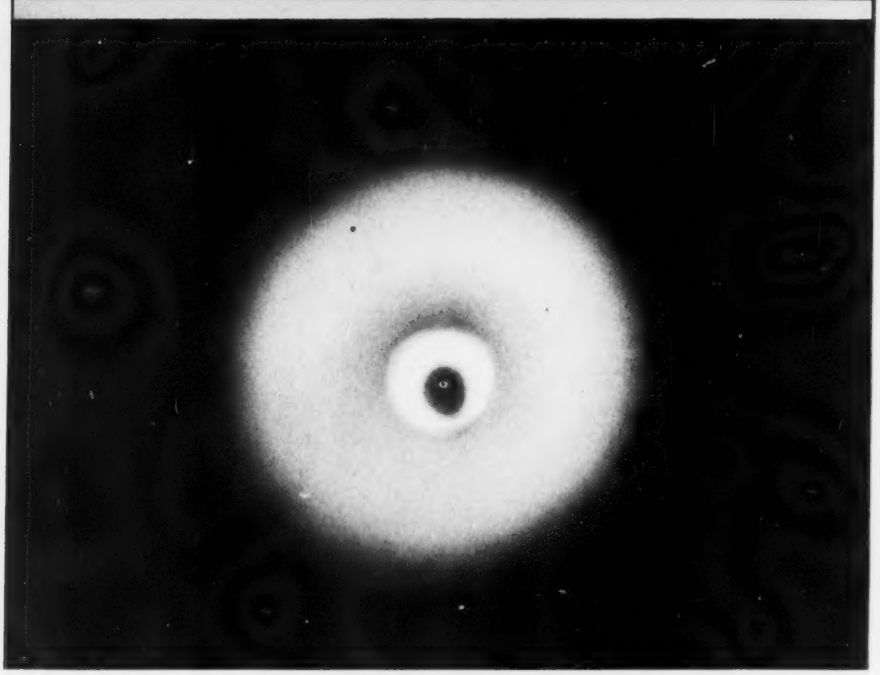

FIG. 4.—Positive of direct photograph of artificial eclipse at second contact

FIG. 5.—Artificial eclipse photographed through scattering-plate

with an over-all gamma referred to the original of over 40, still retaining a high degree of uniformity and reproducibility. This duplicate negative exhibits only areas which are very clear or very dense with quite sharp boundaries between. These are the isodensity contours of the original. A more complete description of the technique and precautions will be published elsewhere.[7] It is this method which we have used for contouring the eclipse negatives.

As a test of the method and to demonstrate the effect shown in Figure 3, an annular source of light was photographed in the laboratory. This source was formed by imaging a concentrated filament lamp upon the photographic objective with a simple lens provided with a decentered disk stop. The angular diameter of the ring, viewed from the camera objective, was 2.4°. A direct photograph is reproduced in Figure 4 (see Pl. I), showing the decentered boundaries of the light source. The photograph shown in Figure 5 was made by breathing upon a plane parallel plate and holding it in front of the objective. The annular source of light is, of course, very much overexposed in order to bring out the diffraction pattern, just as the inner corona is overexposed in an ordinary eclipse photograph that shows the outer coronal details.

The photograph of Figure 5 has been contoured at two levels of density on the original negative. The Kodalith positives at the lower and higher levels of original negative density are shown in Figures 6*a* and 7*a*, respectively, and the corresponding duplicate negatives in Figures 6*b* and 7*b*. By registering the Kodalith negative with its corresponding positive and printing through the two, the contour lines of Figures 6*c* and 7*c* are produced. The marked eccentricity of the isodensity contours is clearly shown, since the center of the ring source of light (artificial moon) has been marked on the original negative and so prints through in all the reproductions. In Figures 6*d* and 7*d* the contour lines have been printed as in 6*c* and 7*c*, the registered positive and negative rotated together 180° about the center mark, and a second print made on the same photographic material before processing. This shows very clearly the decentering of the diffraction isophotes surrounding the source of light which has been formed to correspond roughly to the innermost corona source

[7] O'Brien and Stewart, *J. Opt. Soc. Amer.*, **28**, 50, 1938.

as seen at an eclipse just after second, or just before third, contact. Another way of showing this eccentricity of the contour lines which will be more directly comparable to the actual eclipse study described below is shown in Figure 8. Here the (artificial moon) center of the Kodalith positive corresponding to a low density of the original negative has been registered with the center of the duplicate negative, Figure 7*b*, the positive and negative here being rotated 180° with respect to each other and a print made through the two. The width of the broad crescent-shaped area represents double the decentering of the isodensity contour lines, or a width 1.25 times the diameter of the artificial moon, the decentering being half this amount.

Nine of the eleven negatives made by Major Stevens with the camera of 24-inch focal length, and about 120 feet of 35-mm motion-picture film made with the 6-inch lens, were available to us. The 24-inch camera negatives were made at intervals of about 10 seconds, Nos. 2 and 11 being separated in time by about 90 seconds. The motion-picture film was driven approximately 70 feet per minute, giving a little more than 100 seconds spread from first to last exposure. Photographs were made near the center of the moon's shadow in late afternoon with the sun 11° above the horizon. The duration of totality was 3 minutes 20 seconds, and the apparent motion of the moon referred to the sun was very nearly 0.′5 per minute of time.

Negatives 2, 3, 6, and 11, made with the 24-inch camera, and three frames near the beginning, middle, and end, respectively, of the motion-picture film, were selected for contouring. Registry marks were made on the original negatives far outside of any coronal image, and long-exposure prints were made to bring out the moon's limb and thus permit a determination of the moon's center, to which all quantities were referred. Kodalith positives at nine levels of exposure were then made from each of the selected 24-inch camera negatives by contact printing, and from each of the selected 6-inch camera motion-picture negatives by projection printing to the same scale as the 24-inch camera contact prints. Upon each of these master-positives the moon's center was marked by registering with the positive its corresponding long-exposure print. The uncertainty in

PLATE II

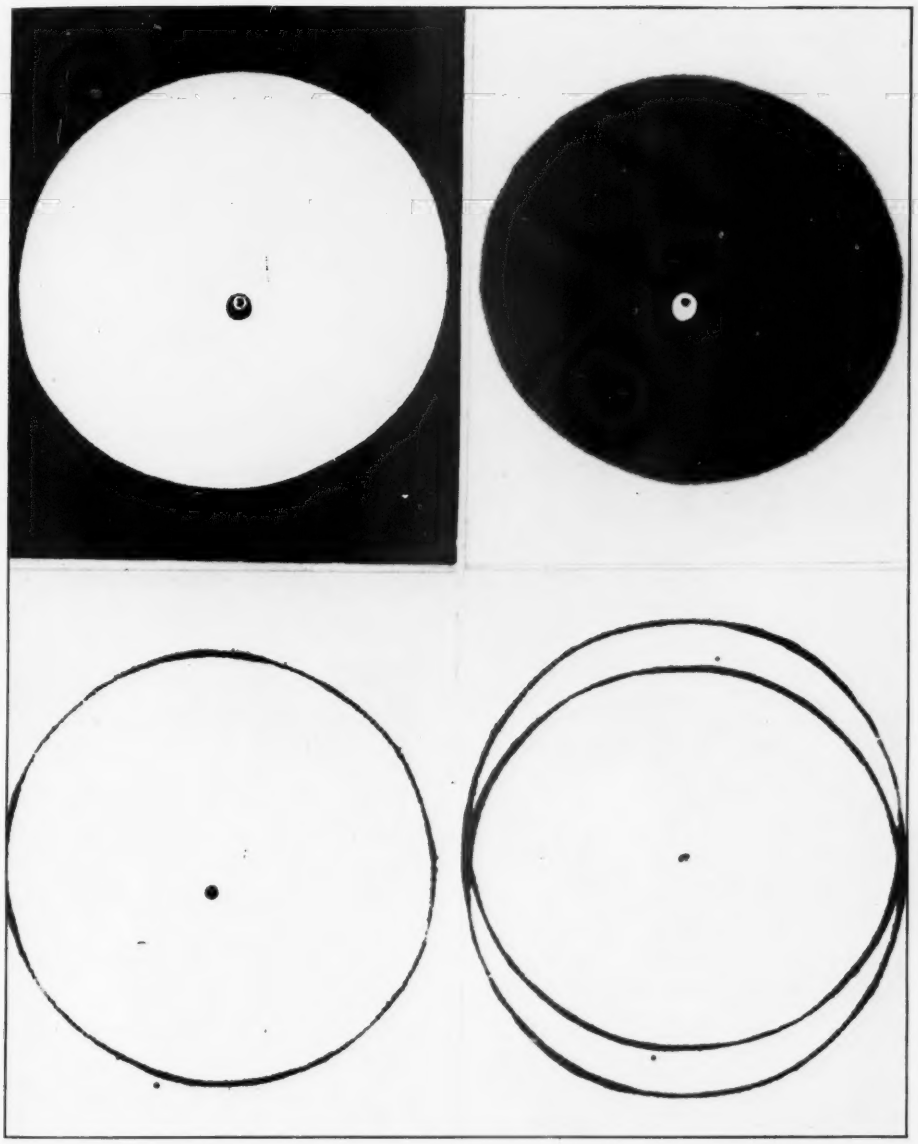

FIG. 6*a*

FIG. 6*b*

FIG. 6*c*

FIG. 6*d*

FIG. 6*a*.—Positive low-density Kodalith contact of artificial eclipse negative

FIG. 6*b*.—Negative low-density Kodalith contact of Fig. 6*a*

FIG. 6*c*.—Isophote contour formed by superimposing Figs. 6*a* and 6*b*

FIG. 6*d*.—Superimposed low-density isophotes centered on moon at second and third contact

PLATE III

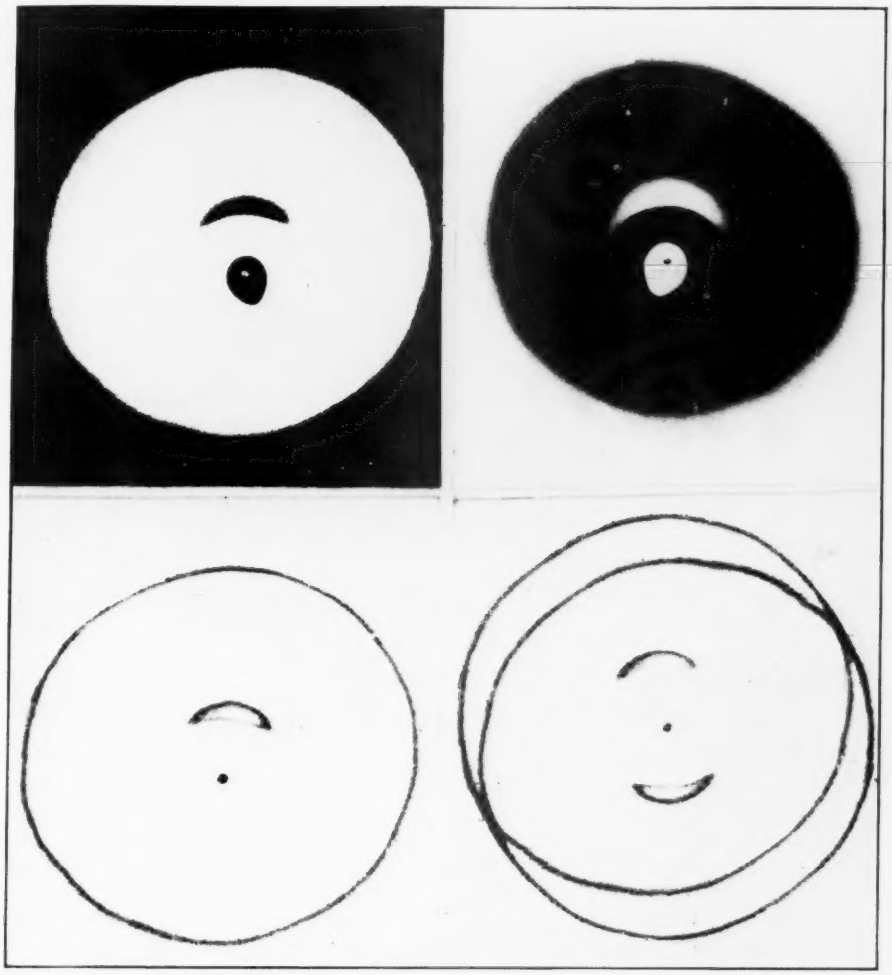

FIG. 7*a*

FIG. 7*b*

FIG. 7*c*

FIG. 7*d*

FIG. 7*a*.—Positive high-density Kodalith contact of artificial eclipse negative

FIG. 7*b*.—Negative Kodalith contact of Fig. 7*a*.

FIG. 7*c*.—Isophote contour formed by superimposing Figs. 7*a* and 7*b*

FIG. 7*d*.—Superimposed high-density isophotes centered on moon at second and third contact.

PLATE IV

FIG. 8

FIG. 9*a*

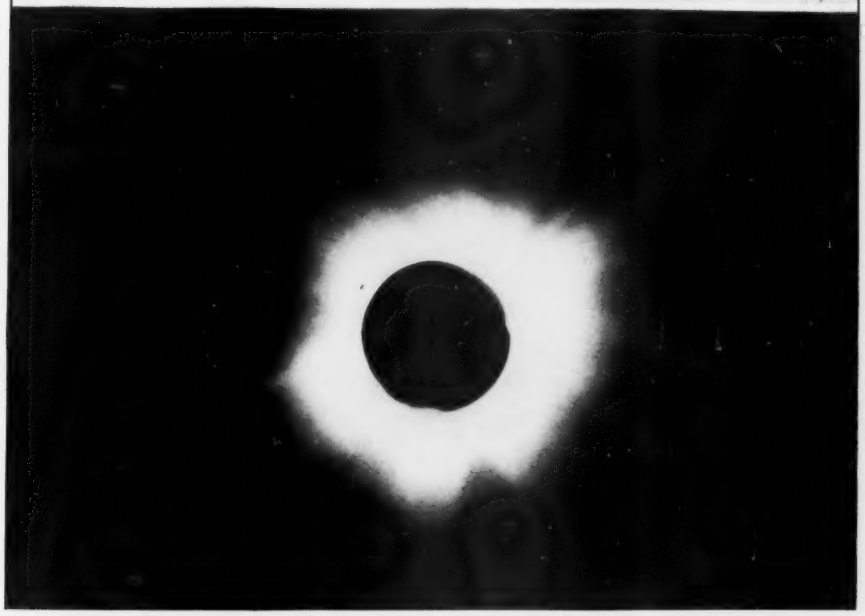

FIG. 8.—Artificial eclipse demonstration of shift anticipated between second-contact low-density positive and third-contact high-density negative, if luminosity depends on scatter in the earth's atmosphere.

FIG. 9*a*.—Positive of solar eclipse photograph

determining the position of the lunar center was not greater than about 1/10 mm on the image, corresponding to about 1/60 of the lunar diameter.

Figure 9*a* is a reproduction of one of the negatives upon low-contrast positive material, showing the characteristic coronal streamers. Figures 10*a*, 10*b*, 11*a* and 11*b* are Kodalith positives and duplicate negatives from the same original at two different exposure levels. The very different appearance of the corona in these is evident, the Kodalith photographs more nearly resembling the

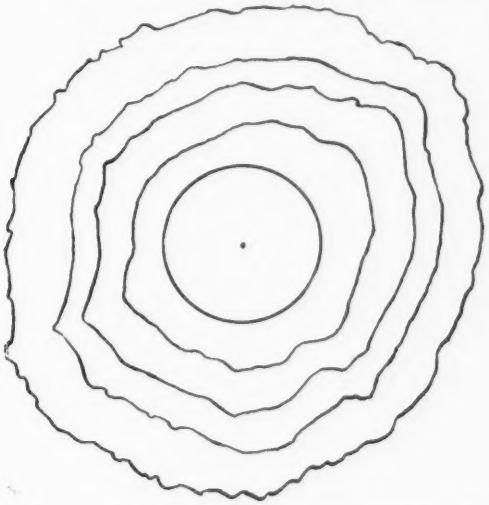

FIG. 9*b*.—Isophote contours about solar eclipse negative

diffuse luminous area observed by Stevens. Figure 12 is a contact print through the positive and negative of Figure 10, registered with reference to the moon's center. It will be noted that the contour line is of substantially constant width, as it should be if the photomechanical reproduction has been properly carried out.

Figure 13 is a similar contour formed by registering, with respect to the moon's center, a positive made from original negative No. 3 with a positive made from original negative No. 11. The non-uniformity of contour band width is evident, the difference in width of the band on opposite sides corresponding to twice the shift of position of the isophotes with reference to the center of the moon. This

is the same kind of shift as that shown in a much greater degree in Figure 8 and is in the proper direction to agree with the concept that the diffuse luminosity surrounding the sun is due to the diffraction phenomenon described above. However, not only is the magnitude of this shift far smaller than would be expected on this concept, but it must be remembered that our co-ordinates are referred to the center of the moon. When the known apparent motion of moon with respect to sun is subtracted from the measured shift of the isophote contours, the results are as shown in Table 1. All quantities are reduced to millimeters, measured on the 24-inch camera negatives.

TABLE 1*

Exposure No.	Interval between Exposures	Mean Shift of Contours Referred to Moon's Center	Shift Referred to Sun's Center
2 and 6	40 sec.	+0.16 mm/min.	+0.06 mm/min.
3 and 10	80	.09	−0.01
A and C	80	+0.06	−0.04

* The estimated probable error of measurement of shift is of the order of 0.04 mm/min.

It is evident from this table that no shift greater than the probable error of measurement occurred in our isophotometric contours of the luminosity surrounding the sun. Moreover, it is evident that our errors are far smaller than any shift which would be expected on a diffraction hypothesis. Compare this result, secured by our method, which is capable of detecting a displacement less than 0.01 lunar diameter, with the shift of 0.63 artificial moon diameter observed in the laboratory experiment described above.

Our conclusion, therefore, which we feel is reached with a rather fair degree of certainty, is that the diffuse luminosity surrounding the sun which has been observed by Stevens is purely a solar phenomenon not related to the earth's atmosphere.

It is interesting to consider why, if this be a real solar phenomenon, it has received so little notice. Actually, it has been observed before. Bergstrand[8] made careful isophote contours of the 1914 eclipse, using a modified Hartmann microphotometer. Although he

[8] Bergstrand, *Off. p. l'Obs. astro. d'Upsala*, 1919.

PLATE V

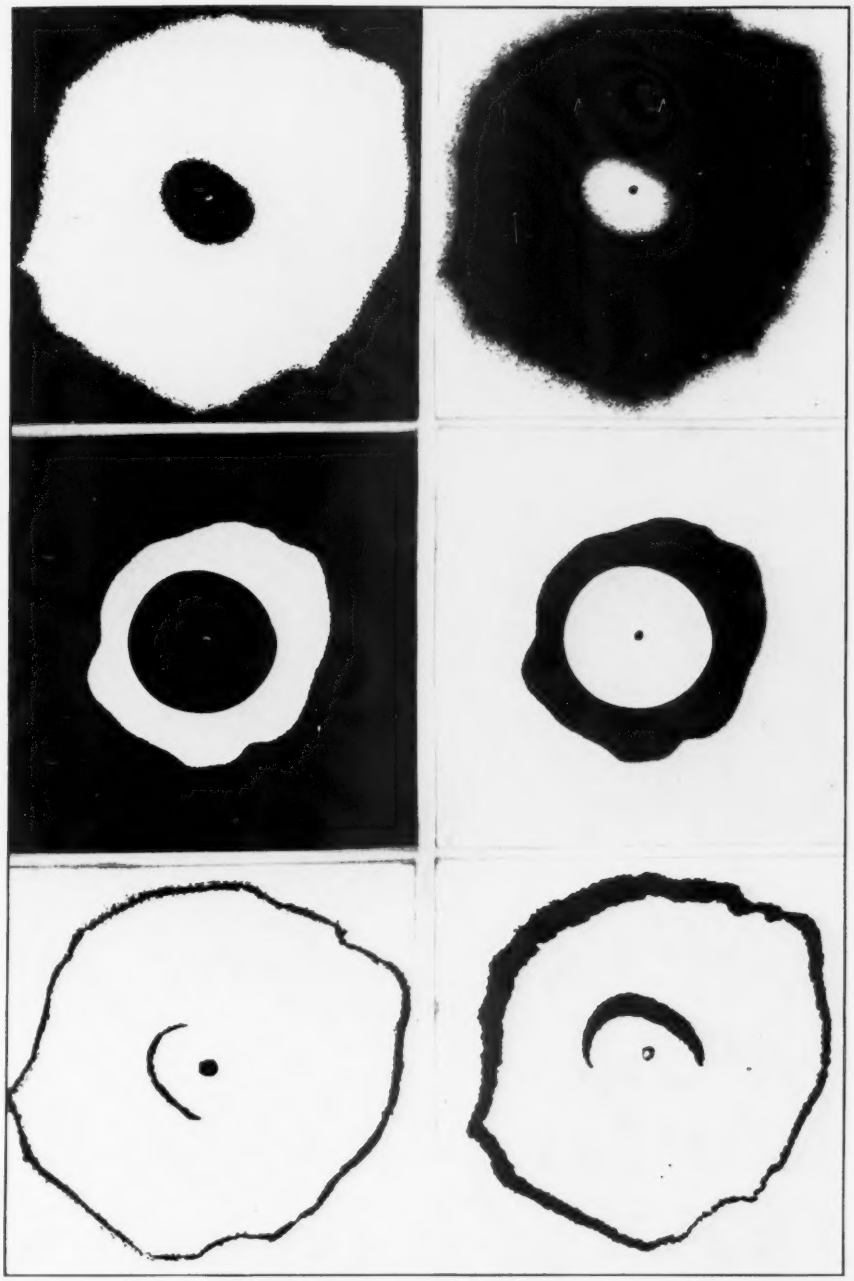

FIG. 10*a*

FIG. 10*b*

FIG. 11*a*

FIG. 11*b*

FIG. 12

FIG. 13

FIG. 10*a*.—Positive low-density Kodalith contact of eclipse photograph

FIG. 10*b*.—Negative Kodalith contact of Fig. 10*a*

FIG. 11*a*.—Positive high-density Kodalith contact of eclipse photograph

FIG. 11*b*.—Negative Kodalith contact of Fig. 11*a*

FIG. 12.—Isophote contour at low density of eclipse photograph formed from Fig. 10*a* and Fig. 10*b*.

FIG. 13.—Solar-eclipse contours shift between second and third contact, corresponding to Fig. 8. Shift shown is due to motion of moon about which contours are centered.

made corrections for scattered skylight, there are certain details of the photographic photometry used which might be open to question. However, his results show the same sort of contours which we have obtained by our photographic procedure, as will be seen from his eclipse photographs and his isophote contours reproduced in the original article. Von Klüber[9] studied photographs of the 1929 eclipse by a procedure similar to Bergstrand's, with very similar results.

The phenomenon appears to have received little attention, in spite of the results of these two authors. It seems probable to us that this is due to two causes. In the first place, both these authors used photographs which had been made at stations not far from sea-level. The Rayleigh scattering in the earth's atmosphere of light from the corona was sufficiently great to produce a background fog upon their plates which had to be taken into account. There seems to have been, rather generally, the feeling that the almost circular isophotes reported by these authors resulted from some contamination of the true coronal image by atmospheric scattering. In the second place, the corona itself and ordinary photographs of it do not look like these contour drawings. The difference in appearance is quite pronounced when one compares Bergstrand's photograph with his contour drawings. The difference is even more pronounced when one views the solar corona itself or a good original photograph of it, since much detail is unavoidably lost in halftone reproduction.

Actually, the difference in appearance between the extended streamers of the corona and the purely photo-mechanical contour lines which show no streamers is a problem in physiological optics. The streamers are undoubtedly present in the solar corona but are not the main feature of the phenomenon, which is missed in viewing either the original or a good photograph. We have carried out an experiment to demonstrate this visual error in the following manner.

An opaque screen of black cardboard had one edge cut to the profile shown in Figure 14*a*, which is simply a contact print of the edge of the cardboard. This screen was mounted against a board in a vertical plane, with the profile edge below. A strip of photographic film to which a weight was attached was slipped between the cardboard mask and the board, with the weighted edge down. This was

[9] Von Klüber, *Zs. f. Ap.*, **3**, 142, 1931.

mounted in a darkroom facing, at some distance, a small source of light covered with a diffusing screen to avoid any pattern in the illumination at the plane of the film. The film was allowed to fall under the acceleration of gravity from behind the black cardboard mask, the light being turned off just before the last of the film strip had left the shadow of the mask. The resulting photograph is reproduced in Figure 15.

It is evident from a moment's consideration of the conditions under which this exposure was made that the contour lines of equal photographic density must be identical with the profile of the lower edge of the cardboard mask as shown in Figure 16*a*. Nevertheless, long streamers are the prominent feature of the resulting photograph in Figure 15, and it is difficult at first to believe that the form of the isodensity contours is as stated.

The explanation of these streamers follows from a property of the visual mechanism which has long been known. The eye is a sensitive indicator of abrupt transition in brightness, even though the actual difference in brightness is small. It is for this reason that the dividing-line in various visual photometric devices, such as the Lummer-Brodhun cube, is made as sharp as possible. On the other hand, the eye is a poor detector of transitions in brightness which occur gradually across the visual field, even though the total change in brightness is quite large. Thus, in viewing the field of a simple equality of brightness photometer with a vertical dividing-line, a gradual transition in brightness from top to bottom of the field may go almost unnoticed, even though the total range in brightness be 2·to 1, while a difference in brightness between the two halves of the field on opposite sides of the vertical dividing-line as small as 2 or 3 per cent will be immediately obvious. Thus, the photograph in Figure 15, which shows a large gradation in brightness from top to bottom and a small but abrupt transition in brightness as one crosses into the square contour region from left to right, has as its prominent feature a long vertical streamer. It should be noted that the triangular profile contour produces a very indistinct streamer, although the departure of the triangular part of the contour from the horizontal position is as great as that of the square part. This, of course, results from the fact that the transition in brightness across that part of the

PLATE VI

FIG. 14*a*

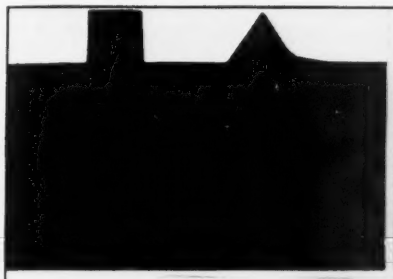

FIG. 14*b*

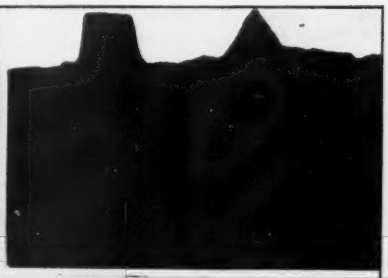

FIG. 15

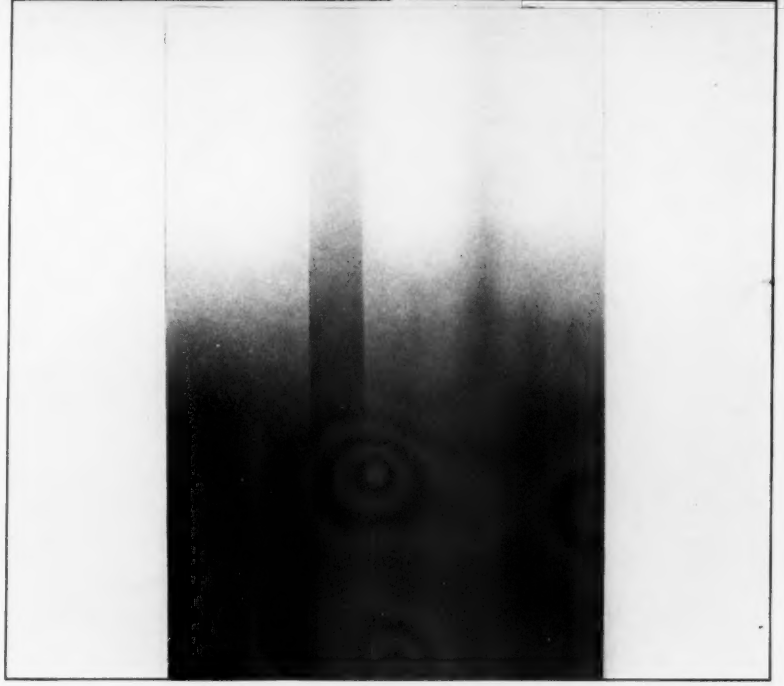

FIG. 14*a*.—Mask used to demonstrate genesis of streamer appearance of solar eclipse.

FIG. 14*b*.—Contour of Fig. 15

FIG. 15.—"Streamers" produced by moving film from under mask shown in Fig. 14*a* during exposure to light source.

photograph corresponding to this triangular notch is more gradual than the brightness transition across those parts of the photograph corresponding to the edges of the square notch.

To further emphasize the foregoing points and to demonstrate the power of the photographic contouring method, the photograph in Figure 15 has been printed to a Kodalith positive and duplicate negative. That the photograph in Figure 15 has, in fact, the contour lines as stated is very clearly demonstrated by the resulting Kodalith contour reproduction of it shown in Figure 14*b*. The slight irregularity in the Kodalith contour is due to actual irregularities in the original photographic image shown in Figure 15, since a duplicate Kodalith contour shows identical irregularities.

In view of the foregoing results, only one conclusion seems possible. The luminosity photometrically contoured by Bergstrand and by von Klüber, observed by Stevens, and photographically contoured by us is the solar corona. It is an extended luminous volume surrounding the sun, with its surfaces of equal brightness exhibiting no large departures from concentric spheres, and with a continuous gradation of brightness outward from the sun's limb. The coronal streamers, so prominent to the eye, are a purely secondary phenomenon resulting from boundaries produced by slight, though abrupt, discontinuities in brightness.

Any satisfactory theory of the corona must take these facts into account. From the optical standpoint, the streamers may be produced by some effect, such as radiation or streams of corpuscles, which effect either adds a slight increment of brightness along roughly radial paths or suppresses slightly the brightness along such paths.

The geometry of those streamers, which exhibit a broad base and a sharp outer point, fits better with the concept of corpuscular or other radiation emitted within sharply defined cones from points on the solar surface, the radiation having the property of suppressing slightly the light emitted from the general corona within the limits of such cones. The broad-base type of coronal streamer would thus be the region between two such cones, within each of which the luminosity is suppressed. Physically this concept seems less probable than the first one mentioned above, in which the bright stream-

ers are due to some agency enhancing the general coronal brightness, although both should be given consideration in view of the optical relations involved.

Unfortunately, the original negatives by Major Stevens do not carry any standard stepped exposure; so it is not possible to produce isophotes at known intervals of brightness. We have, however, produced a few contours of unknown interval, and these are shown in Figure 9*b* on the same scale as the low-contrast direct photograph in Figure 9*a*. This plot may be convenient for comparison with coronal isophotes published by others.

INSTITUTE OF OPTICS
UNIVERSITY OF ROCHESTER

WAVE LENGTHS IN THE SPECTRUM OF ANTARES

DOROTHY N. DAVIS

ABSTRACT

A table of wave lengths, intensities, and identifications of lines in the spectrum of Antares for the region λλ 3600–6600 has been compiled. The table is described and is accompanied by explanatory notes.

Atomic lines in the spectrum of Antares have been discussed in a previous paper.[1] The measurements upon which that study was based are now published in full in the following pages.

DESCRIPTION OF THE TABLE

Column 1 contains the wave length consistent with the velocity adopted for each plate. The presence of a colon after a value indicates that the wave length is believed to be less accurate than others. A question mark indicates that the reality of the line is doubted. Two asterisks preceding the wave length indicate that in the pages following the table there is a note on the corresponding line. Other asterisks in the first column have a meaning which depends upon wave length in the following manner:

*	λλ 4035–4071	Wave length and intensity are from Plate 1096
	4402–4599	Line was measured only on Plate 9378
	4966–4981	Line was measured only on Plate 633[1]
	5358–5371	Line was measured only on Plate 650[2]
***	4549–4570	Line was measured only on Plate 12[2]
	5358–5367	Wave length is mean of measurements on Plates 633[1] and 650[2], while intensity is from Plate 633[1]
	5775–5778	Wave length is mean of measurements on Plates 654[2] and 650[3], while intensity is from Plate 654[2]
	6170–6180	Wave length is mean of measurements on Plates 650[3] and 633[3], while intensity is from Plate 633[3]
****	4585–4970	Line was measured only on Plate 12[2]
	5372–5374	Wave length is mean of measurements on Plate 650[2] and 654[2], while intensity is from Plate 654[2]
	6193–6197	Wave length is mean of measurements on Plates 633[3] and 654[4], while intensity is from Plate 633[3]
(		Wave length and intensity are from Pl. 240W.[2]

[1] *Ap. J.*, **87**, 335, 1938. Table 1 of this paper gives the data for the spectrograms.

[2] Plate 240W was obtained with the two-prism quartz spectrograph and the Crossley reflector of the Lick Observatory. Lines in the region λλ 3400–3700 were measured on

Column 2 contains the intensity estimates. The symbols accompanying the numbers have the following meaning:

BdRv Violet edge of a wide region of absorption, usually containing unmeasurable structures, which gradually decrease in intensity toward the red

BdVr Red edge of a similar sort of region which fades into the continuous background on the violet side

c Center (not the center of gravity) of a wide, possibly blended, line or wide region of absorption

d Apparently double, but components are too close for measurement

d? Possibly double

h Hazy

H Very hazy

n Nebulous

N Very nebulous

r Line has a moderate red wing which may or may not be due to unresolved component on red side

R Line has pronounced red wing

s Line is narrow, giving sharp appearance

v Line has a moderate violet wing

V Line has a pronounced violet wing

w Wide, but not wider than about 0.75 A

W Very wide

Wr When this symbol follows an intensity estimate, it means that the corresponding line is wide and has a red wing. When this symbol occurs alone, it corresponds to the red edge of a very wide line or a region of nearly uniform absorption, which may or may not have a molecular origin

Wv Violet edge of a region of nearly uniform absorption, which may or may not have a molecular origin. When this symbol follows an intensity estimate, it means that the line is wide and has a violet wing

For the first few pages of the table, intensities inclosed in parentheses are those estimated one year after the original measures were made. They are only approximate, owing to underexposure of Plate 1096 for the region concerned.

---

this plate. For various reasons, mainly because of the low dispersion (52.1 A/mm at 3600), measurements of Plate 240W are not comparable with the other measurements. Only a few measurements which supplement those of Plate 1096 in the badly underexposed ultra-violet region have been included in the table.

A verbal description of the meaning of the intensity numbers is as follows:

0	Line barely distinguishable, sometimes not measurable
1	Line barely distinguishable but always measurable (unless too hazy)
2	Line faint
3	Line easily distinguished and measured
2– 5	Moderately faint lines
6– 8	Moderately strong lines
9–15	Strong lines
16 and greater	Very strong lines

Column 3 contains the identifications. In suggesting identifications of the stellar lines, a definite attempt was made to adhere as closely as possible to the notation system employed in the *Revised Rowland Table*. Examples of this system, with modifications and extensions which seemed to be demanded by the nature of the Antares material, are given below:

Fe, Co	Coincidence is of like order in wave length
Fe Co	Coincidence is closer for preceding element
Fe–Co	*Fe* line coincides with violet portion and *Co* line with red portion of stellar line
Fe–	Stellar line is too strong for *Fe* alone, or has a longer wave length than laboratory line, or both. There must be an unknown component to the red
–Fe–	*Fe* line coincides with stellar line within limit of tolerance, but stellar line is so strong that there must be an unidentified component or components on both the violet and red sides
Fe, Co–Cr	*Fe* line and *Co* line of nearly identical wave length coincide with violet portion and *Cr* line coincides with red portion of line
Fe Co–Cr	*Fe* line and *Co* line differing in wave length by more than 0.05 A coincide with violet portion, and *Cr* line coincides with red portion
Fe(K)	An *Fe* line which could be found only in Kayser's *Tabelle der Eisenlinien* coincides fairly well with stellar line
Fe(p)	A predicted *Fe* line coincides with stellar line
Fe?	Identification doubtful for some reason
⊙	Unidentified stellar line coincides with unidentified solar line

As usual, underlining indicates which element predominates. From a study of the unblended lines, it was found that the limit of tolerance in ascribing coincidence is ± 0.05 A. Actually, the majority of the coincidences for unblended lines fall well within this limit.

For plates of relatively low resolving-power and in regions of great line density, blends are so prevalent that it is very difficult to avoid unwieldy and ambiguous identifications. This is particularly true of the ultraviolet. Unless the symbols are separated by commas or dashes, the order of the symbols is dependent directly upon the difference in wave length between laboratory and stellar lines, the element for which the coincidence is closest coming first. When the discrepancy in wave length is more than 0.2 A for any or all of the possible contributors, the symbols have been arranged in order of increasing wave length and separated by dashes. When more than three elements are obviously responsible for a line, the symbols have usually been arranged in order of wave length and inclosed in parentheses.

Believing that the value of such a list of lines and identifications is enhanced if it can be used to select unblended lines without consulting original papers, a definite attempt was made to enter a symbol for each laboratory line which may contribute to a blend, even if the same element contributes more than once to the same line. This rule could be strictly followed in the region λλ 4000–6600. In the ultraviolet, however, two or more strong lines of iron are frequently blended together with lines of another element. In such cases, *Fe* has been written only once. But, if no element other than iron contributes to the line, the symbol *Fe* has been entered twice. This should make it clear that the line must not be mistaken for a single iron line. It will be understood, of course, that the preceding remarks apply to any element.

The identifications of severely blended lines should by no means be considered final.

The intensities in Table 1 should be adequate for identification purposes and should serve until a complete spectrophotometric investigation can be undertaken. It is difficult to judge the reliability of visual estimates of intensity. Even if an observer's intensity scale remains perfectly consistent throughout a series of measurements, systematic errors due to differences in dispersion and resolution, differences in exposure, and variation of plate sensitivity with wave length are bound to enter.

The intensity data in the first part of the table as far as λ 4983.96

have been assembled from six prism plates and two grating plates for which the dispersion ranges from 2.86 A/mm to 12.85 A/mm. The quality and extent of the data would not justify an attempt to reduce the intensities from all the plates to a uniform scale. The originally observed intensities have thus been given, and appropriate notes at the end of the table call attention to unusual cases. In no case have intensities been averaged or altered in any manner. A comparison of intensities of unblended lines measured on more than one plate has shown that no serious discrepancies occur for lines whose intensities are less than 10.

The four grating plates which cover the region from λ 4984.58 to the end of the table were so homogeneous that the intensity estimates for this region probably are sensibly free of serious systematic errors.

TABLE 1

THE SPECTRUM OF ANTARES

λ	*i*	Identification	λ	*i*	Identification
**3600.77	6dcv	Y^+	3670.43..	12wn	$\underline{Ni}$ Mn
02.16		Co–Ni	71.67..	10	Ti
(05.1...	8h	$\underline{Cr}$ $\underline{Co}$ Fe	72.72..	2	Fe
(09.8...	20dc	Mn–Fe–Mn Ni	74.09..	15w	Ni
13.88..	15	Sc^+	74.74..	4	Zr^+
14.78..	10	Zr^+	75.59..	7v	$\underline{V}$ Ca
15.64..	8	Cr	76.17..	Wv	.....
(18.8...	15	Fe	Structure	.....	.....
(21.5...	3	Fe	(77.2...	4h	$\underline{Fe}$ Co BO
22.99..	Wv	.....	78.38..	Wr	.....
(24.4...	11h	(Fe Mn Zr Ca Ni $\underline{Co}$ Ti^+)	78.68..	BdRv	BO
			78.89..	6	Fe
25.26..	Wr	.....	79.92..	(35)W	Fe
26.11..	6	Ti	81.67..	0	Fe
27.86..	10	Co	82.18..	5	Fe
28.72..	8	Y^+	83.08..	15Wr	$\underline{Co}$–$\underline{\underline{Fe}}$ V Pb?
29.87..	4	Ni $\underline{Mn}$	84.17..	5wr	$\underline{\underline{Fe}}$ Yb^+?
(31.0...	17	Ca Sc^+ Co $\underline{Fe}$	84.79..	Wv	.....
33.04..	(50)wrv	Fe–Y^+	86.03..	8w	Fe
35.78..	Wr	Ni Ti Fe	88.44..	(40d)	Ni V
38.07..	(15)Wdc	Ti–Fe	(90.0...	3W	$\underline{Ti}$ Fe Co
39.61..	10wv	Co–Cr	91.28..	1	.....
40.41..	8	Fe	92.01..	Wv	.....
41.50..	20Wv	Ti^+, Ni	94.06..	15w	V–Co–$\underline{\underline{Fe}}$, $\underline{Ni}$
42.79..	25W	Sc^+ $\underline{Ti}$	94.93..	1	Fe
43.71..	8	Fe–Fe	95.80..	5	$\underline{V}$–V
44.23..	Wv	.....	96.65..	1h	Ni(p)? Zr^+?
(45.1...	9	$\underline{Ca}$ Fe	97.26..	Wv	.....
45.60..	Wr	.....	98.60..	2	Zr^+–$\underline{\underline{Fe}}$
46.18..	4	Ti	99.15..	3	Fe
47.76..	15Wn	Co, Fe	3701.01..	5n	Fe
49.25..	(13)wn	$\underline{\underline{Fe}}$ Cr	02.92..	1	Ti?
50.37..	5	Fe	03.34..	Wv	.....
51.63..	(20)Wn	Fe, Sc^+	(05.2...	15vd?	$\underline{\underline{Fe}}$ $\underline{V}$ Co
52.55..	10	Co	06.26..	Wr	.....
53.55..	25Wc	Ti	07.83..	(13)w	Fe
54.59..	8	Ti	09.28..	(12h)w	Fe
55.46..	3h	Fe	10.29..	(10)w	Y^+
56.23..	1	Fe, $\underline{Cr}$	11.35..	7	Fe–Fe
56.96..	5h	Co	12.91..	(7)	Cr^+
58.04..	10	Ti	13.79..	(9)W	Ti Ni
59.52..	7	$\underline{Fe}$ Ti?	14.82..	3	Zr^+–
60.62..	(8)v	Ti	16.49..	2	Fe
61.33..	6	Fe $\underline{Sa^+}$	17.38..	8	Ti
62.03..	10w	$\underline{Ni}$–$\underline{Co}$	19.83..	(35)RV	Fe
64.64..	10	$\underline{V^+}$ Fe $\underline{Ni}$	22.60..	(20)w	Ti Fe Ni
65.20..	1	Nd^+?	24.34..	4h	Fe
65.80..	Wv	.....	26.20..	3	$\odot$–Fe?
(66.5...	4	Sc^+ Fe	26.90..	2	Fe
67.36..	Wr	.....	27.54..	(15)RV	Fe
69.12..	(17)dwn	Fe $\underline{Ni}$ $\underline{\underline{Ti}}$			

TABLE 1—*Continued*

λ	*i*	Identification
3728.24..	0	V^+?
29.77..	(14)w	*Ti*
30.81..	(15)w	*Cr Ni Fe Co*
32.24..	(10)w	*Cr–Fe Co*
33.27..	2w	*Fe*
34.89..	2w	*Fe*
37.08..	2w	*Fe* Ca^+ *Ni*
39.25..	(15)	*Ni*
40.21..	1	*Fe*
41.06..	(20)	*Ti*
42.38..	2h	⊙–*Fe*
43.42..	(10)h	*Fe Fe Cr Cr*
45.77..	15W	*Fe Fe Co*
48.3...	(10)	*Fe*
49.5...	(15)	*Fe Ni Cr*
51.65..	1	*Co* Zr^+
52.72..	10w	*Ti Fe*
53.74..	(6)	*Ti Fe*
54.52..	(12)	*Fe*
55.96..	(10)	*Fe*
58.23..	(10)	*Fe*
59.16..	(10)	*Fe* La^+ *Ti*$^+$
59.93..	(10)	⊙ *Fe* V^+?
61.23..	(10)w	–Ti^+
63.85..	(15)wh	*Fe Zr*
65.50..	4h	*Fe*
67.2...	(13)	*Fe*
68.25..	(8)whr	*Cr Fe Cr*
70.51:.	Structure	Ti^+ *Fe* V^+?
71.66..	6	*Ti*
72.56..	6	*Ni*
73.45..	4	*Fe–Fe*
74.52..	12W	*Co* Y^+
75.56..	7	*Ni*
76.51..	6	*Fe*, Y^+
77.34..	4dw	⊙ *Fe Zr*
78.03..	10	*Ni*
78.69..	9	*V Fe*
79.48..	4	*Fe–Fe*
80.20..	Wv	.....
80.48..	8h	*Zr*
81.22..	7h	*Fe*
82.36..	1wh	*Fe Ti*
83.50..	15	*Ni*
84.65..	(2)h	⊙ *V*
85.88..	6h	*Fe CN*?
86.74..	6h	*Fe*
87.83..	6	*Fe*
88.63..	6	V^+
90.18..	12W	*Fe Mn V*

λ	*i*	Identification
3791.36..	3	*Cr Zr Fe*?
92.33..	5	*Ni Fe Cr*
93.60..	10	*Ni*
95.00..	6	*Fe V*
98.36..	10wh	*Ti Fe Cr*
99.65..	10wh	*Fe V*
3801.71	6Wdc	*Fe Fe*
01.98		*Fe Fe*
02.90..	1h	*Cb? CN*?
03.40..	1h	*V*
03.99..	1h	*Fe*
04.74..	2h	*Cr*
05.45..	2h	*Fe* Nd^+?
07.04..	14W	*Mn Fe–Ni–Fe*
08.32..	3w	*Cr–Co–V*
09.60..	4	*V Mn*
11.24..	4	*Ti Co Fe*?
11.92..	2	*Fe*
12.94..	13R	*Fe–V*
14.12:.	2	Fe^+? *Fe*
14.57..	5h	Ti^+ *Fe*
15.42..	Wv	.....
15.8...	15R	(*V Fe Co Cr Mn*)
17.54..	0	–Zr^+ *Ti*
** 18.29..	2	*V*, V^+–*Cr*
20.37..	15RV	*Fe Cr Fe*
Structure.	.....	*CN*
22.01..	2	*V*
24.46..	10rv	*Fe Mn Cr*
25.92..	8h	*Fe* Sa^+ *Cr*
27.78..	9h	*Fe*
28.55..	3	*V*
29.44..	11	*Mg*
** 30.72..	3Wcd?	*Fe Cr* Sa^+ BO
31.65..	7	*Ni* Sa^+
32.27..	5	*Mg*
32.92..	5	*Ni* Y^+ *Co Fe*
34.21..	10h	*Fe Mn*
Wide abs.	.....	(*Co Zr* Ti^+ Zr^+ *CN*)
38.33..	12	*Mg*
40.4...	10h	*Fe*
41.0...	10h	*Fe Mn Cr*
42.01..	5	*Co Cr*
43.07..	5	Sc^+ Zr^+ *Fe*
44.01..	1	*Mn*
44.48..	2	*V*
45.44..	6h	*Co Fe*
.....	−1	*Fe* BO
47.34..	1	*V* BO
49.96..	8	*Fe Cr*

TABLE 1—*Continued*

λ	*i*	Identification	λ	*i*	Identification
3850.83..	6	*Fe*	3908.73..	6	*Cr*
51.73..	0	*Nd*$^{+}$	09.87..	8	*V Fe Co*
52.27..	1	*Cr Fe*	11.02..	2h	*Fe Fe Ti*
53.71..	0	*Ti*	11.81..	4	*Sc*
54.26..	0	*Cr*	12.93..	4	*V, Ni*
55.30..	1	*–Cr–*	13.73..	3d	*Fe Ti*$^{+}$*–*
56.41..	18v	*Fe V Cr*	14.52..	4dw	*Ti Fe? Ti*
58.27..	6	*Ni Ti*	16.09..	4w	*Cr–Cr*
59.94..	20w	*Fe*	17.23..	4h	*Fe Cr*
61.23..	0h	*Co, Fe*	18.45..	3	*Fe Fe*
62.21..	0	*V*			
62.79..	0	*Ti*	19.16..	4	*Cr Fe*
63.36..	1	*CN Nd*$^{+}$	20.23..	16	*Fe*
64.06..	5h	*Fe Zr V*	22.91..	20	*Fe*
64.84..	2	*V*	24.54..	3	*Ti*
65.54..	5	*Fe*	25.89..	2h	*Fe Fe V*
67.70..	1Wh	*Ti V CN*	27.92..	15	*Fe*
Structure.	.....	*CN*	29.83..	Wv	.....
** 70.0...	0Wcd?	*CN*	**	10r	*Ti–V–Fe*
72.43..	10h	*Fe*	33.15..	Wv	.....
73.15..	10h	*Co Ti*	33.53..	30c	*Ca*$^{+}$
73.93..	9	*Co*	33.98..	Wr	.....
75.15..	6	*V Ti Sa*$^{+}$ *Cr*	35.17..	7hW	*–⊙–Fe*
76.00..	8	*Fe V*	36.82..	8hW	*–Fe–*
76.88..	8	*Co Zr*	39.1...	3H	.....
78.50..	30v	*Fe–Fe*	40.85..	1h	*Fe Co*
81.91..	7h	*Co CN*	41.74..	3hv	*Co Cr Fe*
83.26..	6h	*Cr Fe Fe*$^{+}$*? CN*	43.97..	10hrv	*Al Fe Dy*$^{+}$*?*
84.38..	3	*Fe Co?*	46.14..	2	*–Ni?*
85.21..	4	*Cr Zr Fe*	47.80..	4	*Ti*
86.3...	25	*Fe Cr*	48.68..	5	*Ti Fe*
87.0...	15	*Fe*	50.17..	6w	*Fe–Y*$^{+}$
88.48..	7r	*Fe–Fe*	51.16..	1	*Fe*
90.01..	6w	*Ni–Ti Ce*$^{+}$ *Sa*$^{+}$	52.22..	0	*Nd*$^{+}$*? Co Cr*
		V–Zr	52.97..	1w	*–Co Fe*
91.10..	5w	*Fe–Zr*	56.30..	5h	*Ti Fe*
91.90..	1h	*Fe*	57.08..	0	*Ca Fe?*
92.86..	2	*V*	58.07..	6h	*Co–Ti*
93.34..	2	*Fe Fe*	61.55..	8hv	*Al*
** 94.06..	7	*Co Cr Co*	62.81..	3h	*Ti*
95.68..	20rv	*Fe Ti*	Structure.	.....	.....
98.12..	7dw	*Fe–Fe–Ti*	68.00..	Wv	.....
99.73..	19	*Fe*	68.34..	50c	*Ca*$^{+}$
3900.97..	6v	*Ti*	68.79..	Wr	.....
02.23..	3	*V*	73.57..	4	*–Ni Ca*
02.99..	8	*Fe Cr Cr*	74.75..	3	*Co*
03.94..	2	*Fe*	76.52..	2h	*Fe Cr Fe*
04.76..	2	*Ti*	77.73..	3	*Fe*
05.56..	0	*Si*	78.65..	3	*Co Cr*
06.46..	18	*Fe Co Fe V*	79.54..	5	*Co*
07.50..	4	*Sc Fe*	81.76..	6	*Fe, Ti*

TABLE 1—*Continued*

λ	*i*	Identification
3982.44	6	*Ti*
83.96	ohR	*Fe Cr*
85.43	1	*Fe Ti?*
86.17	1	*Fe*
87.05	1rv	*Co Mg–*
89.77	8	*Ti*
91.11	1	*Zr^+, Cr*
91.76	2	*Co Cr*
92.82	0	*Cr, V*
93.96	0	*Cr*
94.63	1	*Ti Co*
95.33	1	*Co*
96.03:	2	*Fe*
96.61:	2	*Sc*
97.37	1	*Fe*
97.96	2	*Co Fe*
98.66	9r	*Ti*
99.39	3V	*Fe Ti*
4000.64	Wr	*Fe–Dy^+–Fe*
01.66	3V	*Fe*
01.88	Wr	.....
02.71	3V	*Fe Ti, V^+*
03.16	Wr	.....
03.88	3V	*Fe, Ti–⊙*
04.14	Wr	.....
05.22	15	*Fe*
06.56	0v	*Fe–Fe*
07.33	2	*Fe*
08.01	2	*Ti ⊙*
08.90	6	*Ti*
09.68	5	*Ti, Fe*
11.30	3hw	*Fe Ti*
12.42	3hw	*Ti^+ Ce^+ Cr Nd^+*
13.76	2hw	*Fe Ti Co*
14.54	2h	*Fe*
15.45	1	*Ti ⊙*
16.40	1	*Fe Ti*
17.11	0	*Fe Ti*
18.14	6v	*Mn Fe Ti?*
19.13	3h	*Fe Co*
20.34	2	*Sc ⊙*
20.84	2	*Nd^+ Co*
21.87	2wr	*Fe, Ti*
23.64	3v	*Sc V^+? Sa^+?*
24.42	Wv	.....
24.83	5dr	*Ti–Fe–Zr–Ti^+*
26.47	0	*Ti Mn Cr*
27.09	3	*Cr Co Zr*
28.63	0w	*–Fe Ti^+–*
29.58	Wv	.....
4030.74	7	*Mn Ti Fe*
31.82:	0h	*Mn Ti Fe*
33.00	12w	*Mn Fe Ti*
34.49	10	*Mn Ti*

Plate 1400[1]

λ	*i*	Identification
4035.61	10	*Co V^+*
* 35.76	5	*–Mn–*
35.92	10	*⊙, Ti*
36.39	5	*Fe*(p)
36.77	5	*V^+*
Structure	.....	.....
37.16	8	*⊙*
38.78	5	*Fe Fe*
39.33	4	*⊙ Cr*
39.81	8	*–V*
40.27	5	*Ti Fe*
40.73	9	*Ce^+ Nd^+ Fe*
41.43	20	*Mn Fe*
42.22	5h	*Cr*
42.68	10h	*Ce^+ –⊙?*
43.02	10	*⊙ Sa^+ La^+*
43.07	Wr	.....
43.39:	Wr	.....
43.58	15H	*⊙ Cr*
44.02	15H	*Ti–Fe, K? –Fe*
* 45.85	10	*Fe*
47.74	20H	*Y Sc Fe*
47.98	Wr	.....
48.69	11	*Zr^+ Mn Cr*
49.04	4	*Mn*
49.39	8	*Fe, Gd^+*
49.89	7h	*⊙ Gd^+*
50.46	10	*Zr^+ ⊙*
50.98	4	*V*
51.32	10	*V*
51.96	9	*Fe*
52.50	10	*Fe ⊙*
52.93	4	*Co Ti*
53.28	5	*Fe Gd^+*
53.55	6	*Ce^+*
53.81	5	*Ti^+*
54.53	7	*Sc Zr*
54.87	4	*Fe Fe*
55.13	4	*Zr Fe Ti*
55.60	11	*Mn*

TABLE 1—*Continued*

λ	*i*	Identification	λ	*i*	Identification
4056.17..	5	*Ti*+?	4077.90..	wh	*Sr*+ –*Dy*+
56.55..	5	*Pr*+? *Fe*?	78.25..	3	–*Zr Fe*
57.17..	10	*Co V*	78.56..	6r	*Ti*–
57.58..	8	*Mg*	78.76..	Wr	.....
57.89..	8	⊙ *Pb*?	79.21..	8	*Mn Fe*
58.26..	10	*Fe Co*	79.43..	4	*Mn*
58.74..	6	*Co–Fe Cr*	79.77..	8	*Ti Fe*
59.05..	6	*Mn*–	80.20..	5	*Fe*
59.36..	4h	*Mn* ⊙	80.51..	6	–*Ru*
59.65..	3	⊙ *Fe*	80.92..	5	*Fe*
59.96..	4h	*Nd*+?	81.24..	10	*Ce*+? *Zr*
60.22..	9rv	*Ti*	81.77..	3	*Cr*?
61.05..	8	*Nd*+	82.29..	12V	*Fe–Ti Sc*
61.59..	5n	⊙–*Mn*	82.97..	10	*Mn V*
61.98..	4nr?	*Fe*	83.67..	15	*Mn Fe*
62.42..	10s	*Fe*	84.47..	10	*Fe* ⊙
**	100W	*Fe Mn V*	84.80..	Wv	.....
64.21..	10N	*Ti*	84.96:.	9	–*Fe*
64.50..	10N	*Fe*	85.35..	8	*Fe Fe*(p)
64.66:.	Wr	.....	85.78..	9h	.....
65.09..	10	*Ti*	86.26..	10h	*Co Ni*?
65.52..	7	*Ti Fe*	86.69..	10h	*La*+
66.33..	12	⊙–*Co*	87.14..	7h	*Fe*
67.01..	5	*Fe Cr*	Structure.		*Fe*+? *Cr*+?
67.30..	11	*Fe*	87.87..	Wr	.....
67.52..	4	⊙	88.27..	6	*Co*?
67.96..	6	–*Fe*	88.51..	3	*Fe*
68.55..	2h	*Co*	Structure.		.....
68.90..	7	*Ce*+ *Ti*	89.19..	6	*Fe*
69.31..	8	*Nd*+	89.74..	2	.....
69.62..	2	⊙	90.00..	4	*Cr*+? *Fe*?
69.96..	2	*Ir*?–*Fe*	90.56..	8rv	*Zr*+, *V*
70.28..	9	• *Mn*	90.99..	5	*Fe*
70.79..	9	*Fe*	91.55..	5	*Fe*
71.18..	3n?	*Zr*+, ⊙	91.92..	3	*V*
71.54..	12n	*V Fe*(*K*)?	92.33..	9	*Fe V Co*
* 71.73..	9	*Fe*	92.71..	9	*V Ca*
72.67..	8	*Zr Fe*	93.14..	3	*Hf*? ⊙
73.10..	7	–*Dy*+–	93.58..	8	–*V*
73.49..	6	*Ce*+	94.02..	3h	.....
73.81..	8	*Gd*+ *Fe*	Structure.		.....
74.35..	5	*W*?	94.94..	7	*Ca*
74.78..	10	*Fe* ⊙	95.46..	8	*V*
75.22..	9	*Fe*(p)–*Nd*+	96.15..	12cd?	*Fe Fe*
75.79..	8h	*Ce*+ –*Sa*+	96.58..	1h?	–⊙?
76.21..	9h	*Fe Co*	96.84..	5	.....
Structure.		*Fe Fe*	97.17..	5	*Fe*–
76.87..	2	*Fe Fe*	97.65..	3	*Cr*
77.12..	3	*Cr Ti*	98.11..	7	*Cr Fe*
** 77.43..	wh	*V La*+	98.53..	7	*Ca*

TABLE 1—*Continued*

λ	*i*	Identification
4099.01	5	⊙
99.23	5	*Ti*–
99.76	10	*V*
4100.24	3	*Fe* –⊙
00.78	11d?	*Fe, Pr*$^{+}$ *Cb?*
01.26	3h	*Fe*
01.62	10h	*Fe H In?*
01.95	9h	–*V*
02.37	9h	*Y*
02.56	Wr	.....
02.91	4	*Si*
03.34	6	*Dy*$^{+}$
03.67	3	⊙
04.13	6	*Fe*
04.41	4	⊙
04.86	8	*Cr*
05.26	12	*V*–
05.39	Wr	.....
05.78	4	⊙
06.29	7	*Fe*
06.57	5	*Fe*–⊙
06.94	3	⊙
07.41	10	*Sa*$^{+}$ *Ce*$^{+}$ *V Fe*
07.84	4	.....
08.13	4	⊙
08.48	9	*Cr, Zr–Ca*
09.05	9	*Fe*
09.44	10	*Nd*$^{+}$
09.91	9	*V Fe*–⊙?
10.54	10	*Co*
10.81	4	⊙–*Cr*
11.36	3	*Cr*
11.82	11d?	*V Cr* ⊙
12.34	3H	*Fe V*
12.78	12	*Ti*–
13.51	6	*V*
13.81	4	⊙–
14.10	4	⊙
14.48	9	*Fe*
15.07	11	–*V*
15.45	10	*Ce*$^{+}$–
15.87	4	⊙
16.50	20	*V V*
16.91	5	*Fe*
17.25	0	.....
17.49	3	⊙
17.83	5	*Fe*
18.22	4	*V*
18.49	7	*Pr*$^{+}$ –*Sa*$^{+}$ *Fe*
18.81	8	*Co*
4119.48	7	⊙
19.84	3	*Ce*$^{+}$?
20.17	4h	*Fe Ti*
20.54	4	⊙ *Cr?*
20.83	3	*Ce*$^{+}$
21.29	10	*Co Zr*
21.86	7h	*Cr Fe*
22.17	3h	*Cr Ti*
22.58	7	*Fe*–
22.99	Wv	.....
23.61	35Wcd?	*Ti, V Fe Ti La*$^{+}$
24.12	Wr	.....
24.14:	1s	⊙ *V*
24.57	3	⊙–
24.87	6	*Y*$^{+}$
**Structure.	.....	.....
25.83	5	*Fe*
26.16	5	*Fe*
26.54	5s	*Cr*
26.90	4s	*Fe Cr*
27.52	12	*Ti*
28.16	25W	*V Y*
28.43	Wr	.....
28.69	Wv	.....
28.86	4	*Fe*$^{+}$–
29.17	3?	*Fe Cr*
29.69	12HRV	*Eu*$^{+}$
30.64	5h	*Ba*$^{+}$
31.11	4	*Ce*$^{+}$
31.31	3	*Ti, Cr*
32.00	18	*V Fe*
32.95	7	*Fe, Sc*
33.37	5	*Nd*$^{+}$
33.78	4	–*Fe*
34.20	10	⊙–*Fe*
34.54	11	*V Fe*
34.87	7	⊙
35.31	5	*Nd*$^{+}$?
35.75	5	⊙ *Os? Zr*
36.42	6	*V*–*V*
36.60	2?	*Fe*
37.04	8	*Fe*
37.36	3h	*Ti*, ⊙
37.67	2h	*Ce*$^{+}$
38.01	3h	*Fe*(p)
38.37	5	.....
38.82	4	*Fe*
39.17	2?	⊙–*V?*
39.50	6	*Co?*
39.93	12	*Fe*

TABLE 1—*Continued*

λ	*i*	Identification	λ	*i*	Identification
4140.43..	4	*Fe*	4162.32..	2	–⊙?
40.72..	4	⊙	62.65..	3	⊙
41.21..	6s	.....	63.00..	3	*CN*
41.73..	4	*La*$^+$ *Fe*?	63.62..	9	*Cr Ti*$^+$
41.96..	4	*Fe*–⊙	64.16..	6	*Ti*, *Pr*$^+$ *CN*
42.33..	6	*Ni*	64.68..	8	*Ni Cb*?
42.79..	8	*V Fe*?	65.33..	8hW	*Fe Sc Ce*$^+$
43.39..	7	*Fe*	65.62..	Wr	.....
43.71..	15	–*Fe*	65.73..	2	.....
** 44.04..	15	⊙	66.35..	5h	*Ti*
44.53..	3?	⊙ *Tb*$^+$?	66.78..	1?	⊙?
44.96..	3	*Ce*$^+$ *Ti*?	67.38..	8hwd?	*Mg V*
45.25..	7	*Fe*?	68.06..	7	*Cb*? *Fe*?
45.37..	Wr	.....	68.53..	4	–*Fe*?
45.70..	4	⊙?–⊙?	69.03..	6	*Fe*, *Fe*(p)
46.14..	7	*Fe*–*Ce*$^+$	69.39..	3h	*Ti Sa*$^+$
46.71..	5	⊙	69.82..	4	*Fe*?–
47.17..	3	⊙	70.10..	3	–⊙
47.66..	16	*Fe*	70.27..	Wr	.....
48.44..	4	⊙	70.50..	2h	–⊙
48.80..	3	*Mn*	70.96..	9	*Fe Ti*
49.23..	7	*Zr*$^+$	71.55..	1?	⊙
49.74..	9	*Fe*(p)	72.06..	10v	*Ti*$^+$, *Fe*–*Ga*?–*Fe*
49.99..	3	*Ce*$^+$	72.76..	10	*Fe*
50.32..	7	*Fe*–	73.27..	2	–*Fe*
51.00..	8	*Ti Zr*$^+$	73.57..	3	*Ti*$^+$? *Fe*$^+$?
51.36..	2	.....	73.99..	8dc	*Fe*–*Ti*$^+$ *V*
51.78..	Wv	.....	74.44..	0	.....
52.16..	20W	*Fe Sa*$^+$ *Sc*?	74.95..	10d?	*Fe Cr*–
52.63..	6	⊙ *Cb*?	75.64..	6	*Fe*
53.09..	3	*Cr*	75.96..	3	*Cr Fe*(p)
53.38..	4	*Fe*	76.62..	5wd?	–*Fe*–
53.89..	6	*Fe*	77.01..	0?	⊙–*Fe*
54.14..	3	*Fe*	77.32..	4	*Nd*$^+$ *Ti*
54.50..	6	*Fe*	77.58..	10	*V*$^+$, *Fe*
54.82..	5	*Fe*	78.50..	4nw	*V*$^+$–
55.57..	3h	.....	78.95..	0h	⊙?
56.11..	8d?	⊙	79.42..	9	*V Pr*$^+$
56.84..	9	*Fe*	79.88..	2	*Ti Zr*$^+$?
57.83..	7	*Fe*	80.42..	4h	*Fe*(p)
58.38..	3s	⊙	81.10..	4h	⊙?
58.81..	5	*Fe*	81.76..	10cd?	*Fe*
59.20..	2s	⊙	82.29..	2	.....
59.64..	6h	*Ti*	82.52..	8rv	*Fe*–*V*
60.19..	2	⊙	82.81..	2	*Fe*
60.34..	5hwcd?	⊙	83.30..	5	*Ti*
60.44..	3	.....	83.71..	3h	.....
61.17..	6	*Zr*$^+$ *Fe*?	83.97..	2h	⊙
61.54..	5	*Ti*$^+$ *Fe*	84.35..	8	*Ti*$^+$ *Lu*$^+$? *Gd*$^+$
61.95..	3h	*Sr*$^+$?–	84.49..	Wr	.....

TABLE 1—*Continued*

	λ	*i*	Identification
	4184.93	9r?	*Fe Cr*
	85.41	2h	⊙
	85.72	1s	*Ce*+?–
	86.10	9	*Ti*
	86.61	2	*Ce*+
	87.08	13RV	*Fe*
	87.79	13RV	*Fe Fe Zr*
	88.75	7	*Ti*–⊙
	88.95?	2	⊙
**	89.47	5h	–*Pr*+
	89.88	5	*V*
	90.25	2h	*Ti*+
	90.87	13	*V*+? *Co*–*Gd*+
	91.50	13Hw	*Fe, V*
	92.08	9h	*Cr*?
	92.50	3h	–⊙
	93.02:	4h	.....
	93.71	6h	⊙ *Cr*?
	93.90	Wr	.....
	94.91	10V	–*Cr*
	95.04	Wr	.....
	95.46	10hd?	*Fe*–*Fe*
	96.27	7	*Fe*–
	96.64	6	*La*+ *Fe*–*Fe*
	97.12	10	*Fe*(p)
	97.56	3	⊙?
	98.17	7	*Fe*
**	98.54	7	*Fe*
	99.16	10	*Fe*
	4200.02	18cd?	*Fe*
	00.83	9	*Ti Fe*
	01.44	6	*Zr*
	02.07	16wd?	*Fe*
	02.79	3	*Fe*
	03.03	4	*Ce*+–
	03.57	10	*Fe Cr*
	04.07	7	*La*+ *Fe*
	04.72	5	*Y*+
	05.05:	11	*Eu*+ *V*+
	05.31	2?	⊙?
	05.64	2h	*Fe*–
	06.07	1h	–*Sa*+
	06.71	20	*Fe Pr*+?
	07.12	6	*Fe*
	07.39	1	⊙
	07.84	0?	⊙
	08.28	6	–*Cr*?
	08.62	7	*Fe*
	08.98	8	*Zr*+
	09.41	2	*Cr*
	4209.82	9	*Cr, V*
	10.36	10	*Fe Fe*
	11.28	5	–*Cr*
	11.92	12	(*Os*?) *Zr*+ *Gd*+ *Ti*
**	12.58	Wv	.....
	12.71	3	*Cr*?
	13.08	5h	–⊙
	13.62	6s	*Fe*
	13.86	6	*Zr*
	14.37	2h	*CN*?
	14.68	4h	*CN*?
	Structure	.....	*CN*?
	15.19	Wv	.....
**	15.50	30	*Fe*–*Sr*+
	16.22	30w	*Fe Cr*
	16.47	Wr	.....
**	16.94	Wv	.....
	17.21	0	–*CH*?
	17.56	9s	*Fe La*+ *Cr*
	17.94	.....	.....
	18.33	0?	–*Zr*
	18.75	4	*V CH*
	18.84	Wr	.....
	19.40	15	*Fe*
	20.31	10h	–*Fe*
	20.74	3	*Sa*+–
	21.18	3	⊙ *Dy*+?
	21.61	2	*Cr*?
	21.99	Wv	.....
	22.16	13	*Fe*
	23.74	H	⊙
	24.20	(12)H	*Fe*
	25.32	(10)H	*Sa*+ *Pr*+ *Fe*
	26.73:	300RV	*Ca Fe*
	28.79	8H	*Fe*?–
	28.92	Wr	.....
	29.48	4	⊙–*Fe*
	29.80	12Hrv	*Fe*
	30.19	2h	–⊙
	30.51	5h	*Cr? Fe*(p)?
	31.05	4	*Ni*
	31.60	3	*Zr*+
	31.96	0	⊙
	32.40	8	*V Nd*+
	32.77	22	*Fe*
	33.58	9	*Fe*
	34.04	12	*V Co*
	34.58	7	*V Sa*+
	35.24	8	*Mn*
	35.74	6	*Y*+

TABLE 1—*Continued*

λ	i	Identification
4236.02..	12	*Fe Y*
36.64..	3	*V*
37.09..	15	*Fe*(p) *Fe*
37.84..	11wcd?	*Sa*$^+$–*Ti Ti–Fe*
38.35..	4	⊙–*La*$^+$
38.83..	8	*Fe Cr*
39.30..	5	*Zr*
39.81..	15	*Mn, Fe*
40.36..	5	*Zr Ca Fe*
40.74..	1h	*Cr*
41.16..	6	*Fe Zr*
41.66..	5	*Co–Zr*
42.04..	3	⊙? *Al H?*
42.68..	7	*Fe–Fe*
43.46..	6	⊙ *Fe*
43.85..	2	*Fe?–*
44.31..	0	⊙ *Mn*$^+$?
44.70..	2H	*Sa*$^+$ *Ni*$^+$?
45.28..	13	*Fe*
45.98..	6	⊙
46.79..	20	–*Sc*$^+$
47.46..	10	*Fe*
48.36..	12	*Fe–Fe*
48.61?.	4	⊙?–
49.09..	3	–*Ti*
49.52..	4	*CH*
50.08..	15	*Fe*
50.81..	25	*Fe*
51.70..	6	*Ti Gd*$^+$
52.30..	15	*Co*
Structure.	.....	.....
53.47?.	.....	*Gd*$^+$–⊙
54.36..	40WRVcd?	*Cr*
54.77..	Wr	.....
54.99?.	0h	*Fe*
55.24..	0?	*CH*
55.50..	3	*Fe Cr*
55.87..	5	*Fe CH?*
56.37..	6	⊙–*Sa*$^+$
56.83..	0	⊙
** 57.23..	1w	–*V*
57.68..	4	*Mn*
57.98..	Wv	.....
58.35..	50Wc	*Fe*
58.69..	Wr	.....
59.05..	3	*Fe*–⊙–⊙
59.34..	6	*V*
60.07..	4?	*Fe Fe*
60.51..	20Rv	*Fe*
60.95..	Wr	.....
4261.32..	2	–*Cr*
61.68..	3	*CH Ti*
62.17..	6r?	*Cr Gd*$^+$ *Ga*$^+$?
62.77..	2	*Sa*$^+$–
63.21..	10	*Ti Cr*
63.92..	0h	–⊙?
64.32..	8	*Fe*–⊙
64.81..	0	*Fe*–
65.22..	9	*Sa*$^+$–*Fe Ti*
65.90..	9r	*Mn*
66.18..	3	*Ti* ⊙
67.02..	10	*Fe*
67.31..	2h	*CH*?
68.01..	15	*Zr CH Ir?*
68.74..	9	*Fe V*
** 69.38..	3h	*Cr*$^+$–*La*$^+$
69.83..	2h	*V–Fe*(p)
70.20..	3h	*Ce*$^+$ *Ti*
70.59..	3h	⊙
71.12..	12	*Fe*
71.75..	25R	*Fe*
72.44..	8	*Ti*
72.76..	6	⊙?
73.38..	2h	*Ti CH*
73.76..	2h	*CH Fe*

Plate 654 III

4274.36..	Wv	.....
74.77..	30Wcd?	*Cr Ti*
75.21..	Wr	.....
75.64..	4	*La*$^+$
76.34..	Wv	.....
76.59..	8	*Ti–Fe Ti*
77.42..	7	*Zr*$^+$ *CH*
77.68..	Wr	.....
78.38..	6	*Ti Fe*–⊙ *Tb*$^+$?
78.86..	6	*V*$^+$ *Ti CH*
79.48..	Wv	.....
79.75..	6	*Sa*$^+$ *CH*
80.52..	2?	⊙ *Gd*$^+$ *Cr Sa*$^+$
81.32..	6	*Ti Mn*
81.58..	Wr	.....
82.07..	Wv	.....
82.39..	15	*Fe*
** 82.98..	10	*Ca*
83.27..	Wr	.....
83.65..	Wv	.....

TABLE 1—*Continued*

λ	*i*	Identification
4283.95	4	*Fe*(p)–*V Mn*?
84.60	4	*Nd*$^+$–*Ni CH*?
84.96	3	*CH Ti*
85.91	11	*Ti CH Co Fe Sa*$^+$
87.47	6hv	*Ti Na*?
88.03	7	–*Fe Ti*
88.74	Wv	.....
88.95	6	*Fe CH*–*Ti*
89.57	40Wc	*Ca*–*Cr Ti Ti*$^+$
90.27	Wr	.....
90.80	Wv	.....
91.01	7	*Ti CH*?
91.51	15	*Fe*
92.22	2?	*Fe*(p)–*Sa*$^+$–*Fe*(p)
92.72	2?	*Ti*–
94.13	15v	*Fe Ti*$^+$ *Cr*
94.83	7	*Zr Sc*$^+$
95.83	11	*Ti*–*La*$^+$ *V*
96.82	6	*Fe*$^+$–*Cr*
97.85	7	*V*–*V*
98.48	Wv	.....
98.74	14	*Ti*–*Ca Ti*
4300.52	10	*CH Ti Ti*$^+$
01.08	10	*Ti CH*?
01.30	Wr	.....
01.76	Wv	.....
02.55	17	*Ca Zr Ti*$^+$ *CH*?
03.52	15	*Nd*$^+$ *CH*
03.77	Wr	.....
04.26	Wv	.....
04.57	6	*Fe*? *CH*
05.95	18Wv	*Sc*$^+$–*Ti*–*V CH*
07.03	10h	*Ti*–*V CH*
07.97	12h	*Ca*–*Fe Ti*$^+$ *CH*
08.55	6h	*Ti CH Sa*$^+$
09.64	15	*Y*$^+$ *Fe V*
10.51	5w	*Ti*–*CH*–*CH*
11.56	5w	*Ti CH Ir*?
12.78	11v	*Ti*$^+$ *CH Mn*
13.82	Wv	.....
14.16	14	*Sc*$^+$–*Ti CH*
14.92	19	*Ti* –*Ti*$^+$ *Fe*
15.28	Wr	.....
15.96	0	–*Gd*$^+$
17.06	8W	⊙
18.07	1?	⊙

λ	*i*	Identification
Plate 1400[2]		
4318.70	12	*Ca Ti*
19.03	7	*Sa*$^+$–
19.54	5	*Fe*(p)–*Cr*
19.88	2	–⊙?
20.71	15	*Sc*$^+$ *Cr*
21.14	8	*Ti*$^+$–*Cr*
21.72	10	*Fe Ti*
22.12	2	⊙–
22.50	4	*La*$^+$
23.37	11	*Sa*$^+$ –*Fe*(p)–*Cr*
23.92	−1?	*CH*–⊙
24.28	−1?	⊙?–⊙?
24.57	−1?	⊙
24.95	10	*Fe Sc*$^+$ *Cr*
25.62	15s	*Fe*
** 25.92	10	
26.37	8	*Ti*
26.77	4	*Fe*
27.02	10	*Ti Fe*
27.89	11r	*Fe*–
28.98	9	*Sa*$^+$
29.46	8	⊙?–⊙?
30.00	12	*V*
30.69	9	–*Ni, Ti*$^+$–
30.93	2?	*Fe*
31.35	3	–⊙?
31.64	10	*Ni*
32.46	3	⊙?
32.77	22	–*V*
33.84	10	*La*$^+$–*Pr*$^+$
34.06	10	⊙ *Sa*$^+$
34.81	10	*Ti*
Structure?	.....	.....
36.26	4	⊙?
37.02	17cv?	*Fe*
37.50	10	–*Cr*
37.91	10	*Ti*$^+$
38.30	9	*Fe*
38.72	7	*Nd*$^+$? *CH*
39.37	12	–*Cr*
39.72	11	*Cr*
40.29	10	*H Cr*
** 40.58	10	
41.02	9	*V*
41.38	8	*Ti*$^+$
42.08	8	–*Gd*$^+$
42.48	0?	.....
43.17	9	*Cr Fe*
43.72	8	*Fe*–
44.47	30wcd?	*Cr Ti*$^+$

TABLE 1—*Continued*

λ	*i*	Identification
Structure?	.....	.....
4346.00..	8d?	*Sa⁺–Ti*
46.52..	6	*Ti Fe*
46.80..	3s	*Cr*
47.29..	25	*Fe–*
47.86..	8	*Fe Sa⁺–CH*
48.30..	0?	*CH–*
48.55..	0?	⊙?
48.95..	7	*Fe*
49.79..	5	*Ce⁺*
50.13..	0?	⊙
50.46..	4	*Sa⁺*
51.04..	15	*Cr*
51.80..	16wcd?	*Cr Fe⁺–Mg–Sa⁺ CH*
52.83..	13	*Fe–V*
54.05..	6	*Ti*
54.57..	7	*La⁺–Sc⁺*
55.07..	8	⊙–*Ca–Ti*
55.95..	10⁺	*V Ni*
56.77..	5h	*Cr*
57.51..	4h	*Cr*
58.15..	6s	*Nd⁺*
58.68..	10rv?	*Y⁺ Fe*
59.67..	15⁺	*CH Cr Zr⁺?*
60.51..	4	*Ti CH*
60.82..	5	*Fe, Zr Sa⁺*
61.13..	5	.....
61.96..	7	*–Sa⁺*
62.54..	2	⊙
63.09..	3	*Cr–CH*
63.48..	7	⊙ *V Sa⁺*
64.14..	5	*CH –CH*
64.66..	5	*Ce⁺ La⁺*
65.91..	5	*Fe*
66.38..	6	*Zr*
67.58..	4	*CH Fe Ti⁺?*
68.00..	7	*V Sa⁺ Fe*
68.32..	4	*Cr Ni*
68.63..	5	*Nd⁺*
68.96..	2	*Ti–*
69.33..	1?	*SiF*
69.78..	8	*Fe Ti*
70.39:.	0?	*SiF*
71.28..	15V	*–Cr–*
72.31..	5	⊙ *Ti SiF*
73.24..	6	*V Cr SiF*
73.52..	4	*Sa⁺ –Fe*
73.82..	4	*Ce⁺ SiF*
74.21..	2	*Cr–SiF*
74.47..	6	*Sc⁺ SiF*
4374.96..	7	*Sa⁺ V⁺ SiF*
75.39..	1	*Cr*
75.84..	15	*Fe SiF*
** 76.10..	15	
76.79..	4	*Fe SiF*
77.19..	2h	*SiF–SiF*
77.51..	1h	*Cr, SiF*
77.83..	4	*SiF Fe*
78.25..	3	*SiF Sa⁺*
79.23..	15	*V SiF*
79.75..	1	*Cr SiF?*
80.08..	2	*Co? SiF*
80.54..	4	⊙–
81.10..	5	*Cr*
81.78..	2h	⊙?
82.18..	3h	*Ce⁺*
Structure.	.....	.....
83.59..	22wc	*Fe–Fe–*
84.82..	16wcd?	*V–Sc⁺–Cr*
85.66..	6	⊙
86.70..	Wv	⊙*–Ti⁺*
86.78..	5	.....
87.13..	2h	*–V*
87.44..	3h	*Cr–Cr*
87.96..	7	*Fe–Ti*
88.47..	5	*Fe–*⊙?
89.23..	18	*Fe*
89.95..	10	*V*
90.48..	1	*Fe–*⊙
90.96..	9	*Fe Sa⁺ Ti⁺?*
91.73..	9	*Cr Ce⁺ Co*
92.08..	8	*V*
92.58..	3	*Fe*(p)
93.25..	6v	⊙
93.97..	9	*Ti–Ti⁺*
94.48..	2	⊙
94.92..	9	*Ti–Ti⁺*
95.23..	10	*V*
95.86..	5	*Ti⁺*
96.54..	−1h	⊙?
96.91..	−1	⊙
97.23..	2	⊙
98.00..	8	*V⁺*
98.25..	3	*–Ti⁺*
98.79..	3s	⊙
99.25..	3	⊙ *Ce⁺?*
99.76..	5	*Ti⁺*
4400.43..	9	*Sc⁺–V SiF*
00.75..	8	*–Ni?*
01.45..	8h	*Fe Ni*

TABLE 1—*Continued*

λ	*i*	Identification	λ	*i*	Identification
*4402.61	1	*–Co*	4425.95	10	*Ti–⊙–V Ti*
03.32	6H	*⊙–Zr⁺ Cr Sa⁺*	** 27.14	17	*Fe Ti*
03.60	3	*⊙–*	27.43	20	
* 04.08	Wv	.....	27.88	2	*Ti⁺*(p)
04.26	6	*Ti–Ti*	28.48	9	*Cr V*
04.70	14	*Fe*	29.20	8	*⊙ Pr⁺ Ce⁺*
05.12	12	*V, Fe*(p)–	29.84	10	*V–La⁺ Cr*
* 05.39	Wr	.....	30.59	12	*Fe*
05.69	4	*Ti*	31.36	9	*Sc⁺ Ti*
06.10	3	*V Fe*(p)?	32.16	5	*Cr*
06.62	11	*V*	32.59	2	*Fe–*
07.07	3	.....	32.92	2	*V?*
07.62	11	*V Fe*	33.25	5	*Fe*
08.08	10	*–V*	33.89	9	*Sa⁺ Ti Fe*
08.48	10	*V Fe*	34.34	4	*Sa⁺ ⊙*
08.79	3	*Pr⁺*	* 34.74	Wv	.....
09.20	2?	*Ti⁺?*	34.95	15	*Ca*
09.44	8	*Sa⁺–Ti⁺*	** 35.23	15	*Fe*
10.16	4	*⊙–Cr?*	35.63	10	*Ca, Eu⁺*
10.62	5	*Ni–*	36.18	10hd?	*V–Mn*
11.06	7	*Nd⁺ Ti⁺ Cr*	36.62	4	*Ti–Ti*
** 12.01	10	*Mn? Ti⁺ –V*	36.92	4	*Fe Ni*
12.31	11	*Cr–Ti*	* 37.14	Wr	.....
* 12.75	2	*⊙?*	* 37.57	Wv	.....
13.12	3	*⊙?*	37.82	10	*V*
13.71	4	*⊙–Cr*	38.28	4h	*Ti–Fe*
14.09	2	*⊙*	39.03	4	*⊙*
14.42	2	*⊙*	39.81	7	*Fe–Fe*
15.11	20rv	*Fe Mn*	40.35	8	*Ti Fe Zr⁺*
15.52	10wH	*Sc⁺*	40.86:	3	*Fe–Fe*
* 15.83	Wr	.....	41.21	3	*⊙–Ti*
16.48	10	*V Ti*	41.67	9	*V*
16.85	3	*Fe–*	42.35	11	*Fe*
17.28	9	*Ti*	42.86	4	*Fe*
17.69	10	*Ti⁺*	43.20	6	*Fe*
18.34	9	*Ti⁺ Fe*	* 43.65	Wv	.....
18.70	3	*Ce⁺*	43.79	6	*Ti⁺*
18.96	3	*⊙–Gd⁺*	44.21	7	*V Sa⁺*
19.89	10	*V Mn⁺*	44.57	5	*Ti⁺–*
20.53	10	*Os? Zr Sa⁺–Sc⁺*	* 44.79	Wr	.....
21.18	2	*Sa⁺ Co?*	45.48	17	*Fe*
21.55	11	*V Ti?*	46.39	8	*Nd⁺*
21.87	1	*Ti–Ti⁺*	46.81	3	*Fe*
22.54	8	*Fe V⁺*	47.10	8	*Fe*
22.78	8	*Ti*	47.75	10	*Fe*
23.17	6	*Fe–V–Cr*	49.14	9	*Ti*
23.77	2	*Fe*	49.73	8	*?Dy⁺ Pr⁺ V*
24.28	3h	*Cr Sa⁺*	50.41	8	*Ti⁺ Fe*
24.49	3h	*Ti–V*	50.84	8	*Ti Ce⁺*
25.43	8	*Ca*	51.58	7	*Mn Nd⁺*

TABLE 1—*Continued*

	λ	*i*	Identification
	4452.00	7	*V Nd*$^+$
	52.73	6	*Sa*$^+$ ⊙
	53.00:?	.....	*Mn*
	53.27	8	*Ti*
	53.70	7	*Ti*
	54.38	5	*Fe*
	54.76	11	*Ca Zr*$^+$? *Sa*$^+$
	55.30	6	*Mn, Ti Fe?*
	55.86	9	*Ca Mn*
	56.32	2h	*Fe*
	56.61	3h	*Ca*
	57.00	1	*Mn*
	57.42	10	*Ti V Mn*
	58.19	3h	*Fe–Mn*
	58.50	3h	*Sa*$^+$ *Cr*
	59.15	10d?	*Ni–Fe–Cr*
	59.74	5	*V Cr*
	60.29	8	*V Mn Ce*$^+$ *Cr?*
*	60.94	Wv	.....
	61.10	2	*Mn Fe Zr*$^+$?
	61.60	20w	*Fe*
	62.10	15	*Fe Mn–*
	62.41	2	*V–Ni*
	62.48	Wr	.....
	63.01	5	*Nd*$^+$–
	63.44	6	*Ti Ni?–Ti*
	64.31	Wv	.....
**	64.43	4h	*Ti*$^+$
	64.75	4h	*Fe Mn Cr*
	65.05	3h	*Cr–Cr*
	Structure	.....	.....
	65.78	6	*Ti*
	66.60	30w	*Fe*
	67.43	5h	*Sa*$^+$*–Cr*
	67.96	4	*V*
	68.53	9	*Ti*$^+$ *V*
	69.29	6h	*Fe Ti*$^+$
	69.65	5h	*V Co*
	70.13	4	*Mn*
	70.48	4	*Ni*
	70.86	6	*Ti*$^+$
	71.28	7	*Ti, Ce*$^+$–
	71.68	14	*Fe ZrO*
**	71.90	BdVr?	.....
	72.37:	Wv	.....
	72.71	10Wchd?	*Fe Mn Sa*$^+$ *ZrO*
	73.12:	Wr	.....
	73.92	5h	*ZrO V* ⊙
	74.78	7	*V–Ti*
	75.21	2	*ZrO–Cr*(p) *Cr*

	λ	*i*	Identification
	4475.53	2	*Ti ZrO*
	76.02	8	*Fe–Fe*
	76.55	0	*–Ti*
	77.07	2h	*Cr ZrO?*
	77.99	3	⊙ *ZrO*
	78.59	2h	⊙ *Sa*$^+$
	79.33	2	*–Mn*
	79.65	5	*ZrO Fe*
	80.13	4	*Fe*
	80.58	3	*Ti Ni ZrO*
	81.24	6	*Ti*
	81.58	0?	*Fe*
	82.19	25d?	*Fe–Fe*
	82.73:	6	*Ti Fe–Cr ZrO*
*	82.94	Wr	.....
**	83.38	−1	.....
	83.84	2s	⊙*–Ce*$^+$ *Co*
	84.21	3s	*Fe W?*
	84.50	2s	*Co*
**	84.76	−1	⊙?
	85.08	1	*Ti?–*
	85.65	3	*Fe*
	85.98	1	*Cr*(p)?
	86.68	Wv	.....
	86.88	3	*Ce*$^+$
	87.47	0?	*V*
	87.74	0?	⊙
	88.18	4h	*Fe Cr–*
	87.99	6	*V Fe–Ti*
	89.76	20	*Fe*
	90.07	7	*Fe Mn*
	90.71	5	*Ni–Fe V*
	91.61	7h	*Mn Cr*
	92.47	7h	*Cr–Ti*
	93.46	4	*Cr*(p)*–Ti*$^+$
	94.11	3	*Fe*(p)*–*⊙
	94.58	10	*Fe*
	94.94?	0	*–Ti*
	95.45	3	*Fe–Fe*
	96.20	12	*Ti–Ti, ZrO*
	96.85	11	*Cr V*
	97.72	4	*Na Ti*
	98.82	5h	*Cr–Mn*
	99.47	2	*Sa*$^+$
	4500.29	3	*Cr*
*	01.05	Wv	.....
	01.26	7	*Ti*$^+$
	01.84	5	*Cr–Nd*$^+$*–V*
	02.20	3	*Mn*
	02.62	1?	*Fe–*

TABLE 1—*Continued*

λ	*i*	Identification
4503.24..	o?	.....
03.76..	3	*Ti*
04.85..	4h	*Fe*
05.78..	1	⊙
Structure.	.....	*–Y–*
06.25:.	1	*–Ni Ti*
06.63..	3h	*Ca Ti*⁺(p)
07.13..	4h	*Zr Ca*
07.88..	1h	*Ca Ti?*
08.23..	1h	*Fe*⁺
08.72..	1h	⊙?–
09.31..	2h	⊙*Ca*
09.71..	o	⊙
10.16..	3h	*Pr*⁺
10.84..	1h	*Fe*(p)
11.22..	1h	*ZrO Ti In?*
11.85..	3	*Cr*
12.31:.	o	*Ca*
12.71..	10	*Ti*
13.32..	1h	⊙?
13.66..	1h	*Ti Fe*(p)?
14.18..	2h	*Fe V*
14.47..	2h	*–Cr*
15.15:.	2h	*Fe Sa*⁺
15.50..	2h	*Cr–Ti*
** 16.33..	2	.....
16.55..	o	⊙?–⊙?
17.09..	1	*–Co*
17.52..	2	*Fe*
17.99..	9	*Ti*
18.30..	2	⊙
18.64..	4	*Cr*(p)–*Ti*
19.53..	3	*Sa*⁺
20.05..	5hr?	*Ni Fe*⁺
21.17..	1h	*Cr*
21.98..	1h	⊙
22.76..	17rv	*Ti Fe*⁺ *Eu*⁺
23.44..	2	*Fe*
23.93..	2	*Sa*⁺
24.15..	2	*–V*
24.70..	2	*Ti*⁺
25.14..	5	*Fe Ba*⁺
25.91..	2hd?	*Fe–Cr La*⁺
26.44..	6	*Ti Cr Fe*
26.88..	2	*Ca*
27.33..	9	*Ti Cr V*
27.90:.	o?	*Fe Y? V*
28.63..	17	*Fe*
29.61..	6wc	*Fe–Fe–Cr*
30.71..	3	*Cr–Cr*
4531.11..	10	*Fe Co*
31.63..	2	*Fe*
33.22..	15	*Ti*
34.00..	8	*Ti*⁺
34.75..	14	*Ti*
35.55..	14	*Ti*
35.99..	17	*Ti–Ti*
36.54..	o	*Cr?–*
37.17..	o	*Ti*
37.65..	2h	*Fe*
37.93..	2h	*Ti?–Sa*⁺
38.72..	3h	*Fe*(p)–*Fe*
39.81..	3h	*Cr Ce*⁺ *V*
40.37..	Wv	.....
40.49..	8	*Ti Cr*
**Structure?	.....	*Ti? Cr?*
* 41.37..	4h	*V? Fe*⁺
41.71..	Wr	.....
42.14..	3	*Sa*⁺*–Zr*
42.56..	3	*Cr Fe*
43.87..	5	*Co–Sa*⁺ *Ti*⁺
44.67..	9	*Ti Cr*
45.27..	5	*Ti*⁺*–Cr V*
45.94..	9	*Cr*
46.98..	8	*Ni–Fe*
47.83..	3	*Ti Fe*
48.06..	o	*Ti*
48.75..	9	*Ti*
*** 49.34..	2	*–Fe*⁺
49.65..	10d?	*Ti*⁺
50.36..	o?	⊙?
50.79..	1	*Fe*
51.26..	1	*Ni* ⊙

λ = Mean of 1400², 9378, 12¹
Intensity from 1400²

λ	*i*	Identification
4551.72..	o	*Fe*(p)*–V*
52.44..	10	*Ti*
53.03..	2	*Zr, V*
** 54.01..	10	*Ba*⁺
54.41..	4	*–Fe Ru*
*** 54.50..	Wr	.....
55.48..	6	*Ti*
56.12..	4	*Fe*
56.85..	3	*–Fe*
57.42..	–1	.....

TABLE 1—*Continued*

	λ	*i*	Identification
	4558.08..	2	*Ti Fe*
	58.56..	2	*La*$^+$*–Cr*$^+$
	Structure.	.....	.....
*	59.30..	0	*La*$^+$
	59.80..	BdRv?	.....
	60.04..	3	*Ti Ni–Fe*
	60.44..	2	*Sa*$^+$ ⊙?
	60.75..	1	*V*
	61.48..	Wr	.....
	62.59..	10v?	*Ti Ce*$^+$
	63.32..	3	*Cr–Ti*
	63.78..	5	*Ti*$^+$
	64.20..	2h	*Ti Cr?*
	64.75..	3	*Fe–Fe*
	65.56..	10	*Cr–Co Fe*
	66.20:.	0	⊙?
	66.61..	1h	*Fe–Fe*
	66.99..	1h	*Fe*
	67.61..	1	.....
	68.33..	1	*Ti*$^+$
	68.80..	3	*Fe–Fe*
	69.60..	2	*Cr*
	70.42..	1	*V*
***	70.76..	BdRv?	.....
	71.10..	10	*Mg*
	71.96..	9wh	*Ti*$^+$ *V Cr*
	72.27..	2	*Ce*$^+$
	72.99..	4hw	⊙–⊙
	73.80:.	0?	⊙?
	74.24..	3	*Fe*
	74.81..	8	*Fe–La*$^+$
	75.52..	8	*Zr* ⊙
	76.42..	2	*Fe*$^+$*–Ti*(p)
	77.17..	9	*V*
	77.74..	2	*–Sa*$^+$
	78.68..	5	*Ca–V*
	79.32..	3	*Fe*
	80.03..	7	*Cr La*$^+$ *Co?*

λ = Mean of 1400², 9378, 12²
Intensity from 1400²

	λ	*i*	Identification
	4580.39..	10	*V*
	81.48..	5	*Fe Ca*
	82.21..	BdRv?	.....
	82.44..	3	⊙
	82.89..	2	*Fe*$^+$(p)
	83.41..	2	*Ti*$^+$
	83.81..	4	*Fe*$^+$
	84.38:.	1	*Ru*
	84.83..	4	*Fe Fe*
****	85.68..	Wv	.....
	4585.92..	5	*Ca–*⊙
	86.35..	10	*V* ⊙
	86.59..	Wr	.....
	87.06..	4	*Ti*(p)? ⊙*–Fe*
	87.78:.	0?	⊙
	88.30:.	0?	*Cr*$^+$*–*
	88.73..	3	⊙ *Co*
	89.32..	2	*Dy*$^+$
	89.96..	4	*Ti*$^+$
*	90.30..	0	⊙?
	90.65..	2	*Cr? Zr* ⊙
	91.39..	6	*Cr V?*
	92.66..	8	*Fe Ni*
	93.56..	1	*Sa*$^+$
	94.11..	12r	*V*
	95.38..	3	*Fe*
	96.02..	3	*Fe Ni*
	96.50..	1	*Fe*(p)–⊙
	97.08..	4	*Fe*(p)*–*
	97.76..	1	⊙
	98.23..	4	*Fe–Fe*(p)
	Structure.	.....	.....
****	99.01..	5W	*–Ti*(p)*–*
*	99.23..	0	*Ti*
****	99.68..	BdRv	.....
	4600.13..	1	*Cr–*
	00.79..	10r	*Cr*
	02.02..	4	*Fe*
	02.97..	10	*Fe*
	Structure.	.....	.....
****	03.83..	BdRv	⊙?
	03.87:.	0	⊙
	04.24..	2	⊙ *Sa*$^+$
	04.51..	1	*Zr–Fe*
	05.02..	4	*Ni* ⊙
	05.58..	0	⊙
	06.18..	6	*V–Ni*
	06.49..	0	*Sa*$^+$
	06.76..	1	*Cb?*
	07.34..	5	*Sr*
	4607.65..	3	*Fe*
****	08.78..	1	⊙*–*
	Structure	.....	.....
	09.28..	1	*Ti*$^+$(p) *Ti*
	10.02..	0h	⊙?
	11.25..	8	*Fe*
	12.07..	1h	*Cr–*⊙
	12.54..	1h	BO
	13.33..	9	*Cr La*$^+$ *Fe*
	14.16..	2h	*Zr*$^+$*–Fe*

TABLE 1—*Continued*

λ	*i*	Identification
4615.65..	2h	*Fe*–⊙
16.13..	7	*Cr*
17.28..	6	*Ti*
18.01..	−1?	*Ni*?–
18.78..	3	*Fe*–*V Cr*+?
19.31..	2	*Fe Ti Cr*
19.71..	7	*V*–*V*
Structure	.....	.....
20.37..	−1	*Ni*
21.92..	3	*Cr*–*Cr ZrO*
22.58..	0h	BO *Cr*
23.08..	5	*Ti*
24.40..	3	*V*
25.05..	3	*Fe*
***** 26.25..	12h	*Cr Zr V Mn* BO *ZrO*
27.55..	2	*ZrO*
28.20..	3	*ZrO Ce*+
28.86..	5nv	*ZrO Pr*+?
29.37..	8h	*Ti ZrO Fe*+
30.11..	9	*Fe ZrO*
32.21..	1h	BO
32.94..	18	*Fe*
33.98..	14	*Zr Cr*+ *ZrO*
34.75..	3	*Fe ZrO Ti*
35.20..	10	*V ZrO*
35.81..	5v	*ZrO Fe*
36.35..	3	*ZrO*
37.53 } 37.94 }	25W	*Fe* / *Ti*–*Fe*
38.62..	1	*ZrO*
** 39.22..	Wv }	*Ti*–*Ti*–*ZrO*–*Ti V*
40.11..	Wr } 25	
40.82..	10W	*ZrO V*
41.37..	3W	*ZrO*
42.26..	9r	*ZrO Sa*+
43.58..	19Wv	*ZrO Fe V*
45.23..	9	*ZrO Ti La*+
46.14..	30Wr	*Cr V Sa*+
47.41..	10h	*Fe La*+
48.12..	4h	*Cr ZrO Sa*+
48.78..	9vc	*Ni*–*Cr*
49.43?.	1	*Cr ZrO*
49.98..	9whrv	*Ti Fe ZrO*
51.32..	19	*Cr*
52.19..	20r	*Cr*–
53.47..	7	*Fe*(p)
54.51..	22Wc	*Fe ZrO*
55.82..	5Wc	*Ti ZrO*
56.45..	30v	*Ti*
57.40..	8Wc	*Ti*+–*ZrO Fe*

λ	*i*	Identification
4658.30..	3h	*ZrO Fe*(K)?
59.46..	3	*Zr*
59.92..	2v	–*ZrO*
60.47:.	1	*ZrO*
60.89:.	1	*ZrO*
61.39..	2	*ZrO Fe*?
61.98..	5	*Fe Eu*+?
62.66..	4h	*La*+–*Ti*+
63.34..	5	*Cr Co*
63.86..	5	*Cr La*+
64.73..	6h	*Cr Na*
65.86..	Wv	.....
67.55..	20W	*ZrO Fe V*–*Ti*
68.33..	10wc	*Fe*–*Ti*–*Na*
69.42..	11W	*Cr Sa*+ *Fe*–*Sa*+
70.47..	14	*ZrO Sc*+–*V*
72.16..	8WV	–⊙
73.04..	8Wc	*Fe*(p)–*Fe*(p)
74.27..	2h	*ZrO* ⊙
74.51..	Wv	.....
74.91..	19Wrvc	*Y Fe Sa*+ *Ti*
75.32..	Wr	.....
76.37..	2	⊙
76.92..	5h	*Ti Sa*+
77.37:.	2h	–*Ti*
77.53:.	2h	*Ti*?
78.13..	0	⊙
78.87..	7	*Fe*
79.13..	4	–*Fe*?
79.70..	0	*Ti*(p)
80.38..	10	*Fe*–*Cr*
80.78..	5	⊙
81.90..	35WR	*Ti Fe*
83.31:.	BdRv?	.....
83.53..	6	*Fe*
84.41..	5hw	⊙–*Ti*
85.16..	6w	⊙ *Ca*
86.02..	7W	*Ge*?–*Ni Ti*
87.26..	10	*Sa*+–*Fe*(p)
87.75..	8	*Zr*
88.46..	9	*Zr*
89.45..	6	*Cr*, *Fe*
90.28..	5w	*Fe*–*Fe*(p)
90.78..	4	*Ti*
91.36..	13	*Ti Fe*
92.48..	5w	*Ti*(p)?, *La*+
93.68..	15	*Ti Sa*+
95.02..	6w	*Fe*(K)–*Cr*
95.90..	2	*ZrO*
97.02..	7	*Ti*–*Cr*

***** Plate 12[2] begins with λ 4627.55.

TABLE 1—*Continued*

λ	*i*	Identification
4698.67..	25	*Cr–Ti*
99.27..	5r	⊙
4700.41..	7w	*Fe–Fe*(p)*–Cr*
01.24..	6dw	*Fe Mn–Ni*
02.98..	9	*Mg*
03.72..	6w	⊙*–Ni*
04.41..	5	Sa^+
04.97..	5	*Fe*
05.46..	3	*Fe*
06.14..	4	*Cr*?, *V*
06.54..	6	Nd^+ *V*
07.40..	11	*Fe–Fe*
08.03..	5h	*Cr*
08.87..	9dw	Ti^+*–Fe*? *Ti*?*–Fe*
09.70..	6	*Mn*
10.13..	20hw	*Zr Ti Fe*
11.62?.	2	*Fe*? BO?
12.05..	4hv	*–Fe*
13.05..	3hw	Sa^+
14.28..	9wvc	*TiO Ni*
15.28..	22r	Sa^+ *Ti TiO*?*–Ni*
16.51..	1h	⊙
17.08..	2h	.....
17.69..	7r	*V* Sa^+
18.42..	7	*Cr* Sa^+
19.80..	5V	$-Sa^+$
21.02..	5r	*Fe–*
21.46..	3	*–V*
22.63..	8	*Ti*
23.15..	10	*Ti Cr*
24.44..	5h	. *Cr–*
25.13..	2	Ce^+?
26.15..	6w	*Fe* Sa^+
26.86..	Wv	.....
27.38..	10	*Cr–Fe Mn*
27.93..	9	*Co*
28.53..	8	*Fe Co*
29.19..	4	*Sc*
29.81..	4w	*Fe–Mg*
30.67..	Wv	.....
30.71..	3	*Cr*
31.86..	Wv	.....
32.21..	8w	*Co–Zr* C_2?
33.56..	17R	C_2 *Ti–Fe*
34.10..	4	*Fe Sc* C_2
34.68..	4	*Ti*
36.02..	6w	C_2 *Fe*
36.81..	9	*Fe* C_2
37.56..	12wv	*Cr–Sc*
39.32..	11wv	*Mn–Zr*
4740.34..	8	*Fe* ⊙ La^+
41.01..	5	*Sc*
41.58..	7	*Fe*
42.04..	7w	*Sr–Ti*
42.80..	9	*Ti*
43.77..	7	*Sc*
** 44.91..	20Wdc	BO *Fe Cr*
45.75..	9	Sa^+*–Fe*
47.18..	7	*Ti* BO
Structure.	.....	.....
48.08..	1	BO *Na* ⊙
49.63..	9hwr	*–Co–*
51.05..	3	*V–Fe*
51.82..	3h	*–Na Cr*
52.47..	3	*Ni*
53.19..	5	*Sc*
54.05..	13	*Mn*
54.75..	1	*Cr Ni*
56.12..	5	*Cr*
56.52..	5	*Ni*
57.83..	15Wc	*V–Fe–Ti*
59.05..	17Wc	*Ti–Ti*
59.92..	5dWc	*–Cr*?*–*
60.99..	5	*V*
61.52..	6v	*Mn*
62.55..	15Wdc	*Mn–Ni*
63.85..	5	*–Ni*
64.52..	4	*Cr–*Ti^+?*–Cr*
65.48..	5	*Fe*
65.81:.	4	*Mn*
66.53..	6dW	*Ti Mn–V Cr*
68.34..	8WRc	*Fe Ti*
70.89..	Wv	.....
71.09..	5	*Ti Co*
71.60..	5	⊙*–Fe*
72.22..	5r	*Zr*
72.86..	8	*Fe Ni*
74.00..	2	⊙
74.60..	0w	*Cr–*
75.38..	1w	.....
76.29..	8w	*Fe–Co V*
77.78..	5	$-Sa^+$
78.27..	4	*Ti*
79.38..	6	*Sc Fe*
80.02..	5	*Co*
80.87..	1h	⊙?
81.67..	10	*Ti*
82.44: 82.62 82.84	3w	*MgH*? BO?

TABLE 1—*Continued*

λ	*i*	Identification	λ	*i*	Identification
4783.41..	12	*Mn Ti*	4820.42..	10	*Ti*
83.85..	4	⊙? *MgH?*	21.34..	2W	*Ti?*–⊙
84.48..	5	*V*	23.47..	14	*Mn*
84.98..	5	*Zr*	24.27..	7	*Zr*
86.66..	30WdV	*V Ni* V^+–*Fe V*	25.50..	7	*Ti* Nd^+
87.06..	Wr	.....	27.45..	12	*V ZrO*
87.73..	6	–*Fe*	Structure.....		*Zr*
88.74..	5	*Fe*	28.92..	2	–*MgH*–
89.57..	20W	Sa^+ *Fe Cr*	29.35..	10w	*Cr* Sa^+ *Ni*
89.75..	Wv	.....	30.64..	0?	–*ZrO*
91.34..	7W	*Fe–Sc*	31.61..	11	*V*
92.22..	Wv	.....	32.40..	14r	*V Sr*
92.45..	8r	*Ti Cr*	33.31..	0	–*ZrO*
94.20..	5W	*MgH–Fe*(p)? Sa^+	34.52..	5	*Fe* Sa^+
96.32..	7	*Ti–Co*	36.02..	9	*Fe–Ti*
97.00..	6	*V* Nd^+?	36.96..	1w	*MgH ZrO Cr*
98.66..	10v	*Ti*–Ti^+*Fe*	38.61..	3w	*Ni Fe*
99.42..	2	*Fe MgH?*	39.56..	4	–*Fe*–*V*
99.77..	10	*V Ti*	40.28..	4	*Co Fe*
4800.86..	8w	*Fe–Fe Cr*	40.86..	10	*Ti ZrO*
01.92..	4	⊙	41.77..	2	*Fe*(K)?
02.93..	4	*Fe*	43.24..	8h	*AlO Fe*
03.81:.	Wv	*TiO*	44.15..	8h*AlO*	*Fe Ti*–Sa^+
** 03.90:.	3HW	*TiO*	45.63..	2wh	*Fe V*
04.56..	0	*Fe*	46.39..	2w	⊙?
04.92..	Wv	.....	47.28..	2w	*Ca Zr* ⊙
05.21..	6w	Ti^+–*Ti TiO*	48.41..	6	⊙ *Ti*
05.52..	Wr	.....	48.96..	7	*Fe*
05.87..	1	*Zr*	51.41..	15	*Zr–V*
06.32..	0w	Ti^+ *Cr*	52.54..	3	–*Ni?*
06.91..	1w	–*Ni*	54.66..	Wv	.....
07.57..	1w	*V Fe*	55.41..	20Wc	*Ni Fe ZrO Ti*
09.00:.	2w	La^+ *TiO*	56.18..	Wr	.....
Structure.....		.....	57.36..	4	*Ni*
09.38..	Wr	.....	58.12..	4	⊙?
09.95..	1	*Fe*	59.03..	5	Nd^+ *Fe*
09.48..	Wv	.....	59.76..	7	*Fe Y*
10.61..	3h	*Zn–Cr*	60.71..	Wv	.....
11.33..	4h	Nd^+	61.34..	100Wc	*H Cr*
12.21..	3w	*Ti Sr*	62.15..	Wr	.....
13.99..	3	*Ti–Fe*	62.60..	2d	*V?*
13.52..	2	*Co*	63.66..	5	*Fe*
14.33..	3	*Cr*	64.72..	10	*V*
15.07..	4	*Zr*	65.44..	Wv	.....
15.78..	8wc	Sa^+ *Zr Ni*	65.62..	3	–Ti^+(p)
16.47..	4	⊙ *MgH?*	66.20..	5	*Zr–Ni*
17.23..	2s	.....	66.73..	3	Nd^+
17.88..	6	*Fe*–	67.72..	6	*ZrO Co*
18.97..	3	*Ti? V?*	68.27:.	7	*Ti*
19.67..	2	–*MgH*	69.33..	2W	*Ru?*–⊙

TABLE 1—*Continued*

λ	i	Identification	λ	i	Identification
4870.09..	4	*Ti*	4922.20..	5	*–Cr*
70.83..	1w?	*Ni Cr ZrO*	.....	0w	.....
71.30..	11w	*Fe V*	23.99..	6	*Fe+–*
72.12..	10	*Fe*	24.74..	7	*Fe*
** 73.16..	Wv	.....	25.51..	6	*Ti-Ni*
75.44..	15R	*V Fe*(K)	26.11..	5	*–Ti*
78.16..	12r	*Ca Fe*	27.21..	Wv	.....
80.34..	5w	*–⊙–V*	27.86..	13Wc	*–Fe–*
81.52..	25	*Zr–V–Fe*	28.31..	5	*Ti*
82.22..	5	*Fe–Ti*	28.51..	Wr	.....
82.79..	1	*Co–*	28.93..	0	*Ti*
83.74..	8	*ZrO V+*	30.27..	4	*Fe*
84.84..	Wv	.....	30.78..	3h	*Ni?*
85.03..	8	*Ti*	31.95..	4r	*–V*
Structure.	.....	*Fe–Cr–Fe*	33.30..	5h	*Fe*
87.03..	8	*Cr Ni Fe*(K)	** 34.08..	50	*Ba+ Fe*
87.36..	Wr	.....	36.10..	7Wdvc	*Ni–Cr*
.....	0	.....	37.20..	Wv	.....
88.59..	4	*Cr–Fe*	**Structure.	.....	.....
89.00..	12	*Fe*(K)–*Fe*	37.56..	6w	*Ni–Ti*
90.86..	18	*–Fe*	38.24..	6	*Sa+ Fe–Ti*
91.52..	20	*Fe*	38.84..	5	*Fe*
92.76..	BdRv	*TiO?*	39.70..	25	*Fe*
93.06..	6W	*–Ti–*	40.38..	0	*⊙?–*
Structure.	.....	.....	41.31..	7wv	*Ti Ti*
96.46..	2	*Fe*	42.50..	9	*Cr*
97.45..	1w	⊙	42.99..	4h	*–Ti*
98.29..	0w	⊙	43.92..	3h	*⊙?*
99.99..	15wvr	*Ti La+–Ba+–Y+*	44.55..	4h	*Cr? Fe*(K)
4902.09..	6	.....	45.47..	4	*Ni*
03.29..	9	*Cr–Fe*	46.42..	7	*La+ Fe*
04.37..	5	*V Ni*	47.05..	0	.....
05.13..	4h	*Fe*(K)	48.07..	7	*Ti–Ti*
07.14..	1s	.....	48.76..	2	*⊙ Sa+*
07.82..	5	*Fe–⊙*	50.12..	6r	*Fe–*
08.56..	1s	*Ti*(p)? *Fe*(p)?	51.59..	0h	.....
09.15..	6	*Ti Fe*	52.43..	4	*Fe*(K) *Sa+–Fe*
10.25..	8W	*Fe–Fe–Fe*	53.21..	6	*Ni*
11.06..	Wv	.....	54.47..	Wv	*TiO*
** 11.85..	Wc	*Fe*(K) *Ni Ti+*?	54.91?.	7W	*TiO Cr*
12.43..	3h	*Co*	57.05..	Wv	*TiO*
13.08..	7	*–Sa+*	57.51..	18Wr	*Fe–Fe Ti*
14.42..	3	⊙	59.17..	3s	*TiO*
15.16..	4v	*–Ti*	59.67..	4	*TiO*
17.28..	4	*Fe*	61.33..	5hw	*TiO*
18.30..	7Wc	*–Ni*	62.34..	5hw	*Sr TiO Sa+*
18.97..	9	*Fe*	64.91..	10	*Cr TiO Ti*
19.90..	4c	*Ti*			
20.65..	20w	*Fe La+*			
21.79..	5	*Ti La+*			

TABLE 1—*Continued*

λ	*i*	Identification
	λ = Mean of 12[2] and 633[1] Intensity from 633[1]	
4966.01..	12	*TiO Fe*
* 66.61..	6	*Co TiO*
67.31..	9	*Ti? TiO*
* 67.90..	5	*Sr Fe*
68.57..	10	*TiO Ti*
* 69.16..	2h	*TiO*
* 69.85..	10	*–Fe*
**** 70.55..	7h	*Fe*
71.36..	4	*Ni*
* 71.96..	4	*TiO Li?*
72.98..	12w	*Ti Fe*
* 73.80..	4	*TiO*
* 74.53..	4Wc	*TiO*
75.39..	6	*Ti TiO*
76.32..	6	*Ni TiO*
* 77.68..	7	*Ti Fe*(K)
* 78.60..	8	*Fe Na TiO*
80.10..	12W	*TiO–Ni*
* 81.17..	Wv	.....
81.66..	30W	*Ti*
82.61..	6	*Fe–Na*
83.22..	3	*TiO Fe–Fe*
83.96..	10	*Fe–Ni*
	Plate 633[1]	
4984.58..	2	*TiO*
85.08..	?BdRv	.....
85.39..	15rc	*Fe–TiO–Fe*
** 87.82..	7	*TiO*
89.05..	15	*Fe–TiO–Ti*
89.93..	2	*TiO?*
91.09..	17w	*Ti*
91.87..	4	*Fe TiO?*
92.67..	2	*TiO*
93.23..	2	*TiO*
94.05..	20w	*–Fe*
Structure.....		*TiO MgH? MgO?*
97.03..	20	*TiO–Ti*
98.31..	7w	*Ni–TiO*
99.41..	17w	*La*[+] *Ti TiO?*
5000.34..	7	*Ni TiO*
01.04..	8	*Ti*
01.86..	7	*Fe TiO?*
02.73..	9	*–Fe*
03.53..	Wv	*Ni–Cr*
5004.49..	Wr	.....
05.03..	7	*–Ti*[+]*?*
05.95..	18Wd	*Fe–Fe*
07.29..	15w	*Ti–Fe–Co?*
08.8...	(2)	*MgH?*
09.61..	15	*Ti*
10.2...	(4)	*Ni–Ti*[+]*?*
11.03..	6wc	*Ni–TiO*
12.06..	25w	*Fe*
13.27..	4	*Ti–Cr*
14.20..	18rv	*Ti Fe?*
16.17..	13	*Ti*
16.90..	1	*Fe*
17.59..	5	*Ni*
18.42..	13	*Fe*[+]
19.17..	5	*Cr*(p)
20.00..	14	*Ti*
20.76..	5w	*Fe? ⊙*
21.46..	??BdRv	*Fe?*
22.35..	9W	*Fe*
22.87..	10	*Ti*
23.45..	.....	*Ti–*
24.82..	8	*Ti*
25.57..	10	*Ti*
26.36..	3	*MgH?*
27.19..	10w	*Fe–Fe*
28.03..	13w	*–Fe*
28.86..	2	*–MgH*
29.70..	9	*Fe–*
31.01..	12	*Sc*[+]
31.95..	3	*Fe*(K)
32.73..	4	*Ni*
33.53..	3	*–⊙?*
Structure.....		.....
34.88..	2	*MgH?*
35.39..	6	*Ni*
35.87..	15	*Ti*
36.48..	15	*Ti*
36.93..	3	*Fe Fe*[+](p)
38.42..	10	*Ti*
39.23..	8	*Fe–Ni*
39.95..	11	*Ti*
40.48..	Wv	*Ti* BO
Strong abs. Structure.....		.....
40.92..	25d?	*Fe–Fe*
41.74..	25W	*Fe Ca*
42.63..	1h	*Mn*
43.51..	10d	BO *Ti*
44.24..	9	*Fe*
45.42..	10	*Ti*

TABLE 1—*Continued*

λ	*i*	Identification	λ	*i*	Identification
5046.52..	3	*Zr*	5086.15..	0	C_2
47.18..	3	*MgH?*	86.99:.	12	*Sc*
48.46..	18Wdc	*Fe*	87.41:.	8	*Ti–V*+?
48.77..	10	*Cr Ni*	88.18..	2	*Fe*(K)?, V? ⊙
50.68..	3	*Fe*?(K)	89.84..	7	⊙
51.69..	30w	*Fe Cr*	90.78..	8	*Fe*
52.66..	BdRv	C_2?–*Sa*+?	91.87..	8	*Cr*
52.89..	10whR	*Ti–*	92.88..	7	⊙–
54.04..	2	*–Ti*	93.47..	5	*Cr*
54.66..	6	*Fe*?(K)	94.41..	2	*Ni?*
55.54..	2h	.....	95.19..	6hv	C_2*Co?*
56.78..	7	*–Fe*?(K)	95.44..	Wr	.....
57.48..	7	*Fe*(K)	96.91..	7hv	*Sc–Fe*
57.95..	6	*–Fe*(K)	97.54..	3	⊙–
58.47..	5	*Fe*(K)	98.68..	12	*Fe*
59.04..	4h	.....	99.22..	8c	*Fe*(K)? *Sc Ni?*
60.08..	28	*Fe*(K)	** 99.28:.	.....	.....
62.09..	8V	*Fe*(K)?–*Ti*	5100.08..	7	*Ni–*
62.32:.	Wr	.....	01.26..	8dw	*MgH Sc* C_2
62.95..	1h	*–MgH?*–C_2	02.39..	5	.....
63.63..	3h	*MgH–*	03.04..	9	*Ni–Sa*+
64.55 } 65.05 }	30Wr	*Sc–Ti* *Fe*	04.09:.	6	C_2?–*Fe*(K)?
65.94..	9	*Cr–Ti*	04.46:.	4	*Sa*+
67.12..	8	*Fe*	05.54..	15	*Cu*
67.69..	7	*Cr*	06.61..	3h	C_2
68.29..	8r	*Cr Ti*	07.56..	20w	*Fe–Fe*
68.79..	9	*Fe*	08.95..	1	*Co–*
69.43..	8	*Ti Sa*+	09.55..	8	*Ti, Fe*
70.17..	7	*–Sc?*	10.49..	30w	*Fe*
71.46..	9	*Ti*	11.56..	3hw	*MgH*, C_2
72.13..	8	*Fe Ti*+	12.48..	9	*Cr*
72.87..	10	*Cr Fe*(K)?	13.40..	11v	*MgH–Ti*
73.94..	6	.....	14.61..	4	*La*+*–MgH–*
74.75..	8	*Fe*	15.37..	3	*Ni*
75.29..	5	⊙	15.89..	0	C_2? *Fe*(K)?
75.76..	6	*BeO? Sc?*	16.61..	3w	*MgH–Sa*+*–*C_2
76.44..	8h	*Fe–MgH–*C_2	17.75..	Wv	.....
77.22..	4	*–MgH?*	17.95..	4r	*Mn Fe*(K)*–MgH*
78.18..	4	.....	19.03..	6w	*MgH–*C_2*–V*+?
79.12..	12	*Fe–Fe*	20.38..	7	*Ti*
79.79..	14	*Fe Ni*	21.60..	4	*Fe* C_2
80.54..	7	*Ni*	22.13..	6	*Cr*
81.08..	6	*MgH?–Ni*	23.52..	40Wv	*La*+*–Cr–Fe*
81.59..	7	*Sc*	24.15..	Wr	.....
82.38..	7	*Ni*	25.18..	6	*Fe–*C_2
83.35..	25w	*Fe*	26.17..	3h	C_2*–Co–Fe*(K)
84.14..	4	*Ni*	27.50..	30Wc	*Fe–Fe*(p)
84.64:?	1h	*MgH?*	28.52..	4	*V* C_2
85.44..	12	*Ti–Sc*	29.42..	12W	*Pr*+ C_2
			30.50..	6	*MgH–*C_2*–Nd*+

TABLE 1—*Continued*

	λ	*i*	Identification
	5131.48..	12	*Fe*
	32.28..	4	C_2?
	32.84..	2	*Zr?–Ti?*
	33.61..	12	*–Fe*
	34.63..	3	*MgH–*C_2
	35.16..	3	*Zr? MgH–Y*
	36.14..	3w	*Zr? Fe*(K) *MgH*
	37.17..	18d?	*Ni–Fe*
	38.58..	9wd	*MgH, Cr*(p)? C_2?
	39.42..	20w	*Fe–Fe–Cr*
	40.24..	1h	*MgH* C_2?
	40.99..	1hw	⊙ C_2 *MgH*?
	41.73..	9s	*Fe*
	42.89..	25v	*Fe Fe MgH*?
	43.72..	5h	⊙ *MgH* C_2
	44.66..	4	*Cr MgH* C_2
	45.30..	18w	*Fe–MgH–Ti*
	46.40..	10w	*Ni MgH*
**	47.48..	15	*Ti*
	48.17..	8	*Fe–Fe*
	48.74..	6	*Ni–V*?
**	49.96..	9whv	*MgH*
	50.86..	20w	*Fe* C_2?
	52.05..	35W	*Fe* C_2?–*Ti*
	53.06..	BdRv	C_2?
	53.28..	8	*MgH Cu Fe*(K)
	54.11..	8hr	Ti^+ C_2
	55.10..	3	Sa^+–*Ni*?
	55.80..	6	*Ni*
**	56.67..	9wdr	*MgH* C_2
	57.83..	4hw	C_2
	59.11..	7hwv	*Fe*? C_2
	59.72..	3	*MgH* C_2
	60.32..	7	C_2 *MgH*
	60.98..	2	C_2
	61.73..	4	C_2 *Cr*?
	62.30..	9	*Fe* C_2
	Structure.	.....	.....
	63.06..	2	C_2 *MgH*
	63.60..	3	*MgH* C_2
	64.24..	BdRv	C_2
	64.54..	8hw	*Fe*(K)? C_2
	65.34..	9hw	C_2–*Fe–MgH*
	66.26..	35w	*Cr–Fe MgH*
	67.44..	25W	*Mg–Fe TiO*
	68.93..	25R	*Fe MgH*
	**Structure.	.....	*TiO, MgH*
	71.60..	10n	*Fe*
	72.65..	15wnr	*Mg TiO*
	73.75..	14	*Ti TiO*
	75.89..	7dw	*MgH, TiO, Co*?
	76.66..	5	*Ni? Fe*?(K) *TiO*
	77.32..	6	*MgH MgH, TiO, Fe*(K)? *Cr*?
	77.96..	2	*TiO*
	78.75..	7w	*TiO MgH*
	80.16..	7Wn	*TiO MgH Fe*(K)?
	81.19..	5n	*TiO–MgH*?
	81.90..	3n	*TiO, MgH*
	82.63..	0	*TiO, MgH*?
	83.60..	20wnrv	*Mg–Ti–TiO*
	84.56:	7w	*Ni Cr Fe*(K)–
	84.78:		*ZrO*?
	85.83..	7n	*TiO–*Ti^+?
	86.48..	6n	*Ti–TiO*
	87.74..	7wd	*TiO–Fe*(K)
	88.78..	10	*TiO–*Ti^+*–Ca*
**	89.66..	6r	*TiO*
	90.67..	5	*TiO*
	91.44..	10	*Fe,* Nd^+
	92.28..	9	*Cr Fe*
	92.98..	15n	*Ti TiO*?
	94.03..	7	*Ti*
	94.90..	12	*Fe*
	95.35..	7	*TiO Fe*
	96.06..	5	*Fe*
	96.52..	6	*Cr Mn*
	97.20:.	2	*Ni?–TiO*
	97.72..	10dV	Fe^+*–TiO*
	98.78..	13	*Fe TiO*
	99.61..	1	*Fe*(K)?
	5200.31..	12	*TiO Cr*
	01.12..	5	*Ti*
	01.58..	1h	*TiO MgH*
	02.33..	15R	*Fe TiO*
	03.51..	1s	*MgH*
	04.54..	30w	*Cr Fe*
	06.03..	25wr	*Cr Ti*
	08.45..	30dw	*Cr–Fe–Ti*
	10.38..	20w	*Ti MgH*
**	11.26:.	5w	*Ti TiO*
	12.10..	BdRv	*ZrO*
	12.33..	7	*Cr–Ti–*
	12.84..	2	*TiO Co*
	Structure.	.....	.....
	13.70..	0	*TiO*?
	14.16..	1	*Cr*
	14.67..	1	*Cr–*
	15.25..	8	*Fe*
	16.32..	18	*Fe*
	17.44..	5	*Fe TiO*

TABLE 1—*Continued*

λ	*i*	Identification	λ	*i*	Identification
5218.09..	6w	*Fe*(K)–*Cu*	5251.51..	4	*Ti*
19.05..	4w	*TiO*?	52.09..	15	*Ti*
19.68..	12	*Ti*	53.05..	4	*Fe*(p)
20.15..	7	*Pr*$^{+}$ *Cu*	53.51..	5	*Fe*
20.96..	5	*Cr Fe*(K)?	54.06..	1	*Zr TiO*? *In*?
21.63..	7	–*Cr*	54.97..	22	*Fe Cr*
22.51..	9	*Cr Fe*(K)? *Ti*	55.57..	10w	*Mn–Ti*
23.19..	2	*Fe*(K)	56.77..	4	.....
23.60..	2	*Ti*	57.59..	5	*Co Ti*?
24.27..	10r	*Ti Cr Ti*	58.58..	1hw	*TiO*? *Sc*?
24.94..	5s	*Ti*, *Cr*, *Zr*	59.66..	6w	*TiO–Ti*?
25.56..	25	*Fe*	60.40..	3s	*Ca*
26.97..	45dWc	*Fe–Fe*	60.83..	1	*TiO*?
27.75..	1s	*Cr*(p)	61.67..	7	*Ca Cr*
28.44..	7	*Fe*(K) *TiO*	62.23..	7	*Ca*
29.15..	1	*TiO*	62.91..	1	.....
29.88:.	8	*Fe*	63.36..	6	*Fe Ti–Ti*?
30.21:.	6	*Co Cr*	64.14..	20	*Ca–Ca*
30.95..	1	*TiO*	65.74..	15hwv	*Ca–Cr–Ti*
31.42..	2	*TiO Fe*(K)?	66.57..	10	*Fe Co*?
32.00..	1	*TiO*			
32.96..	18	*Fe*	67.19..	2	.....
33.80..	6	*Ti V*?	68.51..	3	*Co*
34.15..	6	*Nd*$^{+}$	69.48..	25	*Fe*
34.65..	3	*Fe*$^{+}$	70.42..	15	*Ca–Fe*
35.30..	11w	*TiO–Co–Fe*	71.51..	3w	*TiO*?
36.31..	4	*Fe*, *TiO*	72.16..	4	*Cr–TiO*?
37.42..	6hv	*TiO Cr*$^{+}$?	73.32..	14	*Fe–Fe*
38.56..	8	*Ti*	74.29..	4hw	*Ce*$^{+}$? *TiO*?
38.97..	1s	*Cr*	75.22..	7	*Cr*
39.63..	Wv	.....	75.96..	12wdv	*Cr–Fe*$^{+}$?–*Cr*
39.88..	8	*Sc*$^{+}$–*Ti*	76.89..	3	.....
40.44..	1	*Cr*	77.40..	4	*Zr*
40.87..	2	*TiO Y*?	78.12..	2	*TiO*? *S*?
41.50..	2	*Cr TiO*	78.74..	2	*TiO*? *S*?
42.55..	7	*Fe*–	80.41..	6nr	*Cr–Co Fe*(K)?
43.30..	4	–*Cr*	81.77..	8	*Fe*
43.78..	5	*Fe*	82.39..	7	*Ti*
Structure.	.....	.....	83.56..	10	*Ti–Fe*
45.68..	2	*TiO*	84.38..	9	*Ti*
46.28..	Wv	.....	85.14..	2	*Fe*(p)
46.50..	10	*Ti*	85.68..	3	*TiO*? *Fe*(K)?
47.04..	75Wcv	*Fe–Ti*	Structure.	.....	*CaF*?
47.62..	20	*Cr Co*	87.18..	3	*Cr*
48.01..	Wr	.....	87.68..	1	*Co*?–*Co*?
48.42..	2	*Ti*	88.55..	7	*Fe*
49.01..	4	*TiO*? *Fe*(K)?	89.27..	5	*Ti*
49.54..	4	*Nd*$^{+}$	89.86..	3	*Y*$^{+}$
50.20..	20	*Fe*	90.75..	5	–*La*$^{+}$
50.76..	10w	*Fe–Ti*	91.95..	2w	*CaF*?
			92.63..	3	*Fe*(K)

TABLE 1—*Continued*

λ	*i*	Identification
5293.19..	7	*Nd*$^{+}$
93.97..	4	*Fe*
94.60..	4	.....
95.24..	2	–*Fe*(K)?
95.76..	7	*Ti*
96.66..	15	*Cr*
97.31..	10	*Ti Cr*
98.26..	30Rw	*Cr*–*Cr*–*Cr*(p)
99.96..	6	*Ti*
5300.82..	16w	*Cr Co*
02.18..	14dw	*Sc*?–*La*$^{+}$?–*Fe*
03.37..	6w	–*TiO*?–*La*$^{+}$?
04.08..	5w	*Fe*(K)–*Cr*
.....	0	*Zr*? *CaF*?
05.90..	1	*Cr*?–*ZrO*?
06.42..	2v	*TiO*?
07.36..	15	*Fe*
08.44..	3hr	.....
09.22..	1	*TiO*?
09.98..	1	.....
11.43..	6h	*Zr*
11.72..	0	*Zr*$^{+}$? *Hf*$^{+}$?
12.80..	1	*Co*?–*Cr*?
13.23..	4	*Ti*
13.69..	1s	.....
15.03..	3	*Fe*(K)
15.79..	0	.....
16.69..	10h	*Fe*$^{+}$–*Fe*$^{+}$(p)
17.61..	1h	⊙
18.60..	4hw	*Sc*$^{+}$–*Cr*
19.91..	8	*Nd*$^{+}$–*Fe*
Structure	.....	.....
21.11..	3h	*Fe*
22.05..	9	*Fe*
22.78..	4	.....
24.17..	14	*Fe Ti*
25.66..	1	*Fe*$^{+}$–
26.17..	4	*Fe*
26.86..	0	*Fe*?–
28.26..	50W	*Fe*–*Cr*–*Fe*
29.22..	5	*Cr*–*Fe*(K)
29.91..	7	*Cr*–*Fe*
30.82..	4Wc	*Zr*?
31.53..	6	*Co*–
32.92..	15	*Fe*
33.77..	3	*Co*–⊙
34.24..	3	*Sc*$^{+}$
34.94..	3	*Co*(p)
36.06..	1	⊙
36.76..	7h	*Ti*$^{+}$
5337.74..	1	*Fe*$^{+}$–*Cr*$^{+}$
38.35..	6	*Ti*
39.36..	1	⊙
40.01..	7	*Fe*–⊙
41.03..	20	*Fe Mn*–*Sc*
42.04..	1	.....
42.88..	5	*Co*–*Sc*
43.46..	4	*Fe Co*
44.17..	4	⊙
44.73..	3	*Cr*
45.82..	17	*Cr*
48.30..	14	*Cr*
49.24..	Wv	.....
49.56..	12	*Sc*–*Ca*–*Sc Fe*
50.36..	2	*Zr*$^{+}$?
50.73..	2	*Ca*–*Fe*(K) *Sc*
51.07..	2	*Ti*
52.08..	3	*Co*
52.45..	2	.....
53.48..	8	*Fe*–*Ni*–*Co*
.....	1w	.....
55.81, 56.12	5dw	*Sc*–*Sc Fe*(K)
57.13..	4	–*Sc*$^{+}$?
58.16..	3	⊙
* 58.37..	Wr	.....
*** 58.81..	Wv	*TiO*
*** 61.60..	9v	*Nd*$^{+}$–*Fe*(K)?–*Ti*
* 61.88..	Wr	.....
* 62.35..	Wv	.....
*** 62.72..	6hw	*Zr*–*Fe*–*Co*–*Fe*$^{+}$(p)?
*** 64.88..	5	*Fe*
*** 65.44..	5	*Fe*
*** 66.66..	6	*Ti*
*** 67.48..	5	*Fe*
* 68.46..	0	.....
* 69.79..	20W	*Co*–*Ti*–*Fe*
* 71.52..	40W	*Fe*
**** 72.58..	1	.....
**** 73.72..	5	*Fe*

Plate 654[2]

λ	*i*	Identification
5375.28..	1	*Sc*
76.61..	14dr	*Ti*
76.95..	3	*Fe*(K)?
77.62..	5	*Mn*
78.23..	1	⊙
79.54..	8	*Fe*
81.09..	16	*Fe*(K)–*Co*
81.76..	0	*Co*
82.28..	2	⊙
82.88..	1	*Ti*(p)

TABLE 1—*Continued*

λ	*i*	Identification	λ	*i*	Identification
5383.36..	9	*Fe*	5422.37..	2h	*Co*
84.62..	6	*Ti*	24.08..	13	*Fe*
85.17..	6	*Zr, V*	24.65..	10	*Ni*
85.86..	1	.....	25.30..	2h	Fe^+
86.36..	1	*Fe*	26.26..	22	*Ti*
86.91..	5v	*–Fe*(K) *Cr*	29.69..	55wcd?	*Fe Fe*(p) *Ti*
87.55..	3	*Cr*	30.79..	1h	.....
88.39..	6	*Ni*	31.50..	3h	⊙?
89.01..	Wv	.....	32.52..	27r	*Mn Fe*(K)
89.18:.	10	*Ti*	34.53..	40w	*Fe*
89.49:.	6	*Fe*			
90.00..	5	*Ti*	35.20..	0	⊙
90.51..	7	⊙ *Cr*	35.85..	9	*Ni*
91.12..	1	*Ti*(p)	36.64..	13h	*Ti Fe*
91.52..	10w	*Fe–Fe*	37.09..	9wc	⊙ *Fe*(p)
92.06..	1	*Sc*	37.77..	3	*Zr?*
93.22..	17	*Fe*	38.29..	8	*Ti V*
94.66..	30	*Mn*	39.03..	6h	*MgH?–Fe*(K)?
95.34..	0	*Fe*(K)–	39.72..	0h	⊙? *ZrO?*
96.59..	15	*Ti*	40.49..	7	*Ti*(p) *Zr?*
97.14..	6ow	*Fe Ti*	41.35..	5	⊙ *Fe*(K)? *Fe*(K)?
98.29..	4	*Fe*			
98.87:.	–1	⊙	42.36..	8hr	*Fe*(K) ⊙ *Cr*
99.47..	3	*Mn*	43.32:.	0h	*Fe*(K)?–⊙?
5400.54..	13v	*Fe Cr*	44.59..	0	*Co?*
01.36..	10	*Ti*	45.06..	9	*Fe*
01.99..	3	*V*	46.86..	55w	*Fe Ti*
02.74..	8	V^+	48.39..	7h	*Fe*(K) *TiO*
04.04..	15hw	*Ti Fe*	49.10..	9hw	*Ti Ti? TiO*
05.11..	3w	*Zr? Cr*	49.30..	Wr	*TiO*
05.80..	40w	*Fe*	51.14..	9hw	Nd^+ *TiO*
06.77..	2	⊙	52.07..	4	*Fe*(K) *TiO*
07.47..	15	*Mn Co?*	52.86..	1	*Fe*(K) *TiO*
08.13..	2	*Co?*	53.63..	9h	*Ti TiO*
08.98..	10	*Ti Fe*	54.02..	4	*TiO*
09.80..	28	*Cr Ti–*	54.62..	0	*TiO*
10.76..	Wv	.....	55.62..	50w	*Fe Fe TiO*
10.91..	10R	*Fe–*	56.54..	1	*Fe*(K) *TiO* Atm?
12.48..	Wv	.....	57.50..	10h	*Mn Fe*(K) *TiO*
12.71..	3	–⊙	58.14..	0	*TiO*
13.24..	3	Atm?–	Structure.	.....	.....
14.19:.	Wr	.....	59.48..	1wc	*TiO Fe*(K) Atm?
15.23..	15	*Fe*	60.50..	20r	*Ti TiO Cr*(p)
16.34..	4h	.....	61.57..	7	*TiO Fe*(K) *MgH*
17.10..	4	*Fe*(K)	62.46..	7	*Ni TiO*
18.06..	2	.....	63.13..	15wc	*TiO Fe Fe*
18.80..	6	Ti^+	64.11:.	10w	*Fe*(p)? *TiO*
19.19..	2	*Ti*	65.79..	5	*TiO*
20.37..	18	*Mn*	66.43..	6	*Fe V*
21.52..	4h	*Fe*	66.99..	4	*Fe*
			68.38..	3hv	*TiO V*
			69.29..	4	*Co TiO*

TABLE 1—*Continued*

	λ	*i*	Identification
	5470.13..	o	*TiO Fe*(K)
**	70.60..	11h	*Mn*
	71.20..	9	*Ti TiO*
	72.28..	2	*TiO*
	72.71..	3	*Ti Fe?*
	73.41..	3	*V*$^{+}$ *TiO Ti*
	74.19..	15hwr	*Ti Fe TiO*
	75.45..	4wc	⊙?
	76.44..	15wc	*Fe–Fe*
	76.90..	22	*Ni TiO*
	77.70..	7	*Ti*
	78.25..	Wv	.....
	78.41..	5R	*–Fe*
	.....	o	.....
	80.76..	3hv	*V*$^{+}$ *TiO Fe Cr*
	81.35..	10	*Fe–Ti–Mn*
	81.89..	9r	*Ti Sc*
	83.28..	15h	*Fe–Co TiO*
	84.01..	2	*Co–TiO*
	84.69..	4wr	*TiO Sc*
	85.61..	2	*TiO*
	86.08..	1	*TiO*
	87.02..	5w	*TiO*
	87.71..	6	*TiO Fe*
	88.17:.	3	*Ti*
	88.97..	oh	*TiO*
	90.07..	12	⊙*–Ti*
	90.82..	16	*Ti*
	91.78..	1h	*Fe*(K) *TiO*
	92.78..	2h	*Ti? TiO*
	93.46..	2	*TiO Fe*
	94.00..	3	*TiO*
	95.05..	BdVr	*TiO Ni?*
	95.41..	−1	*TiO MgH Y*
	95.65..	4v	*TiO Fe*(K)
	96.54..	o	*TiO*
	97.52..	35r	*Fe V*$^{+}$
	5500.78..	o	*TiO Fe*(K)?
	01.46..	30	*Fe*
**	02.06..	3hwd?	*Zr, TiO Cr*$^{+}$?
	03.09..	4	*Fe Ti? Y?*
	03.76:.	?BdRv	*TiO MgH*
	03.93..	5R	*Ti Sr*
	04.87..	2	*TiO*
	05.86..	9	*Mn*
	06.74..	40w	*Fe Mo?*
	07.70..	4	*V*
	08.44..	4	*TiO* ⊙
	09.08..	2	*TiO–*
	09.92..	9	*V*$^{+}$ *Ni*
	5510.69..	3	*MgH Fe*(K)
	11.30..	o?	*MgH*
	11.80..	9	*Ti*
	12.48..	12	*Ti Fe*
	12.87..	9	*–Ca*
	14.41..	18	*Ti Ti Sc*
	15.14..	6whr	Bo?
	16.74..	9	*Mn*
**	17.14..	4	*Zr V?*
	18.37..	6dwc	*MgH TiO Ti*
	19.49..	4wc	*Ba?–Fe?*
	20.46..	5h	*Sc*
	21.36..	4wvc	*Y?*
	21.70..	Wr	.....
	22.48..	5	*Fe*
	23.27..	4	*Co*
	24.04:.	ow	*TiO*
	25.03:.	o	*Co?*
	25.56..	5h	*Fe*
	26.81..	9	*Sc*$^{+}$
	27.56..	5	*Y Ti*
	28.40..	15	*Mg*
	29.11..	5	*Fe*(K)
	29.91..	1	.....
	30.76..	9	*Co*
	32.07..	3h	*Fe*(K) *MgH*
	32.90..	10h	⊙? *Mo? Fe*(K)?
	33.78..	4	.....
	34.74..	4h	*Fe*(K)?–
	35.40..	11	*Fe Ba??*
	36.54..	4	*Fe*(K)
	37.76..	11	*Mn*
	38.56..	4	*Fe MgH*
	39.25..	4	*Fe*(K)
	40.82..	o	*Fe*(K)
	41.78..	1wv	*V?–Ti?*
	42.70..	2	.....
	43.16..	4	*Fe*
	43.94..	4	*Fe*
	44.47..	?BdRv	.....
	44.67..	3r	*Y?*
	45.94..	4	*V*
	46.49..	4	*Fe*
	47.03..	5	*Fe*(K) *V*
	48.51..	4h	.....
	49.97..	3	*Fe*(K)
	Structure.	.....	.....
	52.21..	1	*Sc*$^{+}$
	53.67..	7	*Ni Fe*
	54.88..	7	*Fe*

TABLE 1—*Continued*

λ	*i*	Identification	λ	*i*	Identification
5555.58..	1h	*–Cr*(p)	5605.63..	o	.....
56.38..	1hw	*MgH?–V–Yb?*	06.31..	o	*V*
57.04..	o	*Al*	07.03..	1	*Ni*
57.42..	3	*V*	07.71..	2hw	*Fe*(p) *Fe*(K)–
57.99..	3	*Fe Al*	08.94..	2hw	*Fe*(p)
58.74..	2r	*V* BO?	10.25..	4hw	⊙ *ZrO*
59.69..	o	.....	11.34..	2hw	–⊙–
60.40..	7wc	*Fe–V*	12.12..	2	*Fe*(K)?–
Structure.	.....	.....	13.77..	os	⊙
62.73..	4	*Fe*	14.31..	os	⊙
63.67..	8	*Fe*(p) *Fe*	14.80..	os	*Ni*
64.72..	oh	.....	15.52..	25w	*Fe–Cr*(p)–*Fe*
65.65..	16w	*Fe Ti*	17.11..	3	*–Fe*(K)
66.71..	1	.....	17.71..	4	*–Fe*(K)
67.40..	8	*Fe*	18.57..	5hv	⊙*–Fe*
68.08..	oh	*MgH?*	19.55..	4h	*–Fe–*
68.90..	1h	*Cr*(p) *Fe*(K)	20.35..	7wc	*Zr–Fe*
69.63..	12r	*Fe*	21.36..	o	*MgH*
70.46..	3	*Mo?–Ti?*	22.12..	owc	*–Si?*
72.90..	17	*Fe Fe*	22.95..	1	⊙
74.00..	2	*V*	23.53..	1	*Fe*(K)
76.10..	13dhr	*–Fe–*	24.08..	1	*Fe*
77.04..	o	⊙	24.67..	15	*V Fe V*
77.72..	o	.....	25.40..	o	*Ni*
78.72..	12	*Ni*	26.00..	4	*V*
79.35..	–1	*Fe*(p)	26.71..	o	*Fe*(K)
80.30..	o	⊙ *Cr*(p)?	27.59..	12	*V*
81.93..	12	*Ca, V*	28.65..	1	*Cr*
83.06..	o	*MgH? Ti?*	29.35..	3w	.....
84.58..	12hr	*V–Fe*	30.16..	1	*Y*
85.68..	o	*Ti*	32.42..	5	*–V*
86.80..	15	*Fe*	34.05..	4	*Fe–*
87.84..	11h	*Ni*	35.65..	Wv	.....
88.76..	15	*Ca*	35.95..	5Wr	*Fe–*
90.12..	8	*Ca*	37.11..	6Wv	*–Ni–*
90.77..	6	⊙	37.48..	Wr	.....
91.33..	o	*Sc*	38.22..	4	*Fe*
92.35..	13	*Ni–V*	38.81..	o	*Ni*
92.95..	5	*V*	39.53..	7	⊙
93.75..	2	*Ni*	** 40.51..	?BdRv	.....
94.51..	13	*Ca Nd*$^{+}$ *Fe*	41.18..	8WRd?	*Sc*$^{+}$*–Fe*
95.92..	oh	.....	42.65..	o	*Fe*(K)
97.11..	o	⊙	43.16..	1	.....
97.81..	5h	*V TiO Ti*	44.09..	10h	*Fe*(K)*–Ti*
98.45..	12	*Ca Fe*	45.53..	oh	*–Si*
5600.10..	7	⊙ *Fe*	46.08..	5	*V*
01.31..	10	*Ca*	47.23..	3	*Co*
02.89..	13	*Ca Fe Fe*	47.85..	oH	.....
03.73..	3	⊙	48.54..	4	*Ti V*
04.94..	7	*V*	49.81..	6Wcd	*Cr–Ni–Fe?–Fe*

TABLE 1—*Continued*

λ	*i*	Identification
5650.68..	2	*Fe*
51.40..	3w	*Fe*(p)(K)
52.22..	3w	*–Fe*
53.30..	0	.....
53.89..	3	*Fe*
54.58..	1	⊙–
55.38..	5hv	*Fe–Fe*
57.41..	4	*V*
57.89..	4	Sc^+
58.74..	20wc	*Fe–Fe*
59.75..	2hw	.....
60.74..	3h	*Fe*(K)
61.40..	3h	*Fe*(K)
62.12..	5	*Ti*
62.52..	5	*Fe*
62.89..	5	*Ti Fe* V^+
63.44..	0	.....
63.99..	3h	*Ni Cr*
64.58..	4	*Zr*
65.56..	3hwv	*–Si*
67.38..	7dwv	Sc^+*–Fe*
68.35..	5	*V*
69.01..	4	Sc^+
69.88..	0w	*–Ni–*
70.84..	12	*V*
71.80..	9	*Sc*
73.36..	1h	*Ti*
74.20..	0h	*Cr* Atm?
75.44..	7h	*Ti*
77.79:.	2	⊙–
78.52..	1	*Fe*(p)*–Fe*(p)
79.02..	2	*Fe*
80.00..	4hwr	*Ti–*
80.89..	3	*Zr*
82.23..	0	*Ni*
82.62..	12	*Na Cr*?
84.07..	BdRv	.....
84.31..	8wdr	Sc^+*–Si* Atm
86.74..	11hw	*Sc Fe*
88.23..	13hr	*Na* Nd^+
89.46..	3v	*Ti*
90.42..	1	*Si*
91.53..	3	*Fe*
92.91..	0w	Atm–
93.66..	2	*Fe Y*?
94.86..	4hv	*Cr–Ni*
96.34..	10	⊙ Atm
98.50..	20v	*V Fe*(K) *Cr Fe*
5700.21..	10	*Sc Fe*(K) *Cu*?
01.57..	11	*Fe*
02.49..	8wc	*Cr–Ti*
03.57..	13	*V*
04.71..	0	*Fe* Atm?
05.42..	1	*Fe* Atm?
06.09..	5	*S? Fe Co*?
06.99..	12	*V*
** 08.24..	6r	*Ti Si Sc*
08.92..	5	*Zr*
09.50..	13	*Ni Fe*
11.08..	5	*Mg*
11.88..	13hwr	*Fe Ni Ti Sc*
12.76..	3	*Cr*
13.90..	3	*Ti*
15.13..	8	*Ti Fe Ni*
15.95..	0	*–Fe*(K)
16.42..	3	*Ti*
17.26..	2	*Sc*
17.99..	6wc	*Fe–ZrO*
19.06..	1h	.....
19.82..	2h	*Cr* Atm?
20.45..	2	*Ti*
20.91..	1	⊙ *Fe*(K)?
21.77..	2hw	*–Fe*(K)? Atm?
24.06..	3hd?	*ZrO Sc* Atm?
24.48..	1	*Fe*(K)
25.66..	2hv	*V*
27.02..	15	*V*
27.66..	10	*V*
29.10:.	2hv	Atm?*–Cr*
29.32..	Wr	*CN*?
29.84..	0	–Atm
30.38..	0	.....
31.24..	12	*V*
31.77..	5	*Fe*
33.77..	BdRv	*TiO*
33.95..	3r	*Fe*(K)?
35.68..	11	*Zr*
37.05..	13	*V*
38.27..	2h	*Fe*(K) Atm?
39.42..	3	*Ti*
39.98..	3	*Ti*
41.02..	5W	*VO Ti*
41.94..	3	*VO Fe*?
42.88..	0	*VO*
43.43..	12	*V*
44.08..	0h	*VO* Atm?
44.84..	1h	*VO–*
46.43..	0	*VO*?
47.14..	0	*VO*
.....	3h	.....

TABLE 1—*Continued*

	λ	*i*	Identification
	5748.34..	7V	*Ni VO*
	48.51..	Wr	.....
	48.90..	1	*V VO?*
	49.35..	0	*VO?*
	50.70..	1	*VO*–Atm?
	51.34..	0	⊙ *VO*
	52.07..	3	*Fe*
	53.11..	4hrvd?	*Fe Ti VO?*
	53.59..	2	–⊙
	54.64..	13	*Ni*
	56.93..	2hv	*VO Fe*
	57.64..	1	*VO*
	59.45..	1h	*VO Fe*
	60.41..	2	*Fe VO*
	60.92..	1	*Ni–VO*
	61.43..	2r	*V Fe*(K)? Atm?
	62.35..	3	*Ti Fe*
	63.01..	4	*Fe*
	66.39..	2	*Ti*
	67.47..	oh	*VO*, Atm
	69.12..	2h	La^+–
	69.92..	oh	*VO?*
	70.61..	1hr	⊙ Atm
	71.57..	1h	*Cr*? Atm
**	72.38..	4hd	*V Si*
	73.33..	oh	Atm
	74.12..	2	*Ti*
***	75.13..	2	*Fe*
***	76.70..	6	*V*
**	77.61..	oh	Ba^+
***	78.46..	5	*Fe*

Plate 650[3]

5780.29..	3	–Atm–
80.67..	15hrv	*Fe Ti Fe*
81.76..	3	*Cr*
82.10..	16h	–*Cu Fe*
83.10..	4	*Cr*
83.85..	8	*Cr*
84.58..	Wv	.....
84.89..	15wc	*Fe–Cr–Fe*
85.90..	19	*Ti–Cr–Ti–V*
86.16..	Wr	.....
87.01..	2	Sa^+, *Cr*
87.81:.	Wv	.....
87.97..	7	*Cr*
88.48..	4	*Cr V* Atm*O*
90.16..	0	⊙ Atm*O*
90.92..	20wd?	–*Cr Fe* Atm*O*
92.33..	Wr	Atm
92.86..	Wv	.....
93.07..	3r	Atm*O–Si*
93.94..	3	*Fe*

	λ	*i*	Identification
	5796.08..	8	*Fe Ni*
	96.66..	0	–*Cr*?
**	97.68..	15	*Zr Si Ti*
	98.25..	10wc	*Fe Cr*
	98.68..	Wr	.....
	99.58..	Wv	.....
	99.86:.	1hw	⊙
	5800.97..	2hw	Atm*O*
	01.84..	2w	.....
	03.14..	0w	Atm*O*
	04.27..	22w	*Ti*
	05.17..	2	*Ni*
	05.81..	3	La^+ Atm*O*?
	06.71..	3	*Fe* Atm*O*?
	07.23..	1	*V*–⊙
	07.87..	3	*Fe*(p) *Fe*(K)
	08.35..	3	⊙–
	09.24..	4	*Fe* Atm*O*
	09.86..	0	Atm*O*
	11.02..	0	.....
	11.72..	3wc	⊙ *Fe*
	12.86..	2h	*Ti* Atm*O*
	13.92..	4h	Atm*O*?–*Ti*
	15.06..	4wc	*Fe–Fe*
	16.34..	5h	*Fe* Atm*O*
	17.03..	2	*V* Atm*O*
	18.76..	2hv	–Eu^+
	18.89:.	Wr	.....
	Structure.		.....
	20.62..	0	*FeO*? Atm*O*
	21.31..	0	*FeO*? Atm*O*
	21.91..	0	*FeO*?
	22.53..	0	*FeO*?
	23.75..	4h	*Ti*
	25.76..	3h	⊙ Atm*O Fe*
	26.62..	2	*Fe*
	27.85..	3	*Fe*(p)
**	28.83..	0	Atm*O*?
	29.84..	0	Atm*O*?
	30.74..	1h	*V*
	31.66..	2h	*Ni, Fe*
	32.57..	1h	*Ti*–
	33.94..	3	⊙ *Fe*
	34.64..	5	–*Fe*
	Structure.		.....
	38.53..	4h	*Fe*(p)–*Cr*
	39.60..	5h	⊙–Atm?
	41.21..	1	⊙, Atm?
	42.40..	3h	–*Fe*
	42.99:.	Wv	Atm?

TABLE 1—*Continued*

	λ	*i*	Identification	λ	*i*	Identification
	5844.38..	Wv	.....	5894.04..	1h	.....
	44.65..	4R	*Cr*–	95.18..	Wv	.....
	46.18..	3	*Fe–V*	95.86..	40Wc	*Na*
	47.00..	7	*Ni*	96.54..	Wr	.....
	48.08..	4	*Fe*	99.30..	13	*Ti*
	49.10..	oh	Atm?–⊙	Structure.	.....	⊙ Atm wv
	49.70..	o	*Fe*(K)–	5900.33..	o	*Fe*(K) Atm wv
	50.11..	Wv	.....	01.05..	1	*Zr*
	50.50..	3Rc	–Atm?–	01.71..	1	*Fe*(K) Atm wv
	52.23..	7	*Fe*(K)	02.41..	1	*Fe*(K) ⊙ Atm wv
	53.25..	6	*Fe*–			
	53.68..	11	Ba^+	03.30..	4	*Ti*
	54.91..	?BdRv	.....	04.67..	?BdRv	*TiO*?
	55.06..	2r	–*Fe*	04.84..	0r	⊙ *Fe*(K) Atm wv
	55.85:.	Wv	.....	05.67..	2h	*Fe* Atm wv
	56.13..	3r	*Fe*–	06.69..	oh	⊙–⊙ Atm wv
	57.47..	10h	*Ca, Co*	07.83..	oh	⊙ Atm wv
	58.45..	4Wdc	*V*?–⊙–⊙ *CN*?	09.98..	5	*Fe*
	59.54..	3	–*Fe*	11.51..	o	Atm wv?
	60.18..	1h	$-Sa^+$	11.99:.	Wv	.....
	61.01..	1h	Atm *wv* ⊙	12.23:.	o	*Fe*(K)
**	62.44..	3h	*Fe*–	13.52:.	??Bd	*FeO*? Atm wv
	64.52..	Wr	.....	13.73..	5	*Ti*
	65.17..	2v	.....	14.14..	6w	*Fe* Atm wv
	65.37..	Wr	.....	15.54..	3	*Co*
	66.42..	17	*Ti* Atm *wv*	16.25..	7	*Fe*
	67.55..	2	*Ca*	16.84:.	o	*Cr*(p)–
	68.18..	2	–*Zr*	17.55..	o	*FeO*? Atm?
	.....	1WH	Atm *wv*	18.58..	10	*Ti*
	72.58..	Wv	.....	19.36..	o	Atm wv
				19.93..	o	Atm wv
	72.95..	5Wrc	$-Eu^+$–*Fe*	20.49..	o	*FeO*?
	76.41..	3w	Atm *wv Cr*	Structure.	.....	Atm wv
	77.80..	4w	–*Fe*(K)–	22.12..	10	*Ti*
	78.90..	1	.....	22.90..	o	Atm wv
	79.77..	6w	*Zr* Atm *wv*	23.78..	Wv	*ZrO? Ni?* Atm wv
	80.21..	5	*Ti Fe*	24.58..	0s	Atm wv
	81.24..	1	*Fe*(p) Atm *wv*	25.16..	oh	*Zr* Atm wv
	81.76..	1	*Fe*(p) Atm *wv*?	25.90..	1w	*Ni*(p) *Fe*(K)
	82.57..	Wv	.....	27.26..	0s	Atm?
	82.73..	1r	Atm *wv*?	27.82..	1h	*Fe*
	83.85..	3	*Fe*	28.79..	o	Atm wv
	84.....	o	Atm *wv*	29.64..	1	–*Fe*(K)?
	85.56..	2	*Zr*			Atm wv?
	86.18..	1	Atm *wv*	30.23..	2h	*Fe*
	Structure.	.....	Atm *wv*	30.68..	o	*FeO*?
	87.86..	Wv	Atm *wv*?	31.85..	Wv	*FeO*?
	89.19..	Wv	.....	32.21..	4Wc	*FeO*? Atm wv
	89.87..	50Wc	*Na*	33.00..	o	*FeO*, Atm wv
	90.57..	Wr	.....	33.66..	2w	.....
	92.84..	8	*Ni Fe*(K) Atm *wv*	34.60..	5hw	–*Fe*
				35.32..	5	*Co Zr*

TABLE 1—*Continued*

λ	*i*	Identification
5936.23..	2	–Atm wv–
36.96..	3	⊙
37.77..	6	*Ti*
39.10..	1	*Sa*$^{+}$ *–Fe*
39.82..	0	*Ta?*
40.67..	8	*Ti*
41.74..	9h	*Ti* Atm wv
42.77..	0	Atm wv
43.55..	1h	*Fe*(p)
44.04..	7	*Ti* Atm wv
45.66..	0	.....
46.41..	0v	Atm wv
47.50..	1wv	⊙ Atm wv
48.57..	1w	*Si* Atm wv
49.33..	7h	*Fe* Atm wv
49.96:.	0?	Atm wv?
51.39:.	0	Atm wv–
52.10..	0	Atm wv–
52.75..	2	*Fe*
53.16..	8h	*Ti*
54.56..	0	Atm?
55.34..	5h	*Zr* Atm wv
57.71..	12	*Fe*
58.30..	4h	*Fe*(K), ⊙ Atm wv
59.72..	1	*FeO?*
Structure.	.....	*Fe*(K)? *Fe*(K)? Atm wv
63.28..	3hwv	*Fe*
64.57:.	0w	*Fe*(K)
64.71:.	.....	.....
65.82..	7	*Ti*
67.04..	0?	Atm wv
67.87..	0	⊙
68.88..	0h	Atm wv
69.70..	0	*Fe*(K), Atm wv
70.38..	0	Atm wv
70.99..	Wv	–⊙ Atm wv
72.74..	Wv	*VO?*
75.13..	Wv	Atm wv
75.40..	5R	*Fe*
76.78..	5	*Fe*
78.56..	7h	*Ti*
80.81..	4	*Ti, V*
81.97..	0	*FeO?*
82.70..	0?	*FeO? Cr*(p)?
83.77..	2w	*Fe–Lu*$^{+}$?
84.63..	8h	*V Ti Fe*
87.09..	3h	*Fe*
88.48..	2	*Fe–Ti*
89.24..	3w	⊙
90.56..	3h	⊙
5991.33..	0	*Fe*$^{+}$(p) Atm wv?
91.89..	6hw	*Co* ⊙? *CN?*
93.55..	0	Atm wv–
94.09..	1h	–Atm wv?
94.37..	Wr	.....
95.37..	0	.....
95.89..	2hV	*Ti–Ti*
96.12..	Wr	.....
96.85..	0	*Ni–*
97.77..	3	*Fe*
99.03..	2	*Ti*
99.70..	3w	*Ti*
6000.81..	2w	*Co*–Atm wv
02.10..	Wv	.....
02.44..	8w	*V–Ti*
02.98..	5w	*Fe*
03.20..	Wr	.....
** 05.61..	3	*Fe–*
07.30..	3	*Ni*
08.01..	2	*Fe*
08.60..	4	*Fe*
09.36:.	0	⊙
12.21..	3	*Ni*
12.80..	0	⊙
13.50..	7	*Mn*
15.30..	2	*Fe*(p)
16.69..	9h	*Mn–*
17.80..	1w	*–V?*
18.51..	4h	*Ti–Ti*
18.34..	0	⊙ Atm wv?
20.13..	6	*Fe*
21.80..	7	*Mn Fe*(K)
23.39..	2h	*V*
24.07..	4V	*Fe*
25.39..	2h	*Zr?*
27.07..	4	*Fe*
30.62..	2	⊙, Atm wv
31.66..	7w	*–Ti*
32.59..	2w	*Zr Fe*
34.26:.	1w	*Fe*(K) Atm wv–
35.30..	0w	⊙
36.42..	1w	⊙
39.72..	8	*V*
41.14:.	0	.....
42.10..	2h	*Fe*
43.36..	2	*Ce*$^{+}$
44.04..	0w?	.....
44.77:.	0w	.....
45.34:.	0w	.....
45.86..	0w	*Zr*

TABLE 1—*Continued*

	λ	*i*	Identification
	6047.07..	o	⊙
	47.74..	o	*Cr*?–
	48.65..	1w	⊙
	49.45..	2w	*Zr*?–*Eu*+?
	50.99..	o	*Fe*(p)?
	51.81..	2	⊙
	52.73..	ow	.....
	53.42..	Wv	.....
	53.83..	3w	*Ni*–
	55.08:.	o	.....
	56.01..	3	*Fe*
	57.06..	3w	⊙
	58.12..	5	*V*
	58.76..	0s	*Ti*(p)
	60.64..	3	*Ti*
	62.83..	9r	*Fe* *Zr* *Cr*(p)
	64.62..	9	*Ti*
	65.49..	14	*Fe*
**	68.60..	o	.....
	69.21..	o	.....
	70.84..	Wr	.....
	71.54..	Wv	.....
	73.76..	Wr	.....
	74.24..	Wv	.....
	76.30..	o	.....
	76.87..	−1	⊙
	77.45..	o	*V*?
	77.59..	Wr	.....
	78.46..	2h	*Fe*
	79.11..	2h	*Fe*
	81.43..	10	*V*
	82.66..	10	*Co*–*Fe*
	83.98..	0wc	*Fe*(p)–*Fe*+(p)
	85.26..	10	*Fe* *Ti*
	86.07..	Wv	–*Ni*?
	87.44..	Wv	.....
	89.55..	2	*Fe*
	90.23..	10	*V*
	91.20..	3	*Ti*
	91.87..	o	⊙ *Fe*(K)?
	92.62..	Wv	.....
	92.96..	6wc	*Ti*–*Co*
	93.79..	1	*Fe*–*V*
	94.43..	1	*Fe*(K)
	95.59..	o	.....
	96.44..	Wv	.....
	97.12..	8Wc	*Fe*(p)
	98.44..	5wc	⊙–*Ti*
	6100.28..	3wv	⊙ *Fe*(K)?
	02.28..	8	*Fe*–
	6102.73..	15	*Ca*
	03.14..	8	*Fe*
	03.98..	Wv	.....
	04.65..	1	*V*?
	05.68..	Wr	.....
	06.98..	2hv	*V*
	07.14:.	Wr	.....
	08.14..	9	*Ni*
	09.18..	ow	*V*? *Fe*?
	10.01..	Wv	.....
	10.24..	ow	*V*?
	Structure.		.....
	11.65..	8	*V* *VO*?
	12.70..	Wv	.....
	13.36..	4	*Fe*+(p)
	14.20..	4	.....
	15.38..	ow	*Fe*(K)?
	16.19..	4	*Ni*
	17.02..	3	*Co*
	18.14..	ow	.....
	19.53..	10	*V*
	20.26..	6	*Fe*(p)
	20.96..	5	*Zr* *Ti*
	22.22..	30w	*Ca*
	.....	−1	.....
	24.87..	4h	*Zr* *Si*? *Fe*(K)?
	26.21..	10	*Ti*
	27.26..	Wv	.....
**	27.43..	6	*Zr* *Fe* *V*
	28.58..	Wr	.....
	29.01..	5	*Ni*
	30.29..	1wv	*Ni*–
	30.50:.	Wr	.....
	31.60..	Wv	.....
	31.77..	2hr	*Si*–*Si*
	32.49:.	o	*Fe*(K)?
	34.52..	7	*Zr*
	35.31..	7	*V*
**	36.72..	40w	*Fe*
	37.69..	16	*Fe*
	38.45..	1	*Si*(p)?, *V* *Ti*?
	39.58..	1	.....
	40.46..	2	*Zr*
	41.70..	25	*Ba*+ *Co*? *Fe*(K)
	43.19..	10	*Zr*
	45.69..	Wr	.....
	46.27..	4r	*Ti* *Fe*(K)?
	47.82..	3	*Fe*
	48.49..	Wv	.....
	50.14..	8V	*V*

TABLE 1—*Continued*

	λ	*i*	Identification
	6150.41..	Wr	.....
	51.65..	10	*Fe*
	54.26..	5	*Na*
	55.21..	1r	Fe^{+}(p)? *Si*
	55.85..	Wv	.....
	56.04..	2r	*Ca Si*
	57.73..	7w	*Fe V*?
	59.05..	7Wc	*–Ti–*
	59.55..	Wr	.....
	60.53..	Wv	.....
	60.80..	8	*Na*
	61.33..	7	*Ca*
	62.22..	25w	*Ca*
	63.68..	20	*Ca Ni*
	65.36..	5	*Fe*
	66.50..	7	*Ca*
	66.71..	Wr	.....
*	68.76..	Wv	.....
*	69.04..	9	*Ca*
*	69.56..	8	*Ca*
***	70.40..	10	*V Fe*
***	71.16..	1h	.....
***	71.93..	2h	.....
***	72.69..	2w	.....
***	73.36..	11	*Fe*
***	74.32..	2h	.....
***	75.36..	2h	*Ni*
***	76.60..	Wv	.....
*	77.11..	15Wc	*Ni–Ni*
	77.54..	Wr	.....
	78.30..	3hw	*–Zr*?*–*
***	80.23..	15h	*Fe*
*	81.86..	2h	*V*
*	83.70..	6hWc	⊙*–*
*	85.06..	Wv	.....
*	87.42..	1h	*Fe*(p)
*	88.06..	5h	*Fe*
*	89.18..	18w	*Co, V*
*	90.49..	4hw	BO?
*	91.45..	22Wc	*Ni–Fe–V*
*	91.93..	Wr	.....
****	93.70..	4hw	*Sc*
****	97.62..	1s	.....

	λ	*i*	Identification
	Plate 654[4]		
	6198.45:.	0	*Fe*(p)
	99.21..	15r	*V*
	6200.33..	8	*Fe*
	01.73..	2	.....
	02.44..	1	*–Fe*(K)?
	03.19..	1	.....
	03.91..	0	*Fe*?
	04.64..	3s	*Ni*
	05.21..	3h	⊙
	06.45..	0	.....
	07.32..	0	*Fe*?, *V*
	09.94..	1	.....
	10.73..	11	*Sc Fe*?
	11.83:.	1wc	.....
	13.58..	30Wvc	*Fe–V*
	14.12:.	Wr	.....
	15.19..	4h	*Fe–Ti*
	16.40..	10h	*V*
	17.96..	3Wc	.....
	19.29..	12	*Fe*
	20.54..	0	*Ti*
	21.49..	4w	*Ti–Fe*?
	21.84..	Wr	.....
	22.35..	Wv	*TiO*?
	22.63:.	4r	*V Ti*
	24.54..	6	*V*
	26.08..	Wv	.....
	26.58..	4Wv	*–Fe*?
	26.98..	Wr	.....
	27.45..	Wv	.....
	27.74..	3hr	⊙*–*
	28.28..	0w	.....
	29.03..	Wv	*ZrO*?
	29.30..	5hr	*Fe–*
	Structure.	.....	.....
	30.83..	22w	*V? V Fe*
	32.73:.	4w	*Fe–*
	33.21..	5	*V*
	34.10..	1s	.....
	36.09..	2V	.....
	36.36..	Wr	.....
	37.31..	3h	⊙?
	38.50..	2h	Fe^{+}*–*
	39.16..	Wv	.....
**	40.07..	20Wc	*Sc–Sc–V–Fe*
	40.92..	Wr	.....
	43.12..	22w	*V V*
	45.02..	Wv	.....
	45.45..	6Wc	*V–*Sc^{+}
	46.37..	7	*Fe*

TABLE 1—*Continued*

λ	*i*	Identification	λ	*i*	Identification
6247.36:	Wv	.....	6299.57..	4	Atm*O O*
47.61..	1hr	*Fe*+?–	6300.38..	3hr	.....
49.56..	5	*Co*	01.51..	7	*Fe*
50.48..	3	.....	02.46..	7	*Fe* Atm*O*
51.82..	10	*V*	03.76..	7	*Ti*
52.61..	11rc	*Fe*	05.62..	17dwr	*Sc* Atm*O*
54.27..	10	*Fe*	06.88..	0	Atm*O*
55.07..	1w	.....	07.89..	1w	⊙
56.33..	9	*Ni, Fe*	09.71..	Wv	.....
56.87..	5	*V*	09.99..	4R	*Sc*+–Atm*O*
57.99..	21	*Ti*	11.49..	5	*Fe*
58.73..	20	*V*–*Ti*–*Sc*	12.24..	7	*Ti*
Structure.	.....	.....	13.05..	4r	*Zr*–
61.12..	11	*Ti V*	14.68..	8	*Ni*
62.27..	3h	*Sc La*+?	15.36..	3	*Fe* Atm*O*
63.84..	0	.....	15.86..	1	*Fe*
65.13..	11	*Fe*	16.59..	0	*Ni*? Atm wv?
66.23..	6	*Ti*–*V*	18.13:.	11	*Fe Ti*–
68.77..	9	*Ti*(p)–*V*	18.67..	0	⊙
70.24..	4	*Fe*	19.25..	0	Atm*O*
71.03..	Wv	.....	20.23..	Wv	.....
71.37..	3wR	*Fe*(p)–	20.45..	4R	⊙, Atm wv?
73.40..	5	*Ti*	22.72..	10	*Fe*
74.64..	10	*V*	25.16..	11v	–*Ti*
76.27..	3v	*CaH*–*Sc*	26.82..	3	*V*
76.47..	Wr	.....	27.60..	8	*Ni*
76.91..	Wv	.....	30.11..	11	*Cr*
77.16..	4	Atm*O*	30.93..	1w	*Fe*–
77.75..	3	Atm*O*	32.23..	2w	*CN*?
77.92..	Wr	.....	35.35..	13	*Fe*
78.43..	4	Atm*O*	36.11..	4	*Ti*
79.11..	Wv	.....	36.84..	8	*Fe*
80.60..	13	*Fe* Atm*O*	37.81:.	Wv	.....
81.49..	3v	Atm*O*	39.04..	5	*V Ni*
82.09..	Wv	.....	39.30..	Wr	.....
82.57..	10Wrc	–*Co* Atm*O*	40.04..	2	⊙?–
84.09..	2	Atm*O*	41.73..	4wc	.....
85.14..	10	*V*	44.10..	10	*Fe*
Structure.	.....	Atm*O*	45.03..	4	.....
89.67..	oh	Atm*O*	45.92..	1s	.....
90.57..	4	Atm*O*	46.55..	Wv	*ZrO*
91.00..	3	*Fe*	48.39..	1	.....
91.91..	1	*CaH*	48.65..	Wr	.....
92.78..	11	Atm*O*–*ZrO*–*V*	49.53..	4	*V*
93.22..	3	Atm*O*	50.46..	1s	.....
93.96:.	0	*Fe*(p)	51.74..	1Wcd?	.....
95.29..	5h	*Ti* Atm*O*	53.79..	5v	–*Fe*(p)
96.53..	15	*V Ti*	54.01..	Wr	.....
97.85..	10	*Fe*	55.04..	9	*Fe*
98.81..	2	Atm*O*	57.29..	3	*V*

TABLE 1—*Continued*

λ	*i*	Identification
6358.69..	20	*Fe*
59.86..	8	*Ti*
60.57..	Wv	.....
.....	1W	.....
61.67..	Wr	.....
62.86..	10	*Cr*
63.78..	0	.....
64.66..	12wd?	*Fe–Ti*
65.52..	0	.....
66.40..	10	*Ti*
68.01..	0vc	⊙–
** 68.24..	Wr	.....
69.28..	0vc	*CaH–Fe*$^{+}$(p)?
69.46..	Wr	.....
70.42..	1vc	*Ni CaH?*
70.73..	Wr	.....
71.57..	2vc	*CaH*
71.83..	Wr	.....
72.78..	2vc	*CaH*
73.06..	Wr	.....
74.46..	2vc	*V CaH*
74.71..	Wr	.....
75.85..	2vc	*CaH*
76.30..	Wr	.....
77.37..	0	*CaH*
78.15..	Wv	.....
** 78.63..	9Wc	*CaH ZrO*
80.52..	Wv	*CaH*
80.83..	7R	*Fe CaH*
82.04..	0	*CaH*
82.79..	2wc	*CaH*
83.60..	Wv	*CaH?*
83.79..	0	*CaH*
84.56..	1	*Mn Ni CaH*
85.17..	0	*CaH*
85.77..	0	*Fe*(p) *CaH*
86.35..	0	*CaH*
87.51..	0	*CaH*
88.37..	1w	*CaH*
89.22..	0	*CaH*
90.49..	6h	*CaH La*?$^{+}$
92.50..	5v	*Fe CaH*
92.73..	Wr	.....
93.59..	15	*Fe CaH*
95.51..	2hrv	*CaH*
96.46..	0	*CaH*
97.26..	0	*CaH*
98.10..	0	*CaH*
Structure.	.....	.....
99.01..	0	*CaH*

λ	*i*	Identification
6400.21..	30	*Fe–Fe*
01.84..	Wv	.....
02.19:.	2wrc	*CaH–Y–CaH*
02.95..	Wv	.....
03.35..	2wrc	*CaH* Atm?
04.18..	Wv	.....
04.46..	0	.....
05.25:.	Wv	.....
05.58..	3	.....
07.04..	1	*Zr? V?*
08.06..	9hr	*Fe*
10.36..	2	.....
11.70..	8	*Fe*
13.29..	8	*Sc*
14.51..	Wv	.....
14.77..	2	*Ni–Fe*(K)
15.49..	2r	⊙?
16.96..	3	*Fe*$^{+}$
17.83..	3	*Co*
19.08..	3	*–Ti*
19.92..	6	*Fe*
20.21:.	Wr	.....
20.74..	0?	⊙?–⊙?
21.39..	14	*Fe*
23.78:.	Wv	.....
25.60..	2	⊙?
25.85..	Wr	.....
28.71..	5h	⊙?
30.82..	25	*Fe V?*
31.87..	2w	*V*–⊙?
** 32.51..	Wv	*Fe*$^{+}$(p)?
34.02..	Wr	.....
35.02..	7	*V*
36.49..	3Wc	*Fe–*
37.95..	3wc	⊙–⊙?
39.06..	15	*Ca*
39.98..	0	.....
40.89..	0w	*–Mn*
Structure.	.....	–Atm?–
45.00..	0	.....
45.78..	0	*Zr*
46.63..	0	.....
47.90..	2w	*V?*
49.02..	1	⊙
50.05..	28wc	*Ca–Co*
51.46..	0	.....
52.27..	7	*V*
Structure.	.....	.....
54.96..	0	*Co*
55.61..	4	*Ca*

TABLE 1—*Continued*

λ	*i*	Identification	λ	*i*	Identification
Structure			6508.16	5	*Ti*
6456.38	0	*Fe*+?	08.90	3	*Ca*
57.83	Wr		09.79	0	⊙–
58.24	Wv		10.56	0	
58.50	1w	⊙?	11.14	0	
59.15	0	Atm?	11.84	Wv	
60.84	0	Atm?	12.28	2Wc	Atm wv?–
62.65	25	*Ca–Fe*	12.80	Wr	
64.69	5	*Ca*	13.20	0?	
65.75	0	Atm?	14.16	0?	Atm wv?
66.97	5h	*V Cr*(p)	14.71	Wv	
69.12	5	*–Fe*	14.99	3wvc	Atm wv
71.62	10	*Ca*	15.28	Wr	
73.38	BdRv	*ZrO*	16.10	3w	*Fe*+ Atm wv?
75.62	9	*Fe*	17.03	2w	Atm wv
78.83	1w		18.46	7	*Fe* Atm wv?
79.05	Wr	*CN*?	19.47	Wv	
81.91	10	*Fe*	19.81	2rw	Atm wv
82.79	7	*Ni*	21.04	1w	
83.59	Wv		22.62	Wv	
83.83	4r	Atm wv *Fe*(p)	22.90	2r	Atm wv?
Structure			23.61	Wv	
84.95	0w	Atm wv	23.85	2r	Atm wv
86.17	Wv		24.66	Wv	
86.41	1r	–Atm wv?	24.96	1r	
88.75:	0w	*ZrO* ?	25.98	0w	
89.61	0w	Atm wv, *Zr*	27.07	6rv	⊙?–⊙?
90.31	2w	⊙?–*ZrO*?	28.62	0r	*Fe–*
91.66	2	*Mn*	29.42	0	
93.78	8	*Ca*	30.22	0	
95.00	15	*Fe*	31.42	7h	*V*
95.56	2h	*ZrO–ZrO*	32.90	6h	*Ni*
96.48:	3	*Fe*	33.96	4	*Fe*
96.90	18	*Ba*+	36.33	Wv	
97.53	Wr			2r	–Atm wv
97.72	3	*Ti*	37.93	6h	*Cr*
98.97	12	*Fe*	Structure		
99.70	5	*Ca*	40.11:	0w	
99.93	Wv		41.07:	Wv	
6501.21	6R	*Cr*	41.30:	3r	
Structure			42.80	0	*Sa*+
02.33	0h		43.48	4h	*V*
03.40	0h		46.25	12	*Fe Ti*
04.20	5r?	*V Sr*	47.23	Wv	
05.23	Wv		47.81	4Wcd	–Atm wv
05.43	3r	*ZrO*	48.41	Wr	
06.14	Wv		49.36	Wv	
06.39	3rc	*Zr*	49.93	4Wcd	*–Sr*
07.17	2	⊙? *ZrO*?	50.49	Wr	
07.91	Wv	*ZrO*	51.59	10	–⊙?

TABLE 1—*Continued*

λ	*i*	Identification	λ	*i*	Identification
6552.84..	w	*Fe*(K)–	75.02..	10	*Fe*
54.21..	10	*Ti*	76.47..	4hw	Atm wv–⊙
56.01..	13	*Ti*	77.78..	1hw	*Fe*(K)
58.06..	2rv	*V V*	78.94..	3hw	*V*
59.30..	Wv	.....	81.13..	13	*–Fe*
59.63..	4R	*Ti*+?	82.62..	Wv	.....
61.86..	Wv	.....	86.30..	5	*Ni Fe*(K)
**62.69..	150Wc	*Hα*	89.14..	0Wvr	Atm wv
63.44..	Wr	.....	91.41..	0wc	*–Fe*
65.36..	Wv	.....	92.89..	12	*Fe*
65.72..	4rc	*Ti*?–*V*? Atm	93.91..	10	*Fe*
66.47..	Wv	.....	95.16..	0h	*–Ti*?
66.70..	3w	*–Fe*	96.08:.	0h	.....
69.16..	7hv	*–Fe*	97.54:.	1h	*Fe*
70.01:.	0	.....			
70.70..	Wv	.....			
70.99..	4hwr	–Atm wv–			
71.34..	Wr	.....			
72.73..	15	*Ca*			
74.16..	12	*Fe*			

NOTES TO TABLE 1

λ 3600.77. Wave length is from Plate 1096, but intensity is from Plate 240W.

3818.29. Laboratory wave lengths and intensities are: .24 (60) *V*, .34 (60) Y^+, and .48 (8) *Cr*.

3830.72. One angstrom wide.

3870.0. Measured on enlargement.

3894.06. Note in measuring-book: "With sharp emission edges."

3930.3. In wing of K line.

4063.58. 8 rv on Plate 1096.

4077.68. 15 on Plate 1096.

4124.87. Gradually fades into background.

4144.04. Duplicity doubted. At λ 4143.83 (8rv) on Plate 1096.

4189.47. From λ 4189 to λ 4197.1, lines are all hazy, as if in wing of strong line or molecular absorption.

4198.33. 10 on Plate 654III.

4212.58. Strong general absorption from λ 4212.58 to λ 4216.47 with atomic lines superposed. Estimated intensities probably all too small.

4215.50. 20 on Plate 1096.

4216.94. Moderately strong general absorption from λ 4216 to λ 4219.

4257.23. Probably a blend of λ 4257.11 8wH . . . . and λ 57.34 7H *V* in Arcturus.

4269.38. Lines from λ 4269.3 to λ 4270.5 appear to be in wing of strong line.

4282.39. A *Ti* line must fall between λ 4282.39 and λ 4282.89, but it apparently went unnoticed.

4325.76. 22rv on Plate 654III.

4340.32. 25rv on Plate 654III.

4375.84. 20 on Plate 654III.

4412.16. 16wd? on Plate 9378.

4427.32. 45 on Plate 9378.

4435.09. 30 on Plate 9378.

4464.43. Structures around λ 4465 are peculiar.

4471.90. Bandlike edge measured also on Plate 9378 at λ 4471.94.

4483.38. Reality of line in doubt.

4484.94. 1 on Plate 9378.

4516.37. 4 on Plate 9378.

NOTES TO TABLE 1—*Continued*

λ4540.49. Structure fades into continuous background at λ 4541.7.

4626.25. 30W on Plate 12^2.

4639.22. Measured violet and red edges of absorption region having intensity 25.

4744.91. Intensity estimated on enlargement.

4803.90. Intensity estimated from enlargement.

4873.16. Uniform absorption up to line at λ 4875.44.

4934.08. About one-half as wide as *Hβ*.

4937.20. Structural details in strong absorption are barely resolvable.

4985.39. Moderate absorption to λ 4987.82.

5099.28. Called "condensation" in observing-book.

5147.48. Note in observing-book: "Probably coincides with band head."

5149.96. At least three *MgH* lines contribute here.

5156.67. Microphotometer tracing of this line would probably look something like this:

Vertical line indicates setting of micrometer wire for measurement.

5168.93. Followed by a definitely band like structure. Broad absorption reaches to next line.

5189.66. Much stronger in Antares than in Arcturus.

5211.26. Position of center of gravity, while geometrical center is at λ 5211.31.

5470.60. Moderate absorption between λ 5470.60 and λ 5471.20.

5502.06. Position of center of gravity, while geometrical center is at λ 5502.14.

5517.14. Question mark following $\underline{V}$ in solar spectrum has been retained.

5640.51. Mean of two sets of settings.

5708.24. There is absorption between λ 5708.24 and λ 5708.92 and λ 5709.50.

5772.38. Examined closely on enlargements. Relative intensities of components are exactly reversed on going from Arcturus to Antares.

5771.61 Faint line observed only on Plate $650.^3$

5797.68. General absorption extends from λ 5797.68 to λ 5798.68.

5828.83. From here on, the structure seems to resemble faint structure in comparison spectrum presumably due to *FeO*.

5862.44. General absorption from λ 5862.44 to λ 5864.52.

6005.61. Intensity of background gradually decreases until line at λ 6005.61.

6068.60. Nothing conspicuous for twelve angstroms. A few slight broad regions of absorption were observable and were recorded. There are no lines in the sunspot spectrum for 11 angstroms.

6127.43. Followed by wide absorption which gradually fades out at λ 6128.58 or λ 6130.50.

6136.72. Possibly a double line.

6240.07. In Arcturus intensities of the four lines causing this bandlike structure increase from violet to red.

6368.24. For 10 angstroms, settings were made on the red boundaries of bandlike structures degraded to the violet. They are probably due to clustering of *CaH* lines.

6378.63. After this line, intensity gradually fades into the background.

6432.51. Intensity gradually decreases from λ 6432.51 to λ 6434.02.

6562.69. Intensity could be estimated only roughly. Absorption in *Hα* is so strong that the plate is clear for the whole width.

THE 82-INCH MIRROR OF THE McDONALD OBSERVATORY*

J. S. PLASKETT

ABSTRACT

Visual tests of the 82-inch mirror made at the center of curvature give a maximum departure of only 0.7 millionths of an inch (0.02 μ) from the true paraboloid. The photographic Hartmann test gave slightly larger departures, but this is caused by the greater accidental errors of the measures. The Hartmann criterion T equals 0.05. The zonal aberrations are all satisfactorily small, and there is no measurable astigmatism.

The Warner and Swasey Company, who have designed and constructed the mechanical parts of the Lick, Yerkes, Victoria, and other large telescopes, have never undertaken, until the contract for the McDonald Observatory was signed in 1933, to supply the optical parts for their instruments. The deaths of Dr. Brashear and Mr. McDowell, who had in recent years provided the optical parts required, and the desire to make the complete telescope were probably the main reasons inducing this famous firm of telescope-builders to include an optical department in their organization. This was established in 1933 under the direction of Mr. C. A. R. Lundin, who had previously acted as chief optician for the well-known firm of Alvan Clark and Sons.

The optical shop was fitted with a grinding and polishing machine for the 82-inch mirror and with a smaller machine for a $57\frac{1}{2}$-inch flat to be used in testing the 82-inch. Work on the latter and on some smaller jobs occupied the time until the arrival of the 82-inch disk from Corning in October, 1934. Grinding was commenced on October 19, 1934; and nearly four years later the mirror was completed, on October 14, 1938. The figuring was not, however, continuous throughout the period, as in the hope of early completion the figuring with the full-size tool was unfortunately continued so far that, early in 1937, the focal length became too short. Even though the parabolizing was nearly completed and the reduced focal length was within the range of adjustment provided in the mounting, neither the

* *Contributions from the McDonald Observatory, University of Texas*, No. 1.

firm nor Mr. Lundin was willing to allow such a departure from the specifications. It required several months' work with the large tool to flatten the curve sufficiently, so that the final figuring—for the earlier close approach to the paraboloid was wiped out in the flattening process—did not begin until October, 1937. Twelve months can hardly be considered an unduly long time to figure an optical surface of this size in a newly established shop.

Early in 1936 I was asked by the Warner and Swasey Company to act as consultant in optical and other scientific matters connected with their instrument work, and in 1937 I visited Cleveland twice—once in May during the flattening process and later, in October, after the commencement of the refiguring. I was summoned again in March, 1938, when it seemed desirable to make a change in methods and remained, with two intermissions, consulting with Mr. Lundin until the mirror was completed on October 14.

During a visit, late in March, of Dr. Struve, the director of the new observatory, and two associates—Dr. Van Biesbroeck and Dr. Kuiper—a different method of testing was proposed, depending on measurements at the center of curvature from which a "curve of shape" was developed, the purpose of which was to give the true form of the surface with exact numerical values of the deviations from the paraboloid. The results from this method, which was extensively used and which will be more fully discussed later, were, however, at first disappointing; and early in May the $57\frac{1}{2}$-inch flat, which had been given a very fine figure by Mr. Lundin a year earlier, was silvered and thereafter was used as the principal means of testing the surface of the 82-inch mirror.

It may safely be said that, after the flat was set up and the shadow pattern at the focus could be observed—the method which Mr. Lundin had always hitherto used in figuring mirrors—the progress toward the final result was steady, if not quite continuous. As is probably the case with all optical work, especially large surfaces, various difficulties and occasional setbacks were encountered. It may be sufficient to mention first a sharply turned-up edge—much preferable, however, to one turned down—which required considerable handwork with small tools to reduce, at which Mr. Lundin is remarkably expert. A second difficulty was irregularity and lack of

general smoothness over the surface, a problem completely solved by substituting for the full-size tool a half-size tool, with a long sweeping stroke.

The final figure came quite rapidly at the last, as can be seen in the graphs in Figure 2, where the units are millionths of an inch and where the curves of shape of September 24, when the half-size tool had barely come into use, and those of the final week of figuring are given. Dr. Struve and Mr. Fred Pearson, of the University of Chicago, paid a visit of inspection on October 6, when, under the knife-edge test at the focus, the figure looked so smooth and uniform that they adjudged it as nearly finished. However, tests at the center of curvature next morning and formation of the curve of shape showed it as still undercorrected to the extent of twenty-millionths of an inch, a whole wave, and work was continued. Progress on one day enabled an estimate of the required time of polishing to be accurately made, and on this basis the paraboloid was considered completed on October 12, when the curve of shape showed deviations only slightly larger than a millionth of an inch, an eighteenth of a wave. Tests at the focus showed a high central zone, which Mr. Lundin reduced to practical invisibility in four short hand workings on October 12 and 13. The mirror was inspected and accepted by Dr. Struve on October 15 and was then made ready for aluminizing, necessary to make the Hartmann test and to figure the secondaries. The mirror was taken out of the vacuum chamber on October 24 and set up in the optical shop, where the visual and photographic tests were completed.

VISUAL TESTS OF THE 82-INCH MIRROR

The method of testing the surface, from the beginning of the parabolizing until last April, was a modification of the well-known method of determining the center of curvature of a number of zones spaced uniformly over the surface and comparing these measured positions with those computed from the properties of the parabola. A cardboard diaphragm was placed in front of the mirror, containing twenty-eight circular 1.5-inch holes, spaced uniformly along a horizontal diameter at a separation of 2.5 inches. The innermost zone, No. 14, has a radius of 7.75 inches; and the outermost, No. 1, of 40.25 inches. A series of shutters before the openings, manipulated by a rod extending through a partition, enabled the zones to be opened at will without going near the mirror. The intersection of the

converging pencils from a *fixed* artificial star was determined at first by an eyepiece and later, more accurately, by a knife edge. Obviously, in this case, the departures of the intersections from the computed positions are double those of the radii of curvature and four times those at the principal focus.

The knife edge is attached to a slide moved parallel to the optical axis by a screw, the positions of intersection being obtained by lines scribed against a straight edge on a stationary aluminum plate,

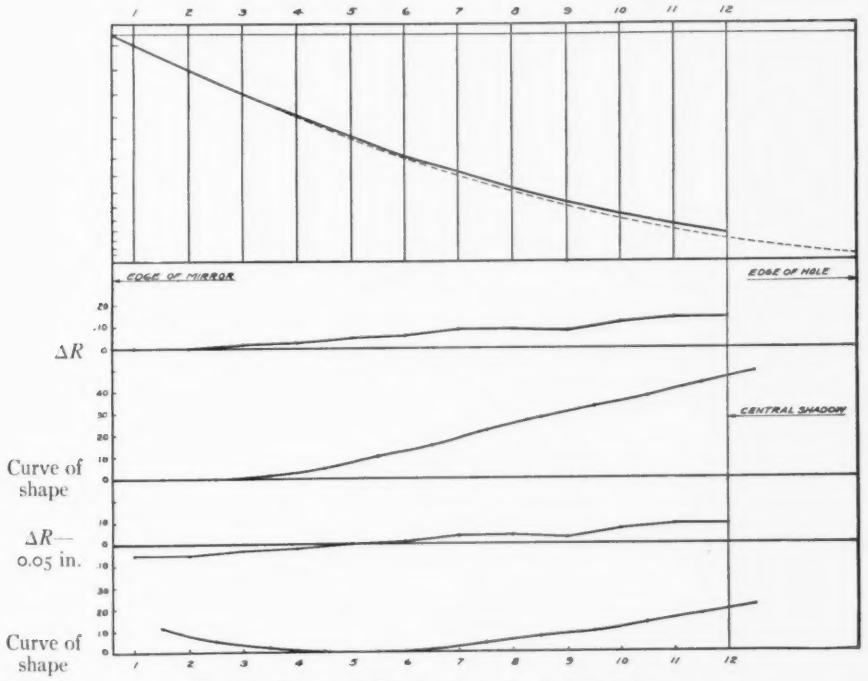

FIG. 1.—Curves of October 5, 1938—82-inch mirror

rigidly attached at right angles to the slide. The positions of the intersections were either directly compared with a standard series in the computed positions, or later, as the mirror approached completion, the separations of the scratches were accurately measured by dividers on a steel scale. A modification developed by Mr. Burrell consisted in plotting the positions of the zonal openings as abscissae and the distances of the corresponding intersections from that at the center of the mirror as ordinates. The method is illustrated in the upper part of Figure 1, containing the measures of October 5, plotted

as a curve which can be directly compared with a normal parabolic curve drawn in a dotted line through the computed positions. Blueprints were made of the fixed parts of this diagram, and the observed curve could be rapidly laid down on one of these prints from the scratches on the plate, the positions of longer radius being above and of shorter radius below the standard curve. The curve was at first considered as indicating where glass should be removed instead of showing where the surface was too flat or too concave.

It was the purpose of the curve of shape proposed[1] by Dr. Struve, Dr. Van Biesbroeck, and Dr. Kuiper to overcome this difficulty and to represent graphically the actual form of the surface and the exact deviations from the paraboloid. The method is simple, the tilt of the element of the surface 2.5 inches wide, centered on any zonal aperture, being determined from the deviation of the intersection of the corresponding pencils from the computed position. The departure of the ends of this element from the paraboloid is thus obtained; and joining these ends together—in other words, algebraically summing the departures consecutively across the surface—gives its true form, the factors being so chosen that the departures of the intersections from normal, hereinafter called ΔR, in hundredths of an inch, correspond to millionths on the curve of shape and on the surface.

Unfortunately, this method is also subject to ambiguity, particularly at the edge of the mirror, as the curve only begins to give reliable information halfway between zones 1 and 2; furthermore, the general slope depends upon the choice of zero, or the starting-point of the measures. This latter point is illustrated in the central part of Figure 1 in the measures of October 5. The deviations of the intersections plotted at the top of the figure with respect to the parabolic curve are repeated directly below, but on a different scale, in the broken curve drawn with respect to a straight-line base. These deviations, in hundredths of an inch, are transformed into the smooth curve of shape immediately below, showing deviations from the paraboloid in millionths of an inch. In the lower pair of curves the broken curve is exactly the same as above except that 0.05 inches is

[1] See, e.g., Danjon and Couder, *Lunettes et télescopes*, p. 517, Paris, 1935; *Amateur Telescope Making*, p. 260, 1933.

subtracted from each measure, or the base line is lowered by 0.05 inches. The curve of shape, however, is quite different, as not only is the slope radically different, indicating an alternative method of reaching a parabola of slightly different focus by removing glass both at edge and center instead of the center only, but also the average curvature is changed. Notwithstanding these difficulties, which rapidly diminish as the paraboloid is approached, the method is of distinct value in representing the exact form of the surface and in giving numerical values of the departure from the theoretical curve. As will be seen below, it was used extensively in the final tests.

As soon as shadow tests at the focus were available, early in May, they were used exclusively as a guide for the next working, as there was then no chance of ambiguity in the readings and the high zones could be accurately located and marked. The knife-edge shadow tests were supplemented and confirmed by the use of a Ronchi plate, where the condition of the surface was shown by the straightness and parallelism of the resultant bands. Measures at the center of curvature were transformed into curves of shape for Dr. Struve about once a week as a numerical record of progress until toward the end of the parabolizing, when it was felt desirable to check the shadow readings by measures at the center of curvature and by the formation of the curve of shape. For the last ten days or so, this was done after every polishing, as, although the shadow test recognizes very minute departures from regularity of figure, it is perhaps not so sensitive to very gradual changes such as those due to slight under- or over-correction.

This was especially true in this instance, where the flat was a little over two-thirds the size of the 82-inch, of which, hence, only a little over half, or just beyond the central hole, could be seen, and consequently the exact position of the knife edge, its exact focusing, was uncertain, with resultant effect on the shadow pattern. As a result, though the shadow test was essential throughout to insure smoothness and regularity of figure and to determine where polishing was required, the final check on complete parabolization depended upon careful measures at the center of curvature and the resultant curve of shape. These were of great value during the last week of figuring, where the proper length of time for the next polishing was deter-

mined solely from past changes in the curve of shape. Thus, on October 11 (see Fig. 2) the time required to complete the parabolizing, $1\frac{1}{2}$ hours, was gauged correctly, as seen in the lowest curve, from the change produced by the two previous workings. And here again, the shadow test was essential, for otherwise the high central zone, which had no effect on the measures at the center of curvature, would have escaped notice and correction.

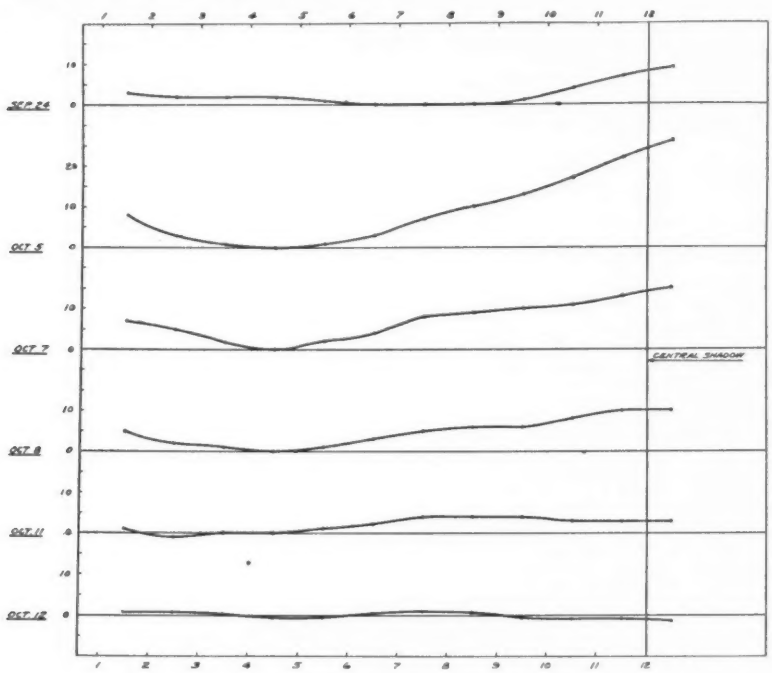

FIG. 2.—Curves of shape of 82-inch mirror

It was considered sufficient in the previous measures at the center of curvature to make two independent sets of measures, one each by Mr. Lundin and myself, as there was rarely a greater difference in the knife-edge settings between the two than 0.02 or 0.03 inches. But when it came to the final determination of October 12, it was considered advisable to increase the number of sets to two each, and these were further added to in three later determinations to make three each, thus making altogether twenty-two measures of the intersections of each of the twelve zones, the measurement of Nos. 13 and

14 being omitted, as they are permanently within the shadow of the center piece carrying the secondary mirrors.

The focal length of the completed mirror was carefully measured before the reductions of the final measures, as 319,656 inches, or 811.928 cm; and with this focal length the positions of the intersections of the twelve zones used in the visual tests and the fifteen in the Hartmann test were computed anew, and are given in Table 1. On the left-hand side the units are inches and on the right centimeters, as the separation of the zones, which are those of the diaphragm used

TABLE 1

POSITIONS OF INTERSECTIONS

(Max. Diam., 0.025 Mm)

Zone	Radius of Zone (In.)	Diff. Radius (In.)	Zone	Radius of Zone (Cm)	Diff. Radius (Cm)	Hartmann Meas.		Mean Astigmatism (Mm)
						ΔR	ΔF	
1.....	40.250	2.539	1....	101.5	6.365	−0.32	−0.08	+0.11
2.....	37.711	2.229	2....	97.	5.808	−0.11	− .03	+ .06
3.....	35.211	1.942	3....	92.	5.224	+0.36	+ .09	− .03
4.....	32.721	1.677	4....	87.	4.653	−0.11	− .03	+ .04
5.....	30.227	1.431	5....	82.	4.149	−0.15	− .04	− .01
6.....	27.736	1.204	6....	77.	3.658	−0.16	− .04	− .02
7.....	25.231	0.996	7....	72.	3.206	−0.12	− .03	+ .07
8.....	22.727	0.809	8....	67.	2.776	−0.17	− .04	+ .08
9.....	20.231	0.641	9....	62.	2.374	+0.13	+ .03	+ .01
10.....	17.738	0.492	10....	57.	2.007	−0.72	− .18	+ .01
11.....	15.217	0.362	11....	52.	1.671	−0 22	− .06	+ .01
12.....	12.744	0.254	12....	47.	1.363	+0.15	+ .04	− .02
13.....	10.277	0.165	13....	42.	1.090	+0.24	+ .06	+ .08
14.....	7.720	0.093	14....	37.	0.846	+0.62	+ .15	− .10
Center..	0	0	15....	32.	0.632	−1.34	−0.33	−0.06

in the Hartmann test, and the pitch of the screw used in measuring the photographs are given in these units. The recomputation was necessary, as the difference between these positions and those for the focal length of 320 inches amounts to 0.005 inches, or 0.12 mm, which is quite significant with so good a mirror as the 82-inch.

The visual measures of the intersections of the pencils from the various zones were made on October 12 and October 14, immediately after the parabolizing was completed, and again on October 25 and November 1 after the mirror was aluminized. There were four independent sets of measures on October 12 and six each on the other

three dates, equally divided between, and alternated by, Mr. Lundin and myself. The separation of the scratches was measured by dividers on a steel rule divided into fiftieths and hundredths of an inch. These measures, or rather the differences between the observed and the computed positions, ΔR, are given in thousandths of an inch, for, although in a single setting three places are not significant, they more nearly approach it in the mean of four, and still more of six settings. The probable errors of the mean of six settings is 0.0022 inches for the outer four zones, 0.0033 for the intermediate, and 0.0043 inches for the inner four zones.

The results of these four measures are given in Table 2, where the first column contains the zone number, the second and third and the succeeding three pairs of columns give the ΔR's, the difference between the observed and computed positions of the zonal intersections, and their transformations into the curve of shape for the four dates. It will be noted that the values of ΔR, which, it must be remembered, are expressed in thousandths of an inch and are four times the longitudinal aberrations at the principal focus, vary somewhat on the different dates, being lower on October 12 and 25 than on October 14 and November 1. While the accidental errors of the means of the sets, varying from ± 0.002 to ± 0.004 inches, and increasing from edge to center of the mirror, may account for a considerable fraction of the variation, there may be something systematic about the differences, such as temperature variations on the different dates, or change of figure produced by irregularities in the thickness of the aluminum coating.

So far as the latter effect is concerned, it may be dismissed as negligible, as there is no appreciable systematic difference in the run of the ΔR's before the coating, on October 12 and 14, and after it, on October 25 and November 1. There may be, however, some evidence of a temperature effect on the figure of the 82-inch mirror. On October 12 and 25, when the variations in the ΔR's were somewhat smaller than in the other two measures, the decrease in temperature, taken from a thermograph near the mirror, between midnight and the time of the tests, about 11:00 A.M., was $1^{\circ}.2$ F, while on October 14 the change was 2° F. However, on November 1 the

temperature was constant within 0°.3 F, so that, on the whole, a variation of figure with small temperature changes is not demonstrated.

We may, hence, consider that the variations in ΔR are mainly accidental and use the mean values of the 22 different settings as best representing the figure of the mirror, and these means are given in the last three columns of Table 2. The mean ΔR's are all remarkably small, less than 0.004 inches, or 0.001 inches at the principal focus,

TABLE 2

VISUAL MEASURES OF ΔR

(Max. Diam., 0.014 Mm)

Zone	Oct. 12		Oct. 14		Oct. 25		Nov. 1		Mean ΔR	Mean Curve	ΔF at Focus (Mm)
	ΔR	Curve	ΔR	Curve	ΔR	Curve	ΔR	Curve			
1	+0.006	+0.7	−0.001	+0.1	+0.001	−0.1	0.000	0.0	+0.0035	−0.4	+0.02
2	− .001	+0.6	.000	+0.1	− .002	− .4	− .003	−0.3	.0000	− .4	.00
3	− .005	+0.2	− .001	0.0	− .001	− .6	+ .001	−0.2	.0000	− .4	.00
4	− .007	−0.4	+ .005	+0.5	.000	− .6	− .008	−1.0	− .0022	− .5	− .02
5	− .003	−0.5	+ .003	+0.8	− .003	− .9	− .003	−1.3	.0000	− .5	.00
6	+ .011	+0.6	+ .011	+1.7	+ .013	+ .2	+ .009	−0.5	+ .0125	+ .6	+ .08
7	+ .003	+1.0	− .001	+1.6	+ .004	+ .4	+ .020	+1.0	+ .0008	+ .7	+ .01
8	+ .001	+0.7	− .016	+0.5	+ .002	+ .5	+ .004	+1.1	− .0015	+ .6	− .01
9	− .025	−0.7	− .023	−1.2	− .006	+ .1	− .023	−0.3	− .0190	− .6	− .12
10	− .004	−0.8	− .017	−2.1	+ .004	+ .3	+ .009	+0.2	− .0005	− .6	.00
11	− .004	−0.8	+ .007	−1.8	+ .008	+ .6	+ .014	+0.8	+ .0078	− .2	+ .05
12	−0.019	−1.4	−0.003	−1.9	+0.010	+0.6	+0.012	+1.5	+0.0015	−0.2	+0.01

except for zones 6, 9, and, to a smaller extent, 11. These indicate only a very small deviation from a perfect figure, the maximum longitudinal aberration at the principal focus in the last column being 0.005 inches, or 0.12 mm, as compared with the 0.4 mm allowed by the specifications. The total area of the three divergent zones is only 15 per cent of the area of the surface, so the effect on the resultant image will be small. The maximum diameter of the circle of confusion, computed geometrically from the largest longitudinal aberrations, is 0.014 mm, as compared with the 0.05 mm of the specifications. Furthermore, 85 per cent of the light is concentrated in a diffusion disk of an average diameter less than one-third the foregoing.

The ΔR's from Table 2 are represented graphically in Figure 3, the scale divisions being in hundredths of an inch, although numbered in thousandths (these being used rather than millimeters since all the measures were more conveniently made in those units). The curves of shape computed from these ΔR's are given immediately be-

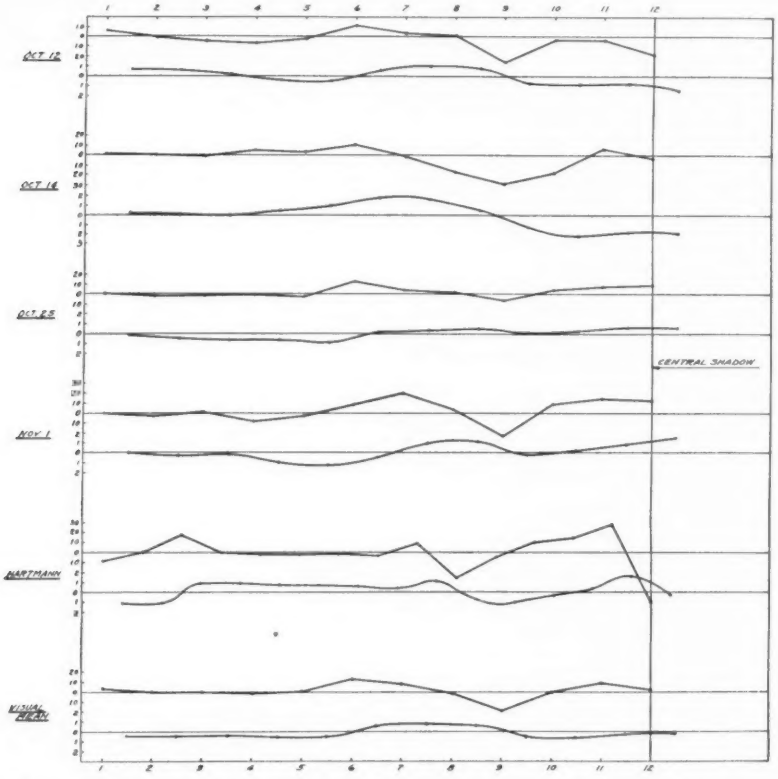

FIG. 3.—Final test of 82-inch mirror. The upper curve of each set of two gives ΔR's; the lower is the curve of shape.

low each curve of ΔR, the units here being millionths of inches. It will be noted that the maximum departure from the mean paraboloid in the lowest curve is 0.0000007 inches, considerably less than a twentieth of a wave.

THE HARTMANN TEST

There remains one further test of the surface, the well-known Hartmann test, which was requested by the purchasers early in the

negotiations, the diaphragm being made according to their specifications. The latter contains sixty holes, each about 38 mm in diameter, spaced along twelve radii 30° apart. The holes cover fifteen zones of the surface twice, the two sets being 90° apart to determine the astigmatism. The radii of the zones are given in Table 1 in centimeters, successive zones being 5 cm apart except that the distance between No. 1 and No. 2 is 4.5 cm. This diaphragm was placed directly over the aluminized mirror, which rested on the table of the polishing machine and was turned into a vertical position for both visual and photographic tests.

Several precautions were taken to insure reliable results on these tests. The principal difficulty encountered in my earlier tests of the 72-inch Victoria and the 69-inch Delaware mirrors had been temperature stratification in the Brashear testing chamber. This difficulty was much less troublesome at Cleveland, owing to the better temperature correction and to the tests being made in an open room instead of the closed 6-foot square tube at Allegheny. Nevertheless, it was still present, as the images of the zonal apertures on the plates were all elongated in the vertical direction. To overcome as much as possible such temperature difficulties, the mirror was always kept horizontal, except for the few minutes the photograph was being made, so that it must have been at practically constant temperature throughout. Four exposures were made in each set, the mirror being rotated 90° each time, so that the longitudinal aberrations and the astigmatism could be tested not only from the two sets of apertures on each plate but also from the horizontal sets only, on successive plates, in the hope of overcoming stratification effects.

Two of the three sets of four exposures were made only on plates outside the focus, as in this case the separation from the optical axis need be only 0.5 inches, about 2.5 minutes of arc, where coma would be very small. In the third set, exposures were made both inside and outside the focus, where the distance from the axis was twice as great and possibly with appreciable coma in an f/4 mirror. Notwithstanding these precautions, the results were disappointing, the photographic measures being much less accordant than the visual. The set yielding the most satisfactory results and the one fully measured was the first made with shorter exposures, the images on

the plates being much smaller and less distorted than the longer exposures and, hence, more easily bisected in the micrometer microscope.

The four plates yielded four determinations of the ΔR's and four of the astigmatism. The average probable errors of the mean values, which, unlike the visual settings, did not increase in the inner zones, was ± 0.21 mm, which, compared with the visual average of ± 0.082, makes the photographic probable error over 2.5 times greater than the visual. The values of the photographic ΔR's and of the longitudinal aberrations at the focus are given in the seventh and eighth columns of Table 1. These, reduced to the same scale as those of the visual tests, are shown graphically in the fifth group of Figure 3. Although these show a trend similar to the visual graphs, they are naturally, owing to the higher probable errors, considerably more ragged and are entitled to considerably less weight.

The principal value of the photographic method is its definite test of the presence of astigmatism. The mean differences between the longitudinal aberrations at the principal focus in two azimuths on the mirror 90° apart are given in the last column of Table 1. If not wholly due to accidental errors, as seems likely from those determined above, there is certainly no systematic trend of the signs, the algebraic mean being only $+0.02$ mm, and it may be safely said that the surface is free from astigmatism.

The Hartmann[2] criterion T, obtained from the formula

$$T = \frac{200{,}000}{F_0^2} \cdot \frac{\Sigma r^2 \Delta F}{\Sigma r},$$

where F_0 is the focal length, ΔF the longitudinal aberration at the principal focus, taken without regard to sign, and r the radius of any zone, simply gives the weighted mean value of the diameter of the geometrical confusion circle expressed in terms of $F_0/100{,}000$, while $2.0626T$ is its apparent diameter in seconds of arc. The values of T were computed for each of the four visual measures and for the single photographic test, and are given in Table 3. This was done for completeness only, as the value of T obtained from the mean of the twenty-two visual measures of ΔR at the center of curvature (given

[2] *Zs. f. Instrumentenkunde*, **24**, 1, 33, 97, 1904.

in the last line of Table 3) is obviously of much greater weight and is taken as more truly representing the optical qualities of the mirror. The maximum diameter of the diffusion disk was calculated above as 0.014 mm, less than one-third the 0.05 mm permitted by the specifications, but is nevertheless nearly four times larger than the average diameter of 0.0039 mm in the last line of Table 3. There is, however, such a small proportion of the total light entering into this expanded disk that, in comparison to the central condensation, it will be quite inappreciable.

TABLE 3

RESULTS OF TESTS

KIND OF MEASURE	DATE	NUMBER OF MEASURES	HARTMANN T	WEIGHTED DIAMETER OF GEOMETRICAL DIFFUSION DISK	
				Millimeters	Seconds
Visual	Oct. 12	4	0.080	0.0064	0.17
Visual	Oct. 14	6	.070	.0052	.14
Visual	Oct. 25	6	.042	.0032	.09
Visual	Nov. 1	6	.085	.0068	.18
Photographic	Oct. 26	4	0.100	0.0078	0.21
Mean of all visual measures		22	0.050	0.0039	0.10

It will be of interest to compare the optical qualities of the 82-inch mirror with those of other large reflecting surfaces which have been similarly tested. For this purpose the criterion T forms the best guide, as the errors or aberrations and the diameter of the geometrical diffusion disks are directly proportional to T. The following list comprises all those known to me, as the Mount Wilson 60- and 100-inch mirrors have had, to the best of my knowledge, no measures of their aberrations published.

72-inch Victoria mirror* ..... $T=0.12$
69-inch Delaware mirror† ..... $T=.14$
74-inch Toronto mirror‡ ..... $T=.20$
82-inch Texas mirror ..... $T=0.050$

* Computed from the aberrations published in *Pub. Dom. Ap. Obs.*, **1**, 41, 1920.

† *J. Opt. Soc. Amer.*, **23**, 293, 1933.

‡ *Pop. Astr.*, **44**, 349, 1936.

Not only has the Texas mirror much smaller measured errors than any other, but such a relatively large proportion of the figuring was performed with large tools that the surface must be remarkably smooth and regular. This was indeed amply demonstrated by the Foucault and Ronchi tests, and it can be safely stated that the quality of the 82-inch mirror of the McDonald Observatory is unequaled by any mirror previously made and tested.

CLEVELAND, OHIO
November 1938

ON THE RELATIVE ABUNDANCE OF *CN*, C_2, *CH*, *NH*, AND *OH* IN THE SOLAR REVERSING LAYER

F. E. ROACH

ABSTRACT

The partition functions of all possible diatomic arrangements of *H*, *C*, *N*, and *O* are computed. From the partition functions and the observed solar intensities of rotational lines in the bands of *CN*, C_2, *CH*, *NH*, and *OH*, the values of log $S \cdot f$ are determined where S is the molecule's abundance and f is the absolute intensity factor. On the assumption that f is the same for all the molecules considered and is equal to 10^{-3}, values of log S are recorded. The values of log S of this paper are systematically higher than those of Russell, the difference increasing in the order *OH*, *NH*, *CH*, *CN*, and C_2, for which Δ log S (Roach *minus* Russell) is 1.1, 1.9, 3.9, 4.5, and 5.5, respectively.

From *CN* (λ 3883) the excitation temperature of the sun is found to be 5630° ± 500° K, and from *OH* (λ 3064), 4640° ± 550° K.

I. INTRODUCTION

In contrast with the extensive results on the relative numbers of atoms in stellar reversing layers, the present knowledge of their molecular composition is rather fragmentary. As a rule, the low dispersion necessarily used for the stars, in general, permits the study of unresolved bands only. On the other hand, with the high dispersion available for the study of the solar spectrum it is possible to examine the individual rotational lines of a band.

In his treatment of the molecular constitution of the sun's atmosphere, Russell[1] employed his own solution of its atomic composition. The dissociation equations for the several molecules then led to a predicted molecular content which was expressed as the logarithm of the abundance, S. For a comparison with this theoretical log S, the observational log S was evaluated as 3, 2, 1, or 0, according as the bands were conspicuous, medium, weak, or barely visible. This method will, at best, give only a qualitative check and may be misleading, since the intensity of a band line depends not only on the number of molecules of the kind in question but also on the absolute intensity factor of the transition, the number of energy-levels, their spacing, and the distribution of the molecules among them.

[1] *Ap. J.*, **79**, 317, 1934.

Concerning the absolute intensity factors of molecular transitions very little is known. The effect of the number and spacing of the energy-levels may be illustrated by a hypothetical example. Consider two molecules: A, with a high moment of inertia, and B, with a relatively low one. A will have rotational energy-levels close together; and the Boltzmann factor, $\exp - E/kT$, will not appreciably reduce the populations of the successive states until the higher rotational quantum numbers are reached. On the other hand, B will have its levels more widely spaced; and the molecules will, for a given temperature, be distributed among fewer levels. Thus, two lines of the same intensity, one due to A and the other to B, will indicate a greater total number of molecules of A than of B.

The purpose of the present paper is to develop a method for the evaluation of the abundance of molecules of a given kind in the solar atmosphere from the intensity of a *single* resolved rotational line. Application will then be made to the following molecules of astrophysical interest: CN, C_2, OH, NH, and CH. The outline of the procedure is as follows: (1) The development of the relationship between the population of a given level and the total number of molecules. (2) The determination, from line intensities, of the population of a given level. This involves the following steps: (*a*) The line intensity is expressed in equivalent milliangstroms. When Rowland intensities alone are available, Mulders'[2] calibration has been employed to express the intensities in the foregoing units. For wave lengths shorter than λ 3900 his calibration is extrapolated. (*b*) From the equivalent width, $N_J \cdot f$ is evaluated by Allen's[3] calibration, where N_J is the number of molecules instrumental in producing the line and f is the absolute intensity factor. (*c*) Since several branches (P, Q, R) may originate in a single level, it is necessary to make observations of all possible lines from this level to obtain $N_K \cdot f$. If this is not possible, the total population of the level may be calculated from the relative transition probabilities of the various branches. (3) By combining the results of (1) and (2), it is now possible to obtain $S \cdot f$, where S is the molecular abundance. (4) From the laboratory knowledge of the absolute value of f it would then be possible

[2] *Zs. f. Ap.*, **8**, 62, 1934.

[3] *Mem. Commonwealth Solar Obs.*, **5**, 22, 1934.

to determine S. The absolute value of f is known only for the case[4] of *OH;* so the final results for S are somewhat uncertain.

II. RELATION BETWEEN THE POPULATION OF A SINGLE ROTATIONAL LEVEL AND THE TOTAL NUMBER OF MOLECULES

The number of molecules, N_K, in a given energy-level, K, is given by

$$N_K = \frac{Sge^{-E_K/kT}}{\prod \sum_K ge^{-E_K/kT}} = \frac{Sge^{-E_K/kT}}{Z(T)}, \tag{1}$$

where the symbol $Z(T)$ is the partition function, g is the a priori probability of the state (or the degeneracy of the level), and S is the abundance of the molecule. The indicated product is to include all possible energy states—electronic, vibrational, and rotational—and nuclear spin. Since our problem is to evaluate S, we find

$$S = N_K \frac{Z(T)}{ge^{-E_K/kT}} = N_K \cdot G. \tag{2}$$

The calculation of the factor, G, is conveniently divided into the separate calculation of the partition function, which can be carried out for a given molecule from the molecular constants, and of the quantity $ge^{-E_K/kT}$ for the particular level, K.

The total partition function, Z, may be broken up into its components due to electronic, vibrational, and rotational energies and the nuclear spin.

$$Z = \sum_{\substack{\text{all electronic} \\ \text{levels}}} Z_r Z_v Z_e Z_n, \tag{3}$$

where[5]

$$Z_r = \sum_{J=0}^{\infty} g_r e^{-E_r/kT} = \sum_{J=0}^{\infty} (2J+1) e^{-\frac{J(J+1)B_v hc}{kT}} \cong \frac{kT}{B_v hc}, \tag{4}$$

[4] Oldenberg and Rieke, *J. Chem. Phys.*, **6**, 439, 1938.

[5] Cf. Mulholland, *Proc. Cambridge Phil. Soc.*, **24**, 80, 1928, for the approximation in eq. (4).

$$Z_v = \sum_{v=0}^{\infty} g_v e^{-E_v/kT} = \sum_{v=0}^{\infty} 1 \cdot e^{-\omega_e v hc/kT} = \frac{1}{1 - e^{-\omega_e hc/kT}}, \tag{5}$$

$$Z_e = (2\Lambda + 1)(2\Sigma + 1)e^{-E_e hc/kT}, \tag{6}$$

$$\left.\begin{aligned} Z_n &= (2S_1 + 1)(2S_2 + 1) \quad \text{for heteronuclear molecules,} \\ Z_n &= \frac{(2S+1)^2}{2} \qquad\qquad \text{for homonuclear molecules.} \end{aligned}\right\} \tag{7}$$

In the case of Z_e (Eq. [6]) there is another factor 2 for Λ-type doubling, for molecules in electronic levels Π and Δ.

The partition functions for all possible diatomic arrangements of H, C, N, and O have been computed from the molecular constants listed in Table 1. Since the factor due to nuclear spin appears in

TABLE 1

MOLECULAR CONSTANTS*

Molecule	Nuclear Spin†	Electronic Level	ω_e	B_v	E_e
C_2	0	$A^3\Pi$	1,641.55	1.6260	0
		$B^3\Pi$	1,792.55	1.7495	19,379.2
N_2	1	$X^1\Sigma_g^+$	2,359.6	1.989	0
O_2	0	$X^3\Sigma_g^-$	1,580.32	1.438	0
		$a^1\Delta$	(1,500)	1.407	7,881.6
		$A^1\Sigma_g^+$	1,432.615	1.392	13,121
H_2	1/2	$^1\Sigma_g^+$	4,276‡	59.354‡	0
CN		$X^2\Sigma^+$	2,068.79	1.8904	0
		$A^2\Pi$	1,788.66	1.6903	10,900
		$B^2\Sigma^+$	2,164.15	1.9590	25,797
CO		$X^1\Sigma^+$	2,168.89	1.916	0
CH		$X^2\Pi$	2,859	14.20	0
		$A^2\Delta$	2,800	(14.20)	23,163
NO		$X^2\Pi$	1,906.5	1.675	0
NH§		$A^3\Sigma$	(3,300)	16.33	0
		$a^1\Delta$	(3,060)	16.46	8,773
		$B^3\Pi$	(3,300)	16.29	29,750
OH		$A^2\Pi$	3,734.9	18.663	0

* From Sponer, *Molekülspektren*, Julius Springer, Berlin, 1935.

† Nuclear spin corresponding to the atom.

‡ ω_0 and B_0.

§ Constants for NH from Funke, *Zs. f. Phys.*, **96**, 787, 1935.

both numerator and denominator of the constant, G, it is convenient to record both the total partition function, Z, and the partition function without the nuclear spin factor, Z_0, in Table 2.

TABLE 2

SUMMARY OF PARTITION FUNCTIONS

Molecule		Temperature (°K)				
		3000	4000	5000	5500	6000
C_2	Z_0	42,500	69,360	102,800	122,700	143,800
	Z	21,250	34,680	51,400	61,350	71,900
N_2	Z_0	1,554	2,460	3,570	4,070	4,860
	Z	7,000	11,060	16,050	18,300	21,850
O_2	Z_0	8,771	16,400	27,620	34,590	46,030
	Z	4,385	8,200	13,810	17,290	23,010
H_2	Z_0	40	60	83	97	110
	Z	80	120	166	194	220
CN	Z_0	3,661	6,467	10,950	14,210	17,650
	Z	10,980	19,400	32,850	42,630	52,950
CO	Z_0	1,696	2,700	3,930	4,620	5,410
	Z	1,696	2,700	3,930	4,620	5,410
CH	Z_0	2,350	3,662	5,262	6,174	7,177
	Z	4,700	7,324	10,520	12,350	14,350
NO	Z_0	24,400	39,400	57,900	68,600	80,500
	Z	73,200	118,200	173,700	205,800	241,500
NH	Z_0	510	849	1,343	1,653	2,008
	Z	3,060	5,094	8,058	9,918	12,050
OH	Z_0	1,613	2,440	3,410	3,960	4,500
	Z	3,226	4,880	6,820	7,920	9,000

III. VALUES OF $N_K \cdot f$ AND $S \cdot f$ FROM OBSERVED LINE INTENSITIES

The application of the procedure outlined in the Introduction is illustrated in detail for *CN* in Tables 3, 4, and 5. In Table 3 are listed the resolved lines of the R_1 and R_2 branches of the λ 3883 band (0 — 0 vibrational transition, $^2\Sigma^+ \rightarrow {}^2\Sigma^+$ electronic). The wave lengths of column 3 are from Uhler and Patterson,[6] and the

[6] *Ap. J.*, 42, 434, 1915.

TABLE 3

CN LINES

Group	$J''-\frac{1}{2}$	λ (Lab.)	λ⊙−λ(Lab.)	Branch	R.I.
I	37	3839.141	0.000	R_2	1
	38	37.877	.013	R_1	0
	38	37.825	.000	R_2	0
	39	36.540	.013	R_1	1
	39	36.494	.009	R_2	1
	40	35.202	.005	R_1	0
	40	35.147	.016	R_2	0
	41	33.785	.000	R_2	0
II	44	29.588	.014	R_2	0
	45	28.211	.015	R_1	0
	45	28.155	.007	R_2	1
	47	25.307	.006	R_1	0
	47	25.239	− .001	R_2	0
	48	23.823	− .003	R_1	0
	48	23.760	− .001	R_2	0
	49	22.322	.008	R_1	0
III	49	22.259	.007	R_2	0
	50	20.807	.004	R_1	0
	50	20.746	.006	R_2	1
	51	19.278	− .003	R_1	1
	51	19.213	− .003	R_2	1
	52	17.732	.004	R_1	0
	53	16.101	.011	R_2	0.N
IV	57	09.755	.002	R_1	0
	57	09.690	.004	R_2	0
	59	06.440	.007	R_1	0
	60	04.696	.002	R_2	1
	61	03.013	− .002	R_2	0
V	62	01.308	− .003	R_2	0
	63	3799.663	.014	R_1	0
	64	97.852	.001	R_2	0
	65	96.184	.004	R_1	0
	65	96.104	.005	R_2	0
	66	94.417	.003	R_1	0
VI	67	92.639	.014	R_1	0
	67	92.565	.002	R_2	0
	69	89.040	.008	R_1	0
	69	88.968	.004	R_2	0
	70	87.228	.010	R_1	0
	71	85.390	.009	R_1	0
	71	85.319	.000	R_2	0
VII	72	83.465	− .001	R_2	−1
	73	81.685	.004	R_1	−1
	74	79.806	.004	R_1	0
	74	79.732	.001	R_2	0
	75	77.919	0.011	R_1	0

TABLE 3—*Continued*

Group	$J''-\frac{1}{2}$	λ(Lab.)	λ⊙−λ(Lab.)	Branch	R.I.
VIII	75	3777.842	0.006	R_2	0
	76	75.944	.007	R_2	−1
	77	74.107	.006	R_1	−1
	77	74.030	.005	R_2	−1
	78	72.180	.010	R_1	−1
IX	78	72.106	.000	R_2	0*N*
	79	70.169	.001	R_2	−1
	81	66.322	.003	R_1	−2*N*
	81	66.247	− .005	R_2	−1
	82	64.277	.009	R_2	−1
X	86	56.332	.009	R_1	−1
	86	56.263	.003	R_2	−1
	87	54.227	.000	R_2	−1
	88	52.258	.009	R_1	−2
	88	52.187	.006	R_2	−2
	89	50.206	.001	R_1	−3*N*
XI	89	50.134	.007	R_2	−2*N*
	92	43.980	.019	R_1	−2
	93	41.817	.018	R_2	−2
	96	35.444	.002	R_2	−2
	99	29.064	.010	R_2	−2*N*
	101	24.732	0.013	R_2	−1

TABLE 4

CN SUMMARY

GROUP	WT.	MEAN			log *EW* (MULDERS)	log $N_J \cdot f$ (ALLEN)	log *i*	log $N_J \cdot f/i$
		J''	E'' (cm^{-1})	R.I.				
I	8	39.5	3,024	0.38	1.34	0.87	1.60	−0.73
II	9	47.5	4,355	0.11	1.24	.70	1.68	0.98
III	6	52	5,210	0.50	1.38	.95	1.72	0.77
IV	5	59.5	6,805	0.29	1.30	.79	1.77	0.98
V	6	64.5	7,986	0.00	1.21	.66	1.81	1.15
VI	7	69.5	9,262	0.00	1.21	.66	1.84	1.18
VII	6	74	10,500	−0.33	1.08	.48	1.87	1.39
VIII	5	77.5	11,501	−0.80	0.90	.25	1.89	1.64
IX	4	81.5	12,711	−1.25	0.71	.02	1.91	1.89
X	7	88	14,808	−1.71	0.50	− .20	1.94	2.14
XI	5	96.5	17,786	−1.80	0.42	−0.28	1.98	−2.26

assignment of the J'' values (col. 2) is from Jevons.[7] The solar wave lengths for column 4 and the Rowland intensities (col. 6) are from the *Revised Rowland*. Because of the rough nature of the Rowland

TABLE 5

log $S \cdot f$ FOR CN

GROUP	log $N_K \cdot f$	log G AND log $S \cdot f$			
		$T = 4000$	5000	5500	6000
I	1.47	2.08	2.21	2.29	2.36
		3.55	3.68	3.76	3.83
II	1.30	2.21	2.30	2.36	2.42
		3.51	3.60	3.66	3.72
III	1.55	2.31	2.37	2.42	2.47
		3.86	3.92	3.97	4.02
IV	1.39	2.50	2.51	2.55	2.58
		3.89	3.90	3.94	3.97
V	1.26	2.65	2.63	2.65	2.67
		3.91	3.89	3.91	3.93
VI	1.26	2.82	2.76	2.76	2.77
		4.08	4.02	4.02	4.03
VII	1.08	2.99	2.89	2.87	2.87
		4.17	4.07	4.05	4.05
VIII	0.85	3.13	2.99	2.97	2.96
		3.98	3.84	3.82	3.81
IX	0.62	3.29	3.14	3.09	3.06
		3.91	3.76	3.71	3.68
X	0.40	3.59	3.35	3.30	3.25
		3.99	3.75	3.70	3.65
XI	0.32	4.02	3.68	3.59	3.52
		4.34	4.00	3.91	3.84
log Z_0		3.81	4.04	4.15	4.25
log $S \cdot f$ (weighted mean)		3.90	3.84	3.84	3.86

intensities, means by groups are assembled in Table 4. From the mean Rowland intensity of column 5, the logarithm of the equivalent width in milliangstroms is obtained from Mulders' calibration ex-

[7] *Proc. R. Soc.*, **112**, 407, 1926.

trapolated to λ 3800 (col. 6). Allen's data of log $N \cdot f$ versus log *EW* for λ 4000 were used to evaluate column 7.

The P_1 and P_2 branches of this band are not as readily observable as the *R* branches, because they are largely concentrated in the region of the band head. The theoretical values of the intensity factors were therefore computed from the formulae found in Jevons,[8] page 137. For the higher quantum numbers the four branches R_1, R_2, P_1, and P_2 comprise all of the transitions which must be considered. Each

TABLE 6

SUMMARY OF *OH* DATA (λ 3064 BAND)

GROUP*	WT.	MEAN			log *EW*	log $N_J \cdot f$	log *i*	log $N_J \cdot f/i$
		J''	E''	R.I.				
I	3	2.5	163.3	0.67	1.36	0.80	0.08	0.72
II	6	6	785	1.50	1.63	1.42	0.48	0.94
III	4	10	2,054	1.50	1.63	1.42	0.70	0.72
IV	3	13.5	3,658	1.33	1.59	1.30	0.83	0.47
V	4	18	6,390	1.00	1.50	1.08	0.96	0.12
VI	2	22.5	9,860	1.00	1.50	1.08	1.06	0.02
VII	2	24.5	11,670	−1.00	0.67	−0.11	1.09	−1.20
VIII	9	2.5	163.3	0.00	1.08	0.38	−0.22	0.60
IX	7	6.2	831	1.00	1.50	1.20	0.18	1.02
X	7	10.1	2,090	1.29	1.58	1.28	0.40	0.88
XI	8	14.4	4,150	0.50	1.29	0.69	0.56	0.13
XII	9	18.2	6,540	0.67	1.36	0.80	0.66	0.14
XIII	9	21.6	9,110	−0.33	0.95	0.21	0.74	−0.53
XIV	7	25.2	12,310	−0.29	0.96	0.22	0.81	−0.59

* Groups I–VII are based on the Q_1 and Q_2 branches; Groups VIII–XIV on the P_1, P_2, R_1, and R_2 branches.

branch is of practically the same intensity, so that the value of $N_J \cdot f$ obtained from a single line is converted into $N_K \cdot f$ for all transitions from a given energy-level by multiplying by a factor 4. Column 8 gives the logarithm of the factor, $gf = i$, which, together with the data in columns 4 and 9, is useful in temperature determinations.

In Table 5 the values of log *G* and finally log $S \cdot f$ are shown for four temperatures. The mean values of log $S \cdot f$ show that for *CN* the choice of excitation temperature has very little effect.

For the molecules *OH*, *CH*, and *NH* the same general procedure

[8] *Report on Band Spectra of Diatomic Molecules*, University Press, Cambridge, 1932.

was followed. For C_2 the data by Adam[9] were used in place of Rowland intensities (Table 9). For reasons of economy, the data for the three hydrides are given in the form of summaries only in Tables 6, 7, and 8. The only difference in treatment as compared with *CN*

TABLE 7

SUMMARY OF *NH* DATA (λ 3360 BAND): AVERAGES OF *R* AND *P* BRANCHES

GROUP	WT.	MEAN			log *EW*	log Nf
		K''	E''	R.I.		
I	4	2.5	143	−0.75	0.82	0.05
II	9	5.2	526	−0.56	0.90	.15
III	11	8.1	1204	−0.27	1.01	.28
IV	10	11.0	2156	−0.40	0.96	.22
V	10	14.0	3430	−0.60	0.88	.13
VI	11	17.3	5160	−0.82	0.78	.01
VII	6	19.7	6660	−1.33	0.55	−0.24

TABLE 8

SUMMARY OF *CH* DATA (λ 4314 BAND): AVERAGES OF *R* AND *Q* BRANCHES

GROUP	WT.	MEAN			log *EW*	log Nf
		J''	E''	R.I.		
I	6	3.3	202	0.67	1.51	1.19
II	9	4.7	380	1.00	1.60	1.39
III	8	7.1	817	1.38	1.68	1.60
IV	8	9.1	1306	1.00	1.60	1.39
V	7	10.6	1747	1.57	1.72	1.65
VI	4	13.2	2660	0.75	1.54	1.27

lies in the evaluation of $N_K \cdot f$ from $N_J \cdot f$, which involves a knowledge of the relative intensity factors for the different branches. The 0 − 0 vibrational band was used in all cases.

OH.—The λ 3064 band of *OH* is a member of the electronic transition $^2\Pi \rightarrow {}^2\Sigma$. There are six branches, P_1, P_2, R_1, R_2, Q_1, and Q_2. The computation of the relative intensity factors, following Earls,[10]

[9] *M.N.*, **98**, 544, 1938.

[10] *Phys. Rev.*, **48**, 423, 1935.

shows that, to a sufficient approximation for the purposes of this paper, the intensities are

$$P_1 = P_2 = R_1 = R_2 = \frac{Q_1}{2} = \frac{Q_2}{2}.$$

Thus, for groups I–VII, inclusive, of Table 6, $N_K \cdot f = 4N_J \cdot f$; and for groups VIII–XIV, $N_K \cdot f = 8N_J \cdot f$.

NH.—The electronic transition is $^3\Sigma \rightarrow {}^3\Pi$. The bands consist of triplet *P*, *Q*, and *R* branches. Because of the near equality of the

TABLE 9

SUMMARY OF C_2 DATA*

Branch	J''	log *EW*	log $N_J \cdot f$
R_1	13	0.34	−0.24
	14	0.68	+ .10
	15	0.93	.40
	17	1.02	.51
	22	1.08	.58
	24	0.70	.18
R_2	12	0.98	.46
	14	0.89	.33
	15	0.85	.28
	16	0.80	.23
R_3	15	0.77	.20
	16	0.99	.48
P_1	28	1.00	.48
	29	1.06	+0.56

* From Adam, *M.N.*, **98**, 544, 1938.

moments of inertia in the two electronic states, the *Q* branch consists of lines very close together.[11] It is therefore convenient to examine the *R* and *P* branches. In the absence of any published theoretical relative intensity factors for this transition, it was necessary to assume that the individual members of each triplet are of the same intensity and to use the formulae for a $^1\Sigma \rightarrow {}^1\Pi$ transition.[12] With these assumptions it is found that the *R* and *P* branches are of approximately the same intensity, and each is about half the in-

[11] Funke, *Zs. f. Phys.*, **96**, 787, 1935.

[12] Weizel, *Handbuch der Experimentalphysik, Bandenspektren*, 167, 1931.

tensity of the Q branch. Thus, it is satisfactory to average the R and P branches and to use the relation $N_K \cdot f = 12N_J \cdot f$.

CH.—The electronic transition is $^2\Pi \rightarrow {}^2\Delta$. The relative intensity factors were computed from the formulae in Weizel,[12] page 167. It turns out that the R and Q branches are of approximately equal intensity and that the average intensity of these branches will yield the correct results if we take $N_K \cdot f = AN_J \cdot f$. The factor, A, varies from 8.95 for $J'' = 4.5$ to 9.76 for $J'' = 11.5$.

C_2.—For the details of this spectrum, including the relative intensity factors, Miss Adam's paper was used. Each of the fourteen entries in Table 9 represents a resolved, unblended line. The factor to go from $N_J \cdot f$ to $N_K \cdot f$ is about 5.8 for the R branches and 6.1 for the P branch.

IV. DISCUSSION OF THE VALUES OF $S \cdot f$

If the absolute intensity factor, f, were unity for molecular transitions, then the entries in Table 10 would be directly comparable

TABLE 10

SUMMARY OF log S · f AND log S

Molecule	log $S \cdot f$				log S (Russell)		log S (Roach)	Δ log S
	4000° K	5000°	5500°	6000°	Computed	Observed	$T=5000°$; $f=10^{-3}$	Column 8–6
CN	3.90	3.84	3.84	3.86	2.3	3.2	6.84	4.5
C_2	3.26	3.41	3.49	3.55	0.9	1.3	6.41	5.5
OH	3.40	3.38	3.40	3.41	5.3	3.0	6.38	1.1
NH	2.75	2.86	2.93	2.98	4.0	2.1	5.86	1.9
CH	3.87	4.00	4.06	4.12	3.1	3.0	7.00	3.9

with the values of log S from Russell's paper. Or, if the absolute f values of the five molecules studied happen to be the same, then the *relative* values of $S \cdot f$ can be compared with the relative values of Russell's S. Recently, Oldenberg and Rieke[4] have succeeded in determining the absolute f values of *OH*. For the early members of the R_2 and P_1 branches their results give, as an average, $f = 1.28 \times 10^{-4}$, and for the first six lines of the Q_1 branch, 2.27×10^{-4}. Recalling that the relative intensity factors of the branches require,

in this case, a factor of 8 for the R and P branches and of 4 for the Q branch to obtain $N_K \cdot f$ from $N_J \cdot f$, it is evident that the absolute value of f for an entire level is about 9.67×10^{-4}.

In the absence of further knowledge concerning the absolute intensity factors of the other molecules, detailed comparison with Russell's predictions is not possible. However, there is some basis for thinking that the absolute intensity factors of at least three of the other molecules are all small compared with unity. Oldenberg and Rieke pointed out that the dissociation products of OH are different for the normal and excited levels, namely,

$$\begin{aligned} OH &\rightarrow O^3P + H^2S \quad \text{(normal)} \\ &\rightarrow O^1D + H^2S \quad \text{(excited)} . \end{aligned}$$

The atomic transition for oxygen, $^3P \rightarrow {}^1D$, is forbidden, which accordingly suggests a low transition probability for the molecular case. If this is the correct explanation of the low observed intensity factor for OH, then it should be expected that CN, CH, and NH will have similarly low intensity factors, since each breaks up into dissociation products that involve forbidden transitions. The following dissociation products are taken from Sponer:[13]

$$\begin{aligned} CN &\rightarrow C^3P + N^4S \quad \text{(normal)?} \\ &\rightarrow C^3P + N^2D \quad \text{(excited)?} \\ CH &\rightarrow C^3P + H^2S \quad \text{(normal)} \\ &\rightarrow C^1D + H^2S \quad \text{(excited)} \\ NH &\rightarrow N^4S + H^2S \quad \text{(normal)} \\ &\rightarrow N^2D + H^2S \quad \text{(excited)} . \end{aligned}$$

In each case there is a forbidden atomic transition which suggests a low molecular intensity factor. On the basis of this observation, column 8 of Table 10 has been computed for 5000° K and $f = 10^{-3}$.

If these values of $\log S$ are even approximately correct, there is a marked disagreement between the values predicted from the sun's atomic constitution and those observed from the molecular lines. A study of the revision in the atomic analysis necessary to bring the two into agreement is reserved for a later investigation.

[13] *Molekülspektren*, Julius Springer, Berlin, 1935.

V. EXCITATION TEMPERATURE FROM BANDS OF *CN* AND *OH*

The intensity of an absorption band line is given by

$$I = N_J \cdot f = gfe^{-E''hc/kT} = ie^{-E''hc/kT} . \tag{8}$$

Solving for T, it is found that

$$T = -\frac{0.4343}{khc}\frac{E''}{\log \frac{N_J \cdot f}{i}} = -0.628\frac{E''}{\log \frac{N_J \cdot f}{i}}, \tag{9}$$

where E'' is in cm^{-1}.

In Tables 4 and 6, the quantities $\log N_J \cdot f/i$ and E'' are recorded for *CN* and *OH*. In Figures 1 and 2 the points are plotted, together with their straight-line least-squares solution. From the slope of the line the excitation temperature may be computed according to equation 9. The slopes are: for *CN*, $-1.116 \times 10^{-4} \pm 0.096$ (p.e.); for *OH*, $-1.352 \times 10^{-4} \pm 0.158$ (p.e.). The corresponding

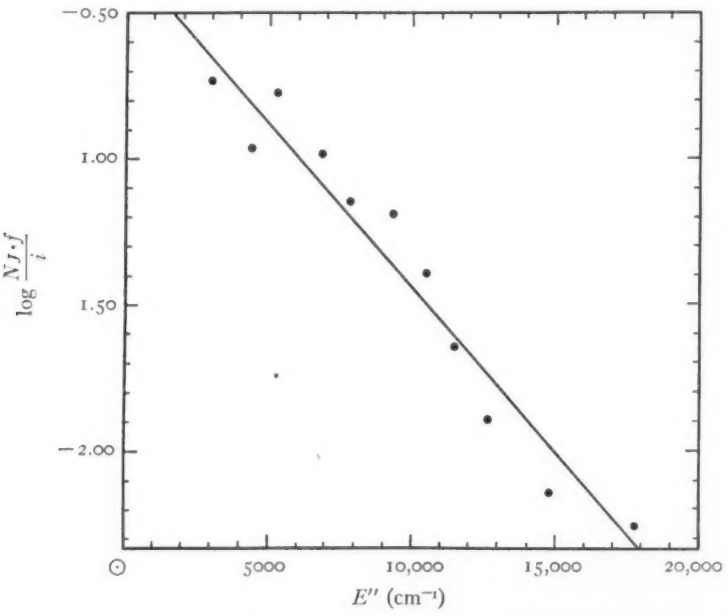

FIG. 1.—Variation of $\log \frac{N_J \cdot f}{i}$ with E'' for *CN* (λ 3883)

temperatures are 5630° K (5180°, 6150°) and 4640° K (4160°, 5250°), where the values in the parentheses are the extremes corresponding to the probable error of the slopes.

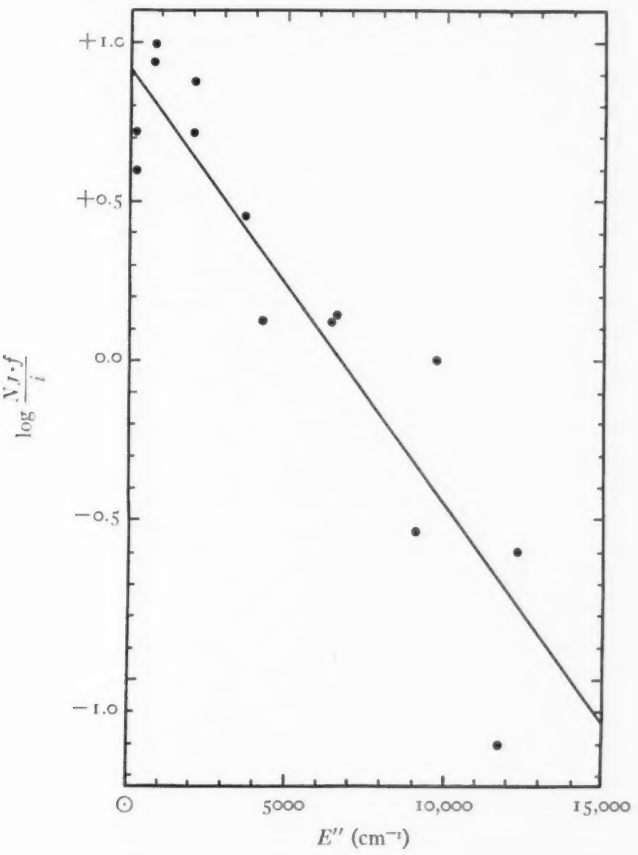

FIG. 2.—Variation of $\log \frac{N_J \cdot f}{i}$ with E'' for *OH* (λ 3064)

In Table 11 are collected the published values of the excitation temperature of the sun. The first five determinations are based on molecular bands, and the last two on atomic lines. With the exception of the determination by Richardson based on the G band, the molecular temperatures are of much lower precision than those based on atomic lines. There seems to be a systematic difference between

the two types of excitation temperature. Giving equal weight to each entry in Table 11, it is found that for the molecules the mean temperature is 5110° K and for the atomic lines, 4300° K. The fact that the molecular temperature is closer to the effective tempera-

TABLE 11

EXCITATION TEMPERATURE OF THE SOLAR REVERSING LAYER

Author	Source	Temperature, °K	Limits	Reference
Birge	*CN* (λ 3883)	4000	4500 3500	*Ap. J.*, **55**, 273, 1922
Richardson	C_2 (Swan)	6000	6700 5300	*Ibid.*, **73**, 216, 1931
		5700	7300 4100	
		5300	5700 4900	
Richardson	*CH* (λ 4314)	5080	5200 4960	*Trans. I.A.U.*, **4**, 55, 1932
Adam	C_2 (Swan)	4550	6700 3400	*M.N.*, **98**, 544, 1938
Roach	*CN* (λ 3883)	5630	6150 5180	
	OH (λ 3064)	4640	5250 4160	
King	*Ti* I	4400	4500 4300	*Ap. J.*, **87**, 40, 1938
Menzel, Baker, Goldberg	*Fe* I	4150	4200 4100	*Ibid.*, **87**, 81, 1938
	Ti I	4350	4550 4150	

ture (5740° K) may be due to the longer lifetime of molecular states compared with atomic. The larger number of collisions per radiation for the former allows a closer approach to the kinetic temperature. Another possibility is that this is evidence for a temperature gradient. The point has been discussed for the molecular case by Rich-

ardson,[14] who found a gradient effect for the G band. For the lower quantum numbers he finds $T = 4430° \pm 160°$ K, and for the higher $6080° \pm 130°$ K.

It is a pleasure to record my thanks to Director Struve for granting me the privilege of carrying on this work at the Yerkes Observatory during the summer of 1938. I am especially indebted to Dr. Karl Wurm, who not only suggested the problem but also gave me much valuable advice during its entire prosecution.

YERKES OBSERVATORY
AND
STEWARD OBSERVATORY
UNIVERSITY OF ARIZONA
August 1938

[14] *Trans. I.A.U.*, **4**, 55, 1932.

THE LANE-EMDEN FUNCTION $\theta_{3.25}$

S. CHANDRASEKHAR

The Lane-Emden function $\theta_{3.25}$ is of considerable interest in the study of stellar models. Thus a stellar model with a uniform distribution of the energy sources ($\eta = 1$), of small mass ($1 - \beta \sim 0$) and on Kramer's law of opacity ($\kappa = \kappa_0 \rho T^{-3.5}$), will be described by $\theta_{3.25}$. Further, if stars have an inner core in which the energy sources are uniformly distributed, they will be described by a point-source envelope fitted onto a polytropic core of index 3.25.[1] For these and similar purposes it has been found necessary to integrate the function $\theta_{3.25}$, which has not been available so far. Table 1 gives the required function and certain other auxiliary functions which are of importance in the theory.

The function $\theta_{3.25}$ has its first zero at $\xi = \xi_1$, where

$$\xi_1 = 8.01894 . \tag{1}$$

At $\xi = \xi_1$ we have

$$\left.\begin{aligned} -\theta' &= 0.030322 , \\ -\xi^2\theta' &= 1.94980 , \\ \frac{\rho_c}{\bar{\rho}} &= 88.153 . \end{aligned}\right\} \tag{2}$$

Applications of this solution will also be found in the author's monograph, *An Introduction to the Study of Stellar Structure*.[2]

Regarding the accuracy of the table, it may be mentioned that an error of more than two (and in extreme cases three) units in the last figure retained is not expected.

[1] This model is being studied by the writer, and the results of this study will be published in due course.

[2] Chicago: University of Chicago Press (in press).

TABLE 1

ξ	θ	$-\theta'$	$\theta^{3.25}$	$\theta^{4.25}$	$-\xi^2\theta'$	$-\frac{\xi}{3\theta'}$
0....	1.000000	0	1.00000	1.00000	0	1.0000
0.1..	0.998336	.033225	0.99460	0.99295	0.0003323	1.0033
0.2..	0.993376	.065809	0.97863	0.97215	0.0026323	1.0130
0.3..	0.985216	.097140	0.95275	0.93866	0.0087426	1.0294
0.4..	0.974009	.126668	0.91797	0.89411	0.020267	1.0526
0.5..	0.959958	.153926	0.87563	0.84057	0.038482	1.0828
0.6..	0.943311	.17855	0.82724	0.78034	0.064277	1.1201
0.7..	0.924345	.20027	0.77439	0.71581	0.098134	1.1651
0.8..	0.903358	.21895	0.71870	0.64924	0.14013	1.2179
0.9..	0.880658	.23454	0.66164	0.58268	0.18998	1.2791
1.0..	0.856553	.24707	0.60458	0.51785	0.24707	1.3491
1.1..	0.831341	.25668	0.54863	0.45610	0.31058	1.4285
1.2..	0.805309	.26353	0.49474	0.39842	0.37948	1.5179
1.3..	0.778720	.26786	0.44360	0.34544	0.45269	1.6178
1.4..	0.751813	.26992	0.39569	0.29749	0.52904	1.7289
1.5..	0.724803	.26997	0.35133	0.25465	0.60743	1.8521
1.6..	0.697877	.26828	0.31066	0.21680	0.68680	1.9880
1.7..	0.671196	.26512	0.27369	0.18370	0.76619	2.1374
1.8..	0.644895	.26072	0.24035	0.15500	0.84473	2.3013
1.9..	0.619086	.25532	0.21047	0.13030	0.92170	2.4806
2.0..	0.593858	.24913	0.18385	0.10918	0.99651	2.6760
2.1..	0.569281	.24232	0.16026	0.091230	1.06864	2.8887
2.2..	0.545408	.23507	0.13943	0.076044	1.13774	3.1196
2.3..	0.522277	.22751	0.12111	0.063252	1.20353	3.3698
2.4..	0.499912	.21976	0.10505	0.052517	1.26583	3.6403
2.5..	0.478327	.21193	0.091014	0.043534	1.32453	3.9322
2.6..	0.457527	.20408	0.078769	0.036039	1.37959	4.2467
2.7..	0.437509	.19630	0.068109	0.029799	1.43103	4.5848
2.8..	0.418263	.18864	0.058845	0.024613	1.47893	4.9477
2.9..	0.399776	.18114	0.050805	0.020311	1.52335	5.3367
3.0..	0.382030	.17382	0.043834	0.016746	1.56442	5.7529
3.1..	0.365004	.16673	0.037798	0.013796	1.60229	6.1976
3.2..	0.348675	.15988	0.032574	0.011358	1.63713	6.6718
3.3..	0.333020	.15327	0.028056	0.009343	1.66906	7.1771
3.4..	0.318014	.14691	0.024152	0.007681	1.69828	7.7145
3.5..	0.303630	.14081	0.020779	0.006309	1.72496	8.2852
3.6..	0.289842	.13497	0.017866	0.005178	1.74925	8.8907
3.7..	0.276627	.12939	0.015352	0.004247	1.77131	9.5321
3.8..	0.263956	.12405	0.013182	0.003479	1.79134	10.211
3.9..	0.251808	.11896	0.011310	0.002848	1.80944	10.928
4.0..	0.240156	.11411	0.009696	0.002329	1.82578	11.685
4.1..	0.228978	.10949	0.008305	0.001902	1.84051	12.482
4.2..	0.218251	.10509	0.007106	0.001551	1.85377	13.322
4.3..	0.207953	.10090	0.006073	0.001263	1.86560	14.206
4.4..	0.198064	.09691	0.005184	0.001027	1.87624	15.134
4.5..	0.188564	.09312	0.004418	0.0008331	1.88572	16.108
4.6..	0.179434	.08952	0.003760	0.0006747	1.89418	17.129
4.7..	0.170655	.08609	0.003194	0.0005451	1.90168	18.198
4.8..	0.162211	.08283	0.002709	0.0004394	1.90831	19.318
4.9..	0.154084	.07972	0.002292	0.0003532	1.91417	20.487
5.0..	0.146261	.07677	0.001935	0.0002830	1.91933	21.709
5.1..	0.138725	.07397	0.001629	0.0002260	1.92388	22.983
5.2..	0.131463	0.07130	0.001368	0.0001799	1.92784	24.312

TABLE 1—*Continued*

ξ	θ	$-\theta'$	$\theta^{1.25}$	$\theta^{4.25}$	$-\xi^2\theta'$	$-\frac{\xi}{3\theta'}$
5.3..	0.124461	0.06875	0.001145	0.0001425	1.93127	25.696
5.4..	.117708	.06633	0.0009553	0.0001124	1.93427	27.136
5.5..	.111191	.06403	0.0007938	0.00008827	1.93691	28.632
5.6..	.104899	.06183	0.0006569	0.00006891	1.93911	30.188
5.7..	.098821	.05974	0.0005411	0.00005347	1.94102	31.803
5.8..	.092947	.05775	0.0004434	0.00004121	1.94264	33.479
5.9..	.087268	.05585	0.0003612	0.00003152	1.94403	35.215
6.0..	.081775	.05403	0.0002924	0.00002391	1.94519	37.014
6.1..	.076459	.05230	0.0002350	0.00001797	1.94612	38.878
6.2..	.071312	.05065	0.0001874	0.00001336	1.94691	40.805
6.3..	.066327	.04907	0.0001481	9.822×10^{-6}	1.94759	42.796
6.4..	.061496	.04756	0.00011158	7.122×10^{-6}	1.94814	44.854
6.5..	.056812	.04612	0.00008952	5.086×10^{-6}	1.94853	46.980
6.6..	.052270	.044740	0.00006828	3.569×10^{-6}	1.94887	49.173
6.7..	.047862	.043420	0.00005129	2.455×10^{-6}	1.94912	51.436
6.8..	.043584	.042157	0.00003783	1.640×10^{-6}	1.94934	53.767
6.9..	.039429	.040947	0.00002732	1.077×10^{-6}	1.94949	56.170
7.0..	.035393	.039788	0.00001923	6.806×10^{-7}	1.94961	58.644
7.1..	.031470	.038677	0.00001313	4.131×10^{-7}	1.94971	61.191
7.2..	.027656	.037611	8.626×10^{-6}	2.386×10^{-7}	1.94975	63.811
7.3..	.023947	.036588	5.402×10^{-6}	1.204×10^{-7}	1.94977	66.506
7.4..	.020337	.035606	3.176×10^{-6}	6.460×10^{-8}	1.94978	69.277
7.5..	.016824	.034663	1.715×10^{-6}	2.885×10^{-8}	1.94979	72.123
7.6..	.013403	.033757	8.1929×10^{-7}	1.098×10^{-8}	1.94980	75.046
7.7..	.010072	.032886	3.2360×10^{-7}	3.26×10^{-9}	1.94980	78.047
7.8..	.006825	.032048	9.138×10^{-8}	6.2×10^{-10}	1.94980	81.128
7.9..	.003661	.031242	1.207×10^{-8}	4×10^{-11}	1.94980	84.288
8.0..	0.000576	0.030466	2.956×10^{-11}	.....	1.94980	87.529

YERKES OBSERVATORY
November 1938

PLATE VII

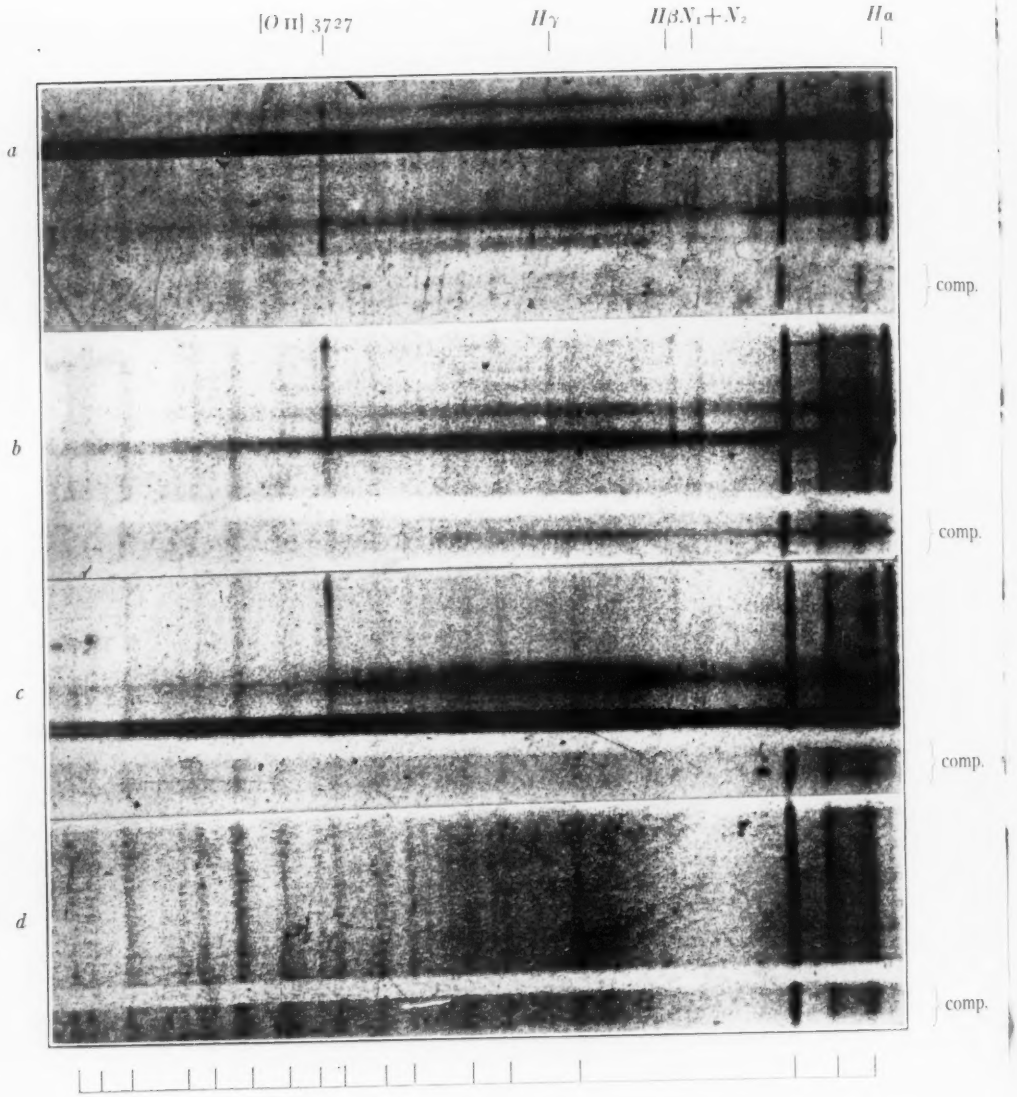

AURORAL LINES

a) Guiding star: +56°2604. Nebula IC 1396
b) Guiding star: +60°504. Loose cluster
c) Guiding star: +59°559. Loose cluster
d) Guided 6′ south of +29°741

OBSERVATIONS MADE WITH THE NEBULAR SPECTROGRAPH OF THE McDONALD OBSERVATORY*

OTTO STRUVE AND C. T. ELVEY

ABSTRACT

Sixteen spectrographic observations of fifteen fields reveal emission lines in eight fields. No emission was found in the luminous rims of dark nebulae in Taurus, in the nebula B 14, or in NGC 884 (one member of the double cluster in Perseus). Two loose clusters north of the double cluster show very conspicuous emission, as does also the galactic cluster NGC 7380.

The present series of observations is a continuation of our former work on the detection of new emission nebulae[1] and on the determination of the character of the spectrum of known, but faint, galactic nebulae. In order to facilitate the identification of the regions which we have observed we have listed them all under new numbers, with their respective identifications, in Table 1. Agfa Super Pan Press film was used for all exposures. Accompanying the table we give the details of our new observations.

The spectrum of the night sky, which was weak in February and very weak in August, is quite strong on all our plates, although it is not as strong as on the spectrograms obtained by Greenstein and Henyey[2] at the Yerkes Observatory in October, November, and December, 1937.

Both nebular emission lines which we have found most useful in our work, *Hα* and [*O* II] 3727, coincide with weak emission lines of the night-sky spectrum. Hence, the detection of emission in the present series was somewhat more difficult than in the two preceding series. Nevertheless, a comparison of the line in the region observed with that given by the comparison mirror has enabled us to record with certainty even small differences in intensity, especially in the case of *Hα*, whose overlying night-sky line is very weak and diffuse.

When we have recorded a region as showing no emission, we wish to indicate that an exposure made as long as was practical does not

[1] *Ap. J.*, **87**, 559, 1938; **88**, 364, 1938. In Plate XVI, Vol. **88**, the index for *Hα* is displaced too far to the left. *Hα* is the line at the extreme right of the photographs.

[2] *Ibid.*, **86**, 620, 1937; **87**, 79, 1938.

* *Contributions from the McDonald Observatory, University of Texas*, No. 9.

TABLE 1

SUMMARY OF OBSERVATIONS MADE WITH THE NEBULAR SPECTROGRAPH

No.	Object	Guiding Star	Date	Identification	Reference to Detailed Description	Result
1	Nebula IC 434	BD − 2°1336	1938, Feb. 22/23	Ross 34; 194 mm from right, 146 mm from bottom	*Ap. J.*, **87**, 563	Very strong emission
2	Nebula IC 434	BD − 2°1345	Feb. 23/24	Ross 34; 199 mm from right, 150 mm from bottom	**87**, 563	Strong emission
3	M 81	.....	Feb. 23/24	.....	.....	No definite emission
4	3° NW. of λ Ori	BD+12°810	Mar. 1/2	Ross 33; 144 mm from right, 125 mm from top	**87**, 564	Strong emission
5	Milky Way	BD+14°1060	Mar. 2/3	Ross 33; 108 mm from left, 98 mm from top	**87**, 565	No emission
6	Coma Cluster	.....	Mar. 2/3	.....	.....	No emission
7	15′ N. of α Sco	.....	Mar. 2/3	Barnard 13	**87**, 565	No definite emission
8	10′ E.; 15′ N. of σ Sco	.....	Mar. 28/29	Barnard 13	**87**, 566	Emission
9	13′ W.; 13′ N. of σ Sco	.....	Mar. 30/31	Barnard 13	**87**, 566	Emission
10	Near γ Cyg	BD+39°4082	Aug. 18/19	Ross 17; 131 mm from right, 157 mm from top	**88**, 364	Strong emission
11	Near γ Cyg	BD+39°4054	Aug. 28/29	Ross 17; 120 mm from right, 170 mm from bottom	**88**, 365	Strong emission
12	Milky Way	28 b² Cyg	Aug. 20/21	Barnard 43	**88**, 365	Strong emission
13	Milky Way	25 Cyg	Aug. 21/22	Barnard 43	**88**, 365	Emission
14	Milky Way	BD+29°3829	Aug. 22/23	Ross 16; 145 mm from right, 174 mm from top	**88**, 365	Faint emission
15	Milky Way	π¹ Cyg	Aug. 23/24	Barnard 48	**88**, 365	Probably faint emission
16	Milky Way	BD+55°2714	Aug. 24/25	Barnard 50; 116 mm from right, 99 mm from top	**88**, 365	Very strong emission
17	Milky Way	BD+54°2708	Aug. 25/26	Barnard 50; 102 mm from right, 99 mm from bottom	**88**, 366	Strong emission
18	Milky Way	δ Cep	Aug. 26/27	Barnard 50	**88**, 366	Weak emission
19	Milky Way	λ Cep	Aug. 27/28	Barnard 50	**88**, 366	Emission
20	Milky Way	γ Cas	Oct. 18/19	Ross 26; 73 mm from right, 122 mm from bottom	**89**, 121	Strong emission

TABLE 1—*Continued*

No.	Object	Guiding Star	Date	Identification	Reference to Detailed Description	Result
21.....	Cluster NGC 7380	BD+57°2601	1938, Oct. 19/20	Ross 19; 101 mm from left, 135 mm from top	*Ap. J.*, **89**, 121	Very strong emission
22.....	Nebula IC 1396	BD+56°2604	Oct. 20/21	Barnard 49	**89**, 122	Very strong emission
23.....	h and χ Per	NGC 884	Oct. 20/21	Barnard 1	**89**, 122	No emission
24.....	B 14	.....	Oct. 22/23	Barnard 5	**89**, 122	No emission
25.....	B 14	.....	Oct. 24/25	Barnard 5	**89**, 122	No emission
26.....	Milky Way	BD+58°2497	Oct. 23/24	Ross 19; 94 mm from left, 120 mm from top	**89**, 123	No definite emission
27.....	Loose Cluster N. of h and χ Per	BD+60°504	Oct. 23/24	Barnard 2; 35 mm from right, 87 mm from top	**89**, 123	Very strong emission
28.....	South of β Cas	BD+57°9	Oct. 24/25	Ross 26; 82 mm from right, 32 mm from top	**89**, 123	No emission
29.....	Loose Cluster NE. of h and χ Per	BD+59°559	Oct. 25/26	Barnard 2; 112 mm from right, 114 mm from bottom	**89**, 123	Very strong emission
30.....	Milky Way	BD+62°2061	Oct. 26/27	Ross 19; 160 mm from right, 60 mm from top	**89**, 123	Emission
31.....	Nebula	BD+29°741	Oct. 26/27	Ross 31; 184 mm from right, 68 mm from top	**89**, 124	No emission
32.....	Milky Way	BD+61°2373	Oct. 27/28	Ross 19; 92 mm from left, 62 mm from top	**89**, 124	Emission
33.....	Nebula	6′ S. of BD+29°741	Oct. 28/29	Ross 31; 184 mm from right, 70 mm from top	**89**, 124	No emission
34.....	Nebula	BD+31°627	Oct. 29/30	Barnard 3; 109 mm from left, 65 mm from top	**89**, 124	Very faint emission (?)
35.....	.....	ζ Per	Oct. 30/31	Barnard 3	**89**, 124	No emission

show a nebular *Hα* or [*O* II] 3727. Short, or otherwise unsatisfactory, exposures have only been used when the evidence was positive.

No. 20.—Guiding star γ Cas. 1938 Oct. 18/19. Exp. 5^h10^m. Comparison mirror $\Delta\delta = -20°$. Slit eq. 45 mm. *Hα* is very conspicuous between 7′ west of γ Cas, and 15′ east of γ Cas. Emission is present, but weak, over the entire length of the slit. The fan-shaped nebulae are too far from the slit to affect the exposure directly. Evidently the entire region near γ Cas has emission nebulosity. [*O* II] 3727 is masked by a fairly strong line of the night sky.

No. 21.—Guiding star +57°2601, sp. F8. 1938 Oct. 19/20. Exp.

30^m. Comparison mirror $\Delta\delta = -30°$. Slit eq. 30 mm. *Hα*, *Hβ*, and [*O* II] 3727 are very conspicuous in a limited region covered by the galactic cluster NGC 7380, which consists of stars between magnitudes 9 and 13. The cluster looks nebulous on Plate 19 of Ross's *Atlas*, but on this small-scale photograph it is difficult to distinguish true nebulosity from the effect of overlapping star images. The emission nebula is quite strong. The exposure was too short to reveal faint extensions of the bright lines east and west of the cluster.

No. 22.—Guiding star +56°2604. 1938 Oct. 20/21. Exp. 3^h25^m. Comparison mirror $\Delta\delta = -30°$. Slit eq. 30 mm. *Hα* and [*O* II] 3727 are very strong; *Hβ* and the blend of N_1 and N_2 are conspicuous, the latter being slightly stronger than the former, thus resembling in intensity the Orion nebula. All lines are strongest near the western end of the slit, in the vicinity of the star +56°2598, mag. 8.7, sp. B8. The lines become slightly weaker at the eastern end, near the star +56°2617, mag. 5.6, sp. Oe5. This is the brightest portion of the large irregular nebula IC 1396, which occupies the central portion of Plate 49 of Barnard's *Atlas*.

No. 23.—Double cluster of Perseus: NGC 884. 1938 Oct. 20/21. Exp. 3^h37^m. Comparison mirror $\Delta\delta = -30°$. Slit eq. 30 mm. No definite trace of *Hα* in the cluster or in the surrounding region. A slight strengthening of the night-sky line, which coincides with *Hα*, in the cluster is probably caused by the strong continuous spectrum of the cluster. The integrated spectrum of NGC 884 shows strong absorption lines of *H* and of *Ca*K, the latter being almost as strong as the blend of *Hε* and *Ca*H. The Balmer line *Hζ* is very strong; *Hβ* is relatively weak, suggesting that the spectrum is composite, the early type predominating in the violet region and the late type in the red region.

No. 24–25.—B 14. 1938 Oct. 22/23. Exp. 3^h55^m and Oct. 24/25. Exp. 6^h. Comparison mirror $\Delta\delta = -20°$. Slit eq. 40 mm. There is no trace of emission at *Hα* or elsewhere. These two exposures were centered upon the feebly luminous nebula Barnard No. 14 (Object 109, Plate 5 of Barnard's *Atlas*). This nebula is located in the middle of a very dense dark nebula in Taurus, the eastern part of which has a slightly luminous edge.[3] The absence of emission supports the hypothesis[4] that this nebula and the luminous rim are produced by reflection.

[3] Struve, *ibid.*, **85**, 194, 1937.

[4] *Ibid.*, p. 211.

No. 26.—Guiding star BD+58°2497. 1938 Oct. 23/24. Exp. 3^h. Comparison mirror $\Delta\delta = -20°$. Slit eq. 40 mm. There is no definite trace of emission at $H\alpha$ or at [*O* II] 3727. The region lies northeast of the bright emission nebula in the cluster NGC 7380 (see above). It looks nebulous on Ross's Plate 19, especially east of the guiding star.

No. 27.—Guiding star BD+60°504. 1938 Oct. 23/24. Exp. 6^h. Comparison mirror $\Delta\delta = -20°$. Slit eq. 40 mm. This region shows an amazingly strong emission spectrum, mostly just east of the guiding star, and again at the extreme eastern edge of the plate, i.e., about 40′ east of the guiding star. The stronger emission lines are, however, visible over the entire height of the spectrum, being relatively weakest about 20′ west of the guiding star. $H\alpha$, $H\beta$, $H\gamma$, [*O* II] 3727, N_1, and N_2 are all well pronounced. N_1 is of about the same density as $H\beta$. The region looks faintly luminous on Plates 26 and 27 of the Ross *Atlas*, especially toward the east of the guiding star. The spectrum of the guiding star is B (perhaps B0), and the photographic magnitude is 7.8.

No. 28.—Guiding star BD+57°9. 1938 Oct. 24/25. Exp. 3^h. Comparison mirror $\Delta\delta = -20°$. Slit eq. 40 mm. There is no trace of emission at $H\alpha$ or [*O* II] 3727. The guiding star is about 8 mm south of β Cas on Plate 20 of the Ross *Atlas*, where the latter is near the center of the photograph. A dark nebula which looks slightly luminous lies east of the guiding star. The spectral class of the latter is B9, and its photographic magnitude is 8.1.

No. 29.—Guiding star BD+59°559. 1938 Oct. 25/26. Exp. 6^h45^m. Comparison mirror $\Delta\delta = -20°$. Slit eq. 40 mm. $H\alpha$ and [*O* II] 3727 are very strong over the entire length of the slit, but especially near its eastern limit. $H\beta$ is present, but $N_1 + N_2$ is weak or absent. This region lies toward the east of BD+60°504, which has a strong emission nebulosity (see No. 27). The entire region looks faintly luminous on Ross's Plate 26. The spectral type of the guiding star is A3, and its photographic magnitude is 7.4.

No. 30.—Guiding star BD+62°2061. 1938 Oct. 26/27. Exp. 4^h3^m. Comparison mirror $\Delta\delta = -20°$. Slit eq. 40 mm. $H\alpha$ is conspicuous over the entire length of the slit but is strongest just west of the guiding star. It is greatly enhanced in the spectrum of the star itself. [*O* II] 3727 is weakly present. The region is very slightly nebu-

lous on Ross's Plate 19 and is shown clearly nebulous on a photograph by C. A. Lower and H. A. Lower, taken at San Diego with an f/1 Schmidt camera. The guiding star is of spectral type B8, and the photographic magnitude is 8.5.

No. 31.—Guiding star BD+29°741. 1938 Oct. 26/27. Exp. 4^h. Comparison mirror $\Delta\delta = -30°$. Slit eq. 40 mm. There is no emission, and the spectrum of the nebula must be continuous. Ross's Plate 31 shows a fairly bright, small nebula in the immediate vicinity of the guiding star, whose spectrum is B9 and photographic magnitude is 7.3. This nebula is a part of the system of dark nebulae and reflection nebulae in Taurus.

No. 32.—Guiding star BD+61°2373. 1938 Oct. 27/28. Exp. 2^h25^m. (Frequently interrupted by clouds.) Comparison mirror $\Delta\delta = -20°$. Slit eq. 40 mm. *Hα* and [*O* II] 3727 are in emission over the entire length of the slit. The region is slightly nebulous on Ross's photograph 19 and also on the red-sensitive photograph by the Lowers. The guiding star is of spectral type B0, and the photographic magnitude is 7.6.

No. 33.—Guided about 6′ south of BD+29°741. 1938 Oct. 28/29. Exp. 7^h. Comparison mirror $\Delta\delta = -20°$. Slit eq. 41 mm. There is no emission, and the spectrum of the nebula which should be near the western end of the slit must be continuous. It is, however, not definitely visible on the background of the strong night-sky spectrum. This region is the same as the one described under No. 31.

No. 34.—Guiding star BD+31°627. 1938 Oct. 29/30. Exp. 5^h. Comparison mirror $\Delta\delta = -20°$. Slit eq. 40 mm. We suspect a faint emission line at *Hα*, but [*O* II] 3727 is not visible in emission, being masked by a fairly strong emission line of the night sky. This region lies about 1° east of *o* Persei. It is faintly nebulous on Barnard's Plate 3. Our experience with other objects suggests that most of the light of this nebulosity must have a continuous spectrum, since otherwise the *Hα* emission line would be much stronger.

No. 35.—Guiding star ζ Persei. 1938 Oct. 30/31. Exp. 3^h30^m. (Interrupted by clouds.) Comparison mirror $\Delta\delta = -20°$. Slit eq. 40 mm. No emission.

McDonald Observatory
November 1, 1938

A NEW ECLIPSING VARIABLE OF LARGE MASS

SERGEI GAPOSCHKIN

ABSTRACT

More than a thousand photographic observations of the new eclipsing variable HD 163181 = HV 7868 = Boss 4520 have been secured from Harvard plates. The light-curve shows slight indications of ellipticity; the minima are well defined, and both are of greater depth than $0^m.4$, so that the photometric relative elements may be regarded as of considerable precision. The velocity-curve published in 1928 by Humason and Nicholson refers to the star that is in front during the primary minimum: it is slightly the larger, slightly the brighter, and slightly the more massive of the two components. There is an indication of a slow apsidal motion.

A photovisual light-curve based on 87 observations confirms the variability and the range. The star is much redder than would be expected from its spectrum (Harvard, Oe; Mount Wilson, B1e; Lick, Bo); the mean color excess is $+0^m.57$.

The principal results obtained are as follows: $P = 12^d.0042$; $i = 88°.4$; $k_{2,1} = 0.917$; $r_1 = 5.71\odot$; $r_2 = 5.23\odot$; $\mu_1 = 44.38\odot$; $\mu_2 = 40.82\odot$; $\rho_1 = 0.23\odot$; $\rho_2 = 0.28\odot$; $L_1 = 0.54$; $\gamma = 1.03$; $b/a = 0.985$.

The star is unique in that its mass is of the same order as that of AO Cassiopeiae or UW Canis Majoris, but the radii are much smaller, being similar to those of the components of Y Cygni. The spectra of all four stars are practically the same. The mass of the heavier component of HD 163181 is about equal to that of the red supergiant component of VV Cephei ($44.5\odot$), but the radius is 420 times smaller than the radius of that star.

A preliminary study of 148 photographic observations of the spectroscopic binary HD 163181 showed it to be an eclipsing vari-

TABLE 1

MAGNITUDES OF COMPARISON STARS

Number of Star	Magnitude IPg	Spectrum	Number of Star	Magnitude IPg	Spectrum
1	$6^m.25 \pm 0^m.07$	A0	6	$6^m.75 \pm 0^m.05$	B3
2	6.85 .07	A0	7	6.82 .04	.....
3	8.08 .05	A0	8	7.58 .07	.....
4	6.60 .06	B9	Variable (max.)	6.56 ± 0.04	Oe5
5	7.70 ± 0.06	.....			

able.[1] Harvard patrol plates have now been used in order to secure all possible observations, and 1069 estimates have been obtained. The estimates were made by the step method, the magnitudes adopted for the comparison stars (based ultimately on the Harvard Standard Regions)—being those given in Table 1.

[1] *Harvard Bull.*, No. 909, p. 20, 1938.

The observations cover an interval from July, 1899, to July, 1937; they were divided into four groups for the purpose of studying possible changes in the appearance of the light-curve during the 34 years. The depth and width of the minima have not changed appreciably; but in the distance between the minima there seems to be a slight progression, as is shown in Table 2. If this slow increase in the dif-

TABLE 2

SEPARATION OF MINIMA OF HD 163181

Interval	Phase of First Minimum	Phase of Second Minimum	Difference
I	$0^{P}.230$	$0^{P}.740$	$0^{P}.510$
II	.225	.745	.520
III	.230	.752	.522
IV	0.231	0.761	0.530

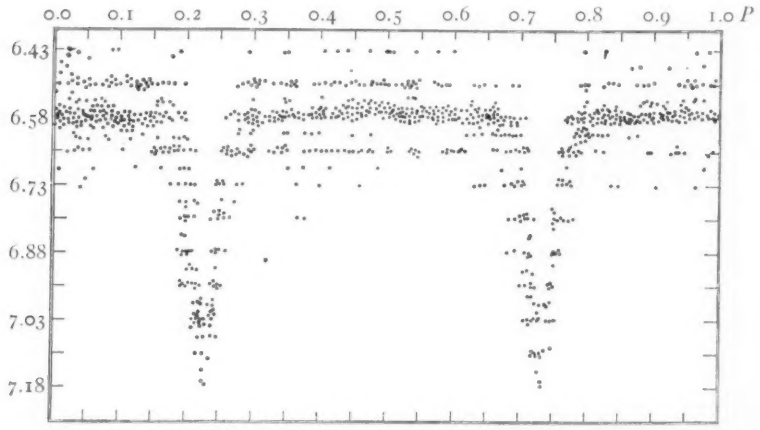

FIG. 1.—Single observations for HD 163181. Abscissae, phases in units of the period; ordinates, photographic magnitudes.

ference is considered to be real, the apsidal motion in this system of heavy, widely separated components must be very slow—of the order of several hundred years.

The mean light-curve is given in Figure 1. There are slight evidences of ellipticity, and the minima are sharp and well defined; the relative photometric elements must therefore be of considerable

accuracy. The star is in a class with Y Cygni and V Puppis. The absolute dimensions are not yet definitive, for the orbital velocity has been observed for but one component. However, the values given below are very probable.

Spectroscopically, the system is of some interest, for it has hydrogen and helium lines in emission which behave in a manner very similar to those of β Lyrae: the emission lines oscillate in position relative to the absorption lines which they flank, and their intensity changes throughout the cycle of light variation. The two systems differ in that the bright lines never disappear from the spectrum of β Lyrae, whereas they disappear periodically from that of HD

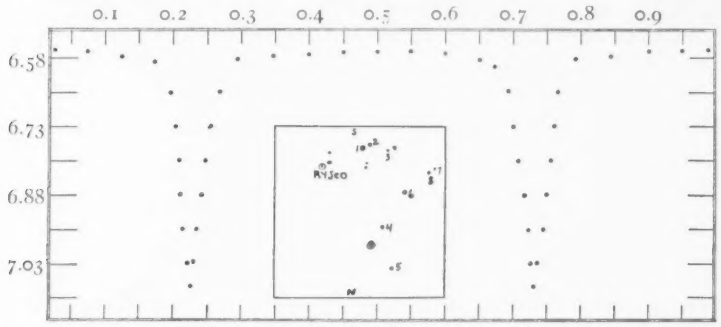

FIG. 2.—Mean light curve and chart for HD 163181. Co-ordinates, same as for Figure 1. Variable in lower circle.

163181; moreover, in the spectrum of β Lyrae they are much stronger in the first half of the cycle than in the second. The first difference mentioned is probably to be explained by the fact that the inclination of the orbit of HD 163181 is nearly 90°; that of β Lyrae is much lower, so that a large portion of the eclipsed area of β Lyrae is always visible. The helium line 4471 appears in emission in the spectra of both systems, being the strongest line in the spectrum of β Lyrae during the first half of the cycle.

The two systems differ somewhat in geometrical properties, for while HD 163181 has well-separated components, only slightly different from each other in size, luminosity, and mass, β Lyrae consists of two slightly separated components that differ considerably in the properties just mentioned. This contrast in geometrical properties probably accounts for some of the spectroscopic differences.

Besides the photographic observations, 87 photovisual estimates of HD 163181 have been secured which confirm the general nature of the variation, although they are not sufficient for the determination of a precise light-curve.

The comparison stars used are all of about the same effective wave length, so that a determination of the color of the variable is not difficult. It is, without doubt, considerably redder than are normal members of its spectral class. The color index is $6^m.56 - 6^m.24 = 0^m.32$; if we take for the normal Bo or Oe star a color index[2] of $-0^m.25$, we derive the large color excess $+0^m.57$. The star lies in the direction of the galactic center, against the background of a bright star cloud.

The relative photometric elements are summarized in Table 3. The mean errors were obtained from a comparison of four independent solutions, made with different groups of material. The spectroscopic elements of the variable, taken from the work of Humason and Nicholson, are given in Table 4.

TABLE 3

PHOTOMETRIC ELEMENTS OF HD 163181

max	$= 6^m.558 \pm 0^m.042$	P	$= 12^d.00421$	L_1	$= 0.54 \pm 0.02$
$\min_1$	$= 6.990 \quad .044$	D	$= 0^d.09$	L_2	$= 0.46 \quad 0.02$
$\min_2$	$= 6.976 \quad .045$	z	$= 0.056$	a_1	$= 0.052$ A $\quad 0.009$ A
A_1	$= 0.432 \quad .061$	$k_{2,1}$	$= 0.917 \pm 0.051$	a_2	$= 0.047 \pm 0.009$
A_2	$= 0.418 \pm 0.061$	i	$= 88°26' \quad 15'$	b/a	$= 0.985$
		$\gamma_{2,1}$	$= 1.02 \pm 0.09$		

TABLE 4

SPECTROSCOPIC ELEMENTS OF HD 163181

$e = 0.065$	$\gamma = 41.8$ km/sec
$\omega = 23°.2$	$a \sin i = 31,700,000$ km
$K = 194.4$ km/sec	$f = 8.84 \odot$

The mass function given in Table 4 refers to the component observed spectroscopically; it passes in front at the primary minimum, and we denote it as the first component, thus avoiding the confusion

[2] See *Harvard Ann.*, **89**, No. 6, 1936.

produced by referring to the "smaller," "lighter," or "fainter" component. This first component is slightly brighter (in total luminosity; not in surface brightness, which is slightly fainter), slightly larger, and slightly more massive than the second component.

From Table 4 it appears that the system is very massive. Humason and Nicholson considered that it ranked next to Plaskett's star in mass. From the photometric and spectroscopic elements we may deduce that the mass ratio of the two components must be less than unity. Using an empirical relation, recently derived, for the mass ratio in terms of the relative luminosities of the components,[3] we find that the mass ratio is 0.92. This value was used in deriving the absolute dimensions, which are given in Table 5.

TABLE 5

ABSOLUTE DIMENSIONS OF HD 163181

$Mass_1$	$= 44.38\ \odot$	$Density_2$	$= 0.28\ \odot$
$Mass_2$	$= 40.82\ \odot$	$Radius_1$	$= 3{,}970{,}020$ km
A	$= 66{,}167{,}000$ km		$= 5.71\ \odot$
$Density_1$	$= 0.24\ \odot$	$Radius_2$	$= 3{,}652{,}418$ km
			$= 5.23\ \odot$

It is evident from Table 5 that the system now discussed is slightly more massive than the heaviest eclipsing systems previously known. The total masses of AO Cassiopeiae, UW Canis Majoris, and VV Cephei are, respectively, 70 ⊙, 71 ⊙, and 80 ⊙, as compared with the value 85 ⊙ now found. The radii of the components, however, are very near to those of the system of Y Cygni, much smaller than those of AO Cassiopeiae or UW Canis Majoris, and 420 times smaller than the red component of VV Cephei, though of approximately the same mass. It must be remembered that the masses of this new eclipsing system may be considerably larger, for the mass ratio, deduced here, is probably overestimated.

HARVARD COLLEGE OBSERVATORY
November 22, 1938

[3] *Proc. Amer. Phil. Soc.*, **79**, No. 3, 327, 1938.

NOTES

THE ENERGY-PRODUCING REACTION IN THE SUN

Recently two different reaction chains have been proposed for the explanation of the energy production in the sun and in the other stars of the main sequence.[1]

The first one, ${}_1H^1 + {}_1H^1 \rightarrow {}_1H^2 + \beta^+$, etc., gives, according to the calculations of Bethe and Critchfield,[2] an energy production which, for the conditions usually accepted in the center of the sun ($T_c = 2 \cdot 10^7$ °C and $\rho_c = 80$), amounts to about 2 erg/gm sec. Since the actual energy liberation in the central regions of the sun should be several times larger (2 erg/gm sec being the observed average energy production), it seems that this reaction might be not sufficient.

The second reaction chain, ${}_6C^{12} + {}_1H^1 \rightarrow {}_7N^{13} + h\nu$; ${}_7N^{13} \rightarrow {}_6C^{13} + \beta^+$; ${}_6C^{13} + {}_1H^1 \rightarrow {}_7N^{14} + h\nu$; ${}_7N^{14} + {}_1H^1 \rightarrow {}_8O^{15} + h\nu$; ${}_8O^{15} \rightarrow {}_7N^{15} + \beta^+$; and ${}_7N^{15} + {}_1H^1 \rightarrow {}_6C^{12} + {}_2He^4$, leads, according to calculations of Bethe,[3] to a just sufficient energy production if one accepts 10 per cent of N-concentration in the sun.

Since the relative energy liberation of the two above-mentioned reactions depends essentially on the adopted concentrations and on the exact values of the central temperatures, it would be interesting to find some other method of attacking the question as to which reaction is really responsible for the observed energy liberation of the sun. This can be done by studying the observed relations between masses M, luminosities L (or absolute magnitudes $M_{bol} \equiv -2.5 \log L + \text{const.}$) and radii R of the stars of the main sequence in the neighborhood of the sun. According to the homology transformations of the fundamental equations of stellar equilibrium in

[1] We must notice that the reaction chain ${}_2He^4 + {}_1H^1 \rightarrow {}_3Li^5 + h\nu$, etc., originally proposed by Weizsäcker (*Phys. Zs.*, **38**, 176, 1937), must be excluded from consideration, as the experimental evidence seems to speak definitely against the existence of ${}_2He^5$ and, consequently, also of ${}_3Li^5$ nuclei.

[2] *Phys. Rev.*, **54**, 248, 1938.

[3] *Phys. Rev.* (in print); the author is grateful to Dr. Bethe for communication of his results prior to publication.

the form proposed by the author,[4] these relations should depend on the exponent in the temperature dependence of the rate of thermonuclear reactions ($\epsilon \simeq AT^n$) in the following way:

$$L \sim M^{\frac{31+10n}{5+2n}} \mu^{\frac{45+14n}{5+2n}} \kappa_0^{-\frac{6+2n}{5+2n}} A^{-\frac{1}{5+2n}}, \tag{1}$$

$$R \sim M^{11-2\frac{31+10n}{5+2n}} \mu^{15-2\frac{45+14n}{5+2n}} \kappa_0^{-2+2\frac{6+2n}{5+2n}} A^{+\frac{2}{5+2n}}, \tag{2}$$

where μ is the effective molecular weight and κ_0 the coefficient of opacity.

In the temperature region around 2.10^7 °C we have for the first chain $n = 3.5$. The rate of energy production in the second chain will be given by the rate of its slowest link, which, according to Bethe, is ${}_7N^{14} + {}_1H^1 \rightarrow {}_8O^{15} + h\nu$; for this reaction we have $n = 18$. Thus we get

$$L \sim M^{+5.5} \text{ (for } H - H) \text{ and } \sim M^{+5.2} \text{ (for } N - H)\,, \tag{3}$$

$$R \sim M^{0.0} \text{ (for } H - H) \text{ and } \sim M^{+0.7} \text{ (for } N - H)\,. \tag{4}$$

These relations are shown in Figure 1 (*a*, *b*), where the expected M_{bol} and $\log R/R_\odot$ are plotted against $\log M/M_\odot$. For the comparison with observations we use 15 stars with $0.4\ M_\odot < M < 2.5\ M_\odot$, for which the masses, radii, and absolute luminosities are fairly well known from the critical investigation by Kuiper.[5] We see from the first plot that the observed data follow the theoretical relation very closely, although no choice can be made here between $n = 3.5$ and $n = 18$.

On the other hand, the second plot ($R - M$ relation) speaks definitely in favor of $n = 18$ (or any sufficiently high value of n). The small scatter observed may be considered as being due to a slightly different chemical constitution of the stars. If we interpret this in terms of different hydrogen content, x, we can express μ, κ_0, and A through x.[6] Using (1) and (2) and accepting $x = 0.60$ for

[4] *Zs. f. Ap.*, **16**, 113, 1938.

[5] *Ap. J.*, **88**, 472, 1938; the author is grateful to Dr. Kuiper for the communication of his results prior to publication.

[6] G. Gamow, *Phys. Rev.*, **10**, 265, 1938.

the sun, we find that (for M = const.), with decreasing x, both L and R will increase if $n = 13$, whereas L will increase and R decrease if $n = 3.5$. A particularly large deviation, both in luminosity and in radius, is shown in Figure 1 for ζ Herculis A. We see that this

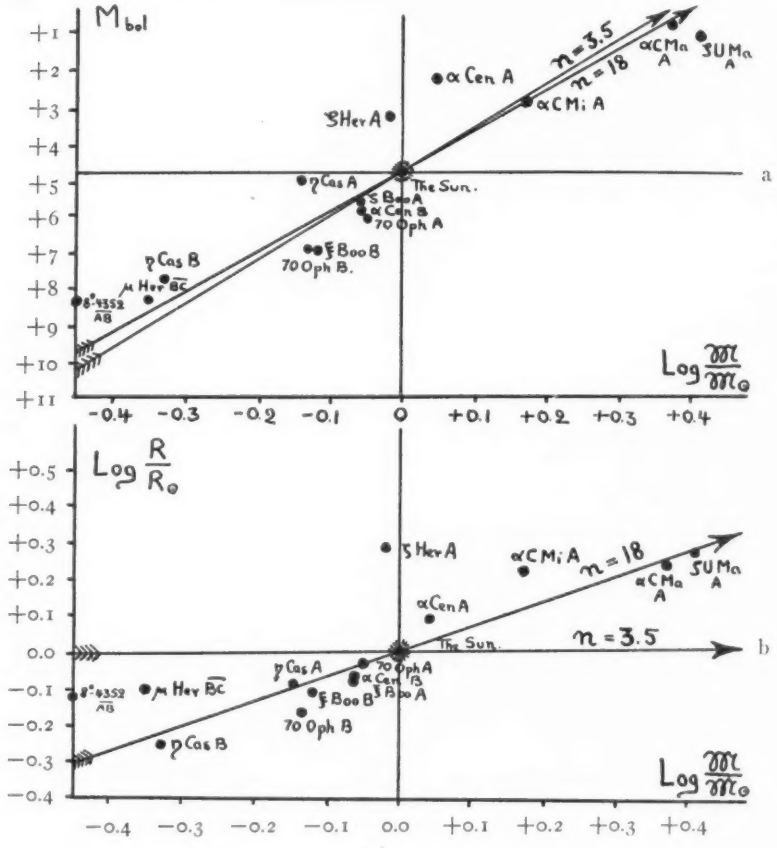

FIG. 1

deviation is in agreement with the theoretical expectation for $n = 18$ and lower hydrogen content.

For stars of considerably smaller masses ($\leqq 0.2\ M_\odot$) the central temperature should be lower and we should expect the $H - H$ reaction to play the most important role; it will make no essential change in the $L - M$ relation but will entail a tendency of the radii to be independent of the mass. The observational data show, however,

quite the opposite: the change of luminosity with mass becomes considerably slower (in fact, so slow that it cannot be obtained from [1] with *any* value of n), whereas the radii still decrease. A possible explanation of this[7] is that, owing to considerably higher densities in the central regions of these stars, the ionization of atoms is not complete and the simple considerations used above are no longer applicable.

G. GAMOW

GEORGE WASHINGTON UNIVERSITY
October 1, 1938

THE IDENTIFICATION AND THE ORIGIN OF ATMOSPHERIC SODIUM

In the September, 1938, issue of the *Astrophysical Journal*,[1] J. Cabannes, J. Dufay, and J. Gauzit describe their recent observations of atmospheric sodium and offer suggestions concerning the origin of the sodium atoms in the high atmosphere. However, this paper does not sufficiently take into account my own contributions,[2] which bring out all the essential facts.[3] I should like especially to call attention to the following points:

1. Prior to the publication of my first note,[4] all that was known on this subject was that there existed in the night-sky spectrum a yellow radiation near λ 5892 (within a few angstroms) and that this radiation was of atmospheric origin. Cabannes and Dufay's first paper,[5] published a few days before mine, did not add anything new to the question, since the new wave length measured by them, λ 5894, was no better than the preceding ones, and the relatively great width of the yellow radiation had already been mentioned in 1935.[6]

[7] This was indicated to the author by Dr. Chandrasekhar in a private communication.

[1] **88**, 164.

[2] *C.R.*, **206**, 448, 928, 1137, 1938; *Nature*, **141**, 788, 1938; *C.R.*, **206**, 1669, 1938; *Nature*, **142**, 164, 1938; *Zs. f. Phys.*, **110**, 291, 1938; R. Bernard and G. Déjardin, *J. de Phys.*, Ser. VII, **9**, 978, 1938; G. Déjardin and R. Bernard, *C.R.*, **207**, 81, 1938.

[3] See my general paper: *Zs. f. Phys.*, **110**, 291, 1938.

[4] *C.R.*, **206**, 448, 1938.

[5] *Ibid.*, p. 221. [6] L. Vegard and E. Tonsberg, *Zs. f. Phys.*, **94**, 413, 1935.

2. In October and November, 1937, I found at the Tromsö Observatory that the yellow line presents at twilight a considerable temporary enhancement, which can only be interpreted as an optical resonance under the action of sunlight.[7] The hypothesis of atmospheric sodium thus received a firm support.

3. Cabannes, Dufay, and Gauzit[8] attribute to Currie and Edwards[9] the discovery of the twilight effect. However, I have clearly shown[10] that Currie and Edwards have never observed the line λ 5892, but sometimes a nitrogen band belonging to the auroral spectrum and sometimes a narrow portion of the continuous spectrum produced by moonlight. More than a year after the publication of Currie and Edwards' paper, and hardly two months before my own observations, H. Garrigue[11] (whose papers are quoted by Cabannes, Dufay, and Gauzit) wrote: "I have not observed any perceptible diurnal variation of the band 5888 A." Thus, the considerable enhancement of the yellow line at twilight, which is much more intense (at least one hundred times) than that reported for the line λ 6300, had escaped all other observers.

4. Concerning the interference analysis worked out simultaneously but independently by Cabannes, Dufay, and Gauzit and by myself, it must be noted that the experimental processes carried out in both cases, as well as the results obtained, are rigorously equivalent. Contrary to what Cabannes, Dufay, and Gauzit seem to assert, there are not two interference methods; there are only different manners of isolating the radiation to be studied. For my own part, I deliberately chose the only one capable of bringing out a result at once clear and easily interpretable, which does not weaken in the least the value of my experiments. If I used colored screens and rejected the large-aperture spectrograph which I had at my disposal, it was because the latter process, on account of the experimental conditions, leads to the study of fragments of rings, on an image of the slit which is too narrow and rather ill defined. My experiments, at twilight as well as at night, were carried out in Febru-

[7] *C.R.*, **206**, 448, 1938; *Zs. f. Phys.*, **110**, 291, 1938.

[8] *C.R.*, **206**, 870, 1938.

[9] *Terrest. Magn. and Atmosph. Elect.*, **41**, 265, 1936.

[10] *C.R.*, **206**, 1137, 1938; *Nature*, **142**, 164, 1938.

[11] *C.R.*, **205**, 491, 1937.

ary, 1938, and were brought to an end on March 6; they were published in their final form, with plate reproductions, as early as March 21. Therefore, I was the first person to obtain and exhibit the interference rings on the *night* radiation; at the same time—and this is a fundamental fact—I reported the characteristic alternating intensities of the D_1 and D_2 components.[12]

5. Taking into account some observations by Garrigue,[13] Cabannes, Dufay, and Gauzit ascribe to the sodium layer an altitude of 130 km, but they do not indicate the precision of their calculation. Such a result is questionable, as was clearly shown by Déjardin and myself.[14] After a discussion of the different causes of errors, it was found that the formula used may give 400 km as well as a few tens of kilometers. Consequently, this does not contradict the value of 60 km deduced from the twilight effect, with an approximation of a few kilometers.

6. Taking up again a hypothesis previously considered by G. Déjardin,[15] Cabannes, Dufay, and Gauzit attribute the origin of atmospheric sodium to meteorites. This hypothesis encounters a serious objection: the absence of the D lines in the spectrum of the polar aurora, and consequently the almost certain absence of sodium atoms in the auroral region where, however, a great number of meteorites disappear.

7. Another more plausible hypothesis ascribes to the sodium a terrestrial origin. In particular, it may be admitted[16] that salt particles from the oceans are carried up by ascending currents to a very great altitude, where their vaporization gives rise to *NaCl* molecules capable of being dissociated under certain influences. This theory has the advantage of explaining quite simply the twilight phenomenon and the absence of sodium in the auroral region. On the other hand, volcanic dust shot to heights of 10–30 km may also constitute an appreciable source of sodium.[17]

RENÉ BERNARD

INSTITUT DE PHYSIQUE GÉNÉRALE
UNIVERSITÉ DE LYON

[12] *Nature*, **141**, 788, 1938.
[13] *Ibid.*, **205**, 491, 1937.
[14] *Ibid.*, **207**, 81, 1938.
[15] *Ibid.*, **206**, 930, 1938.
[16] *Ibid.*, **206**, 1669; **207**, 81, 1938.
[17] *Ibid.*, **207**, 81, 1938.

THE RADIAL VELOCITY OF 59 d SERPENTIS

The following measurements of the G component from spectrograms taken with the single-prism Bruce spectrograph of the Yerkes Observatory are given to supplement the recent results derived by McLaughlin[1] and by Tremblot[2] for this star.

TABLE 1

Date		G.M.T.	Radial Velocity
1928	June 24	4:46	−42 km/sec
	July 8	5.59	− 8
	12	4:48	−34
	17	6:20	−29
	23	3:07	−22
	26	3:23	−39
	27	4:25	−26
	Aug. 28	3:08	−18
	Sept. 1	2:30	−20
	6	2:27	−29
	7	2:23	−24
	16	2:13	−20
1929	April 15	9:32	+ 6
	June 5	6:08	−12

OTTO STRUVE
ALICE JOHNSON

YERKES OBSERVATORY
October 1938

PHOTOGRAPHS OF TWO DIFFUSE NEBULOSITIES

Two of the regions recently examined by Struve and Elvey[1] with the nebular spectrograph of the McDonald Observatory give strong emission spectra. These are Nos. 16 and 21 of their list. Direct photographs have been obtained of these regions with the 24-inch reflector of the Yerkes Observatory, on Agfa Superpan Press emulsion. A Wratten Ciné Red filter was used to eliminate most of the radiation of the night sky on the violet side of λ 6000 and to transmit the *Hα* radiation of the nebulae. An exposure of one hour on Region 21, made on November 24, 1938, shows a large diffuse nebula

[1] *Ap. J.*, **88**, 356, 1938.

[2] *C.R.*, **207**, 491, 1938.

[1] *Ap. J.*, **89**, 120, 1939, Table 1.

PLATE VIII

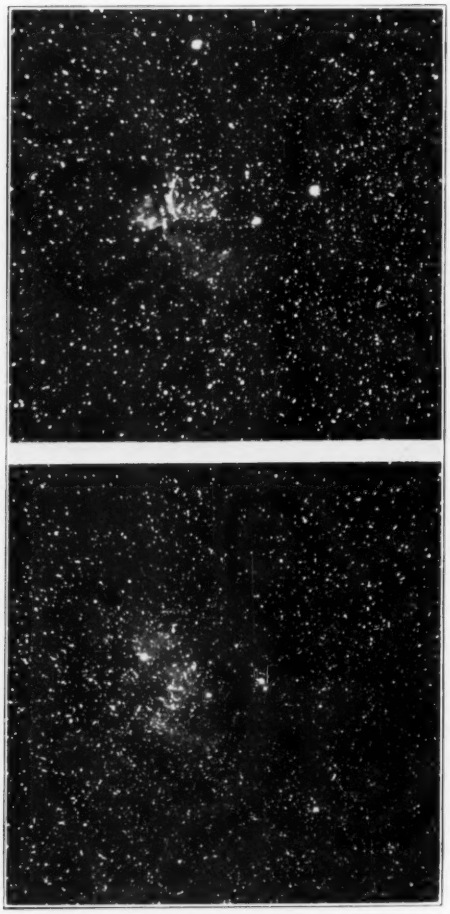

a) Diffuse nebula in cluster NGC 7380
b) Diffuse nebula near BD+55°2724

Please substitute for Plates IX–XIV in
ASTROPHYSICAL JOURNAL, Vol. 89, No. 1

PLATE IX

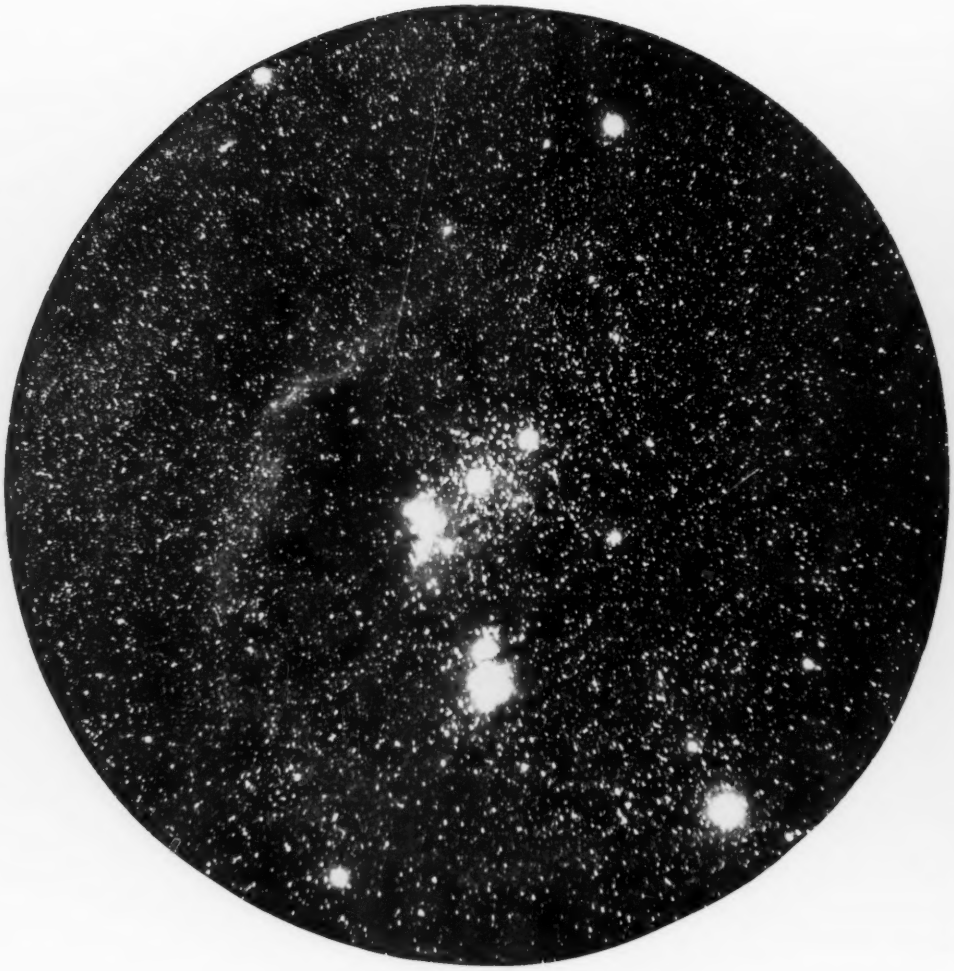

ORION: AGFA SUPERPAN PRESS FILM, NO FILTER

Exposure, 2 minutes. The two meteors were estimated to be of the second and third magnitude.

PLATE X

ORION: AGFA SUPERPAN PRESS FILM WITH RED FILTER
Exposure, 20 minutes

PLATE XI

Region Around μ Cephei: Agfa Superpan Press Film, No Filter
Exposure, 2 minutes

PLATE XII

Region around μ Cephei: Agfa Superpan Press Film with Red Filter
Exposure, 20 minutes

PLATE XIII

Region Centered at about $\alpha\ 6^h13^m$; $\delta + 12^\circ$: Agfa Superpan Press Film, No Filter
Exposure, 2 minutes

PLATE XIV

Region Centered at about $\alpha\ 6^h13^m$; $\delta + 12°$: Agfa Superpan Press Film with Red Filter

Exposure, 20 minutes

2^m east of BD$+57°2601$. This nebula falls in the region of the galactic cluster NGC 7380 and surrounds the stars BD$+57°2615$ and 2617. The nebula shows a considerable amount of structure (see Pl. VIII*a*).

An exposure of 90 minutes on Region 16, made on December 15, 1938, shows a large, faint, diffuse nebula centered about 2^m east of BD$+55°2714$. This nebula surrounds the stars BD$+55°2719$, 2720, 2721, 2722, and 2724; but there seems to be no direct connection between the nebula and these stars. The background fog, presumably due to the night sky, was strong on both films, but particularly on that of December 15; on this night there was a perceptible aurora.

JOHN A. O'KEEFE

YERKES OBSERVATORY
December 1938

PHOTOGRAPHS OF DIFFUSE NEBULOSITIES

A recent series of photographs taken by Charles A. Lower and the writer show that some diffuse galactic nebulae appear very strong when photographed in red light. The increase in density of the nebular images when photographed with Agfa Superpan Press film and with an Eastman Kodaloid filter (which has about the same transmission as the Wratten F filter) is probably due partly to the elimination of sky fog caused by the green component of the atmospheric glow, but mostly to the presence of bright *Hα* in the light of the nebulae. However, not all diffuse nebulosities appear strong on the red exposures. For example, the diffuse nebula around the Pleiades is considerably fainter when photographed in red light.

The photographs shown in Plates IX–XIV were obtained with an 8-inch f/1 Schmidt camera. The original diameter of the negatives was three inches, and the reproductions were made to bring out the faintest nebulosities. They do not do full justice to the quality of the star images. This is especially true of the two photographs of the region in Cepheus which were obtained with the camera slightly out of alignment, resulting in out-of-focus star images at one edge of the field. The blue sensitive plates were secured on the same emulsion but without a filter.

H. A. LOWER

SAN DIEGO, CALIFORNIA
December 1938

NOTE ON EMISSION B STARS

In a recent issue of the *Astrophysical Journal*[1] I outlined a method for the detection of small objects having strong *Hα* emission. The method consists of photographing stars through a red filter at two different focal settings on the same red-sensitive emulsion. One focal setting corresponds to the wave length of *Hα*; the other corresponds to a wave length shorter than that of *Hα*, chosen in such a way that the two images of a normal star on the plate are of equal sizes. The images of an object with strong *Hα* emission will be of different sizes

TABLE 1

Mt. Wilson Cat. No.	*Hα* Int.*	Spectrum	Remarks
3	3	Bone	
5	3	B(o)e	
10	2	B5eβ	
11	3	B(3)e	
12	4	B2ne	
13	< 2	B5s(e)	The bright *H* lines seem to have disappeared since the Harvard observations were made
14	4	B8eβ	
15	2	B8e	
23	3	B3e	
84	4	Bep	The bright lines of *H* are very intense
137	4	Pec	The bright *H* lines are extraordinarily intense. The type is uncertain

* Intensities obtained from *Ap. J.*, **76**, 156, 1932.

and thus can readily be detected from the normal stars on the plate. By using this method, what was believed to be a new Wolf-Rayet star was found. In a recent letter to me, Dr. Paul W. Merrill suggested that this object is identical with No. 315 in the *Mount Wilson Catalogue* of Be stars.[2] This star was observed by him several years ago. There can be no doubt that this identification is correct, and I wish to thank Dr. Merrill for calling this matter to my attention. Dr. Merrill further states that there are no Wolf-Rayet features present in his spectrum of this object. His measure of the *Hα* emission is 4 on his scale of intensities.[3] In another publication[2] he remarks that "the bright hydrogen lines are very intense."

[1] *Ap. J.*, **88**, 527, 1938. [2] *Ibid.*, **78**, 87, 1933. [3] *Ibid.*, **76**, 156, 1932.

In order to investigate the possibility of detecting other Be stars with this new method, photographs were made of the eleven stars listed in the table. These were selected from the *Mount Wilson Catalogue* of Be stars.[2] The films were taken with a 6-inch refractor at the McDonald Observatory, in the manner described above. The images of only two of the stars, Nos. 84 and 137 in the *Mount Wilson Catalogue*, could be distinguished from those of normal stars. These stars are similar to No. 315 mentioned above, inasmuch as they are peculiar Be stars with hydrogen lines of sufficient intensity to warrant remarks by Merrill in the notes to his table.[2] All three stars have an *Hα* intensity equal to 4. The two other stars of *Hα* intensity 4 that were investigated (*Mt. Wilson Cat.*, Nos. 12 and 14) could not be detected by my method. It is noted that these latter stars were *not* marked as peculiar by Merrill, whereas those that could be detected by my method were so indicated. Hence, it is probable that only exceptional Be stars can be detected in this manner.

CARL K. SEYFERT

McDONALD OBSERVATORY
December 3, 1938

PHOTOELECTRIC MEASURES OF γ CASSIOPEIAE

Since the announcement by Cherrington that γ Cassiopeiae was brighter than normal, this star has been observed, when convenient, with the photoelectric photometer of the Washburn Observatory. The cell was the Kunz potassium cell in Corex glass, which has been in use since 1934 for all photoelectric work done in Madison.

The comparison star for the magnitudes recorded in the table was HD 2905 (α $0^h27^m.3$, δ $+62°23'$, 1900) = κ Cassiopeiae, whose spectrum is B0k and whose visual magnitude is 4.24. A rotating sector reduced the brightness of γ by 2.02 mag. to approximate more nearly the brightness of κ. A second star, HD 10516 (α $1^h37^m.4$, δ $+50°11'$, 1900) = φ Persei, whose spectrum is B0ne, visual magnitude 4.19, was also used as a check part of the time. But since φ Persei is at a considerable distance from γ and κ Cassiopeiae and

is slightly and irregularly variable, the magnitudes given in the table are referred to κ alone.

The maximum of γ Cassiopeiae, magnitude 1.57 (photoelectric), was reached on May 7, 1937; a minimum of 2.44 was reached on November 22 and again on December 10, 1937. The secondary

OBSERVATIONS OF γ CASSIOPEIAE

JD	Photoelectric Magnitude	JD	Photoelectric Magnitude
2426583.80	2.17	2428797.64	2.02
6589.78	2.19	8802.77	2.03
8466.58	1.71	8837.71	2.27
8466.72	1.70	8841.78	2.26
8483.73	1.70	8858.56	2.38
8488.69	1.69	8860.68	2.44
8490.56	1.70	8863.68	2.34
8501.58	1.67	8866.63	2.33
8517.68	1.70	8874.63	2.36
8534.58	1.70	8878.61	2.44
8565.57	1.64	8904.67	2.30
8581.65	1.63	8906.59	2.32
8595.57	1.63	8921.54	2.31
8614.59	1.64	8949.55	2.33
8634.87	1.60	9040.86	2.26
8661.85	1.57	9069.78	2.24
8691.82	1.61	9090.74	2.21
8702.77	1.63	9100.75	2.13
8706.80	1.65	9115.67	2.17
8720.73	1.65	9123.64	2.17
8741.72	1.73	9132.70	2.17
8743.68	1.75	9139.64	2.21
8745.70	1.74	9154.58	2.26
8746.74	1.78	9154.64	2.25
8749.73	1.76	9164.68	2.21
8752.71	1.77	9185.66	2.32
8758.69	1.84	9192.58	2.22
8767.66	1.86	9201.56	2.26
8769.66	1.91	9214.56	2.30
8793.70	2.02	9221.67	2.30

variations of about one-tenth of a magnitude appear to be real and nonperiodic. Such variations occurred at approximate dates 8870, 9100, 9150, and 9175 and were of irregular duration (between 18 and 32 days). These variations suggest possible changes in the spectrum near these dates.

In the table are given the observations of γ Cassiopeiae. The dates are given in Julian days; and the magnitudes are photoelectric,

based on an assumed photoelectric magnitude of 4.26 of κ Cassiopeiae. The first two observations were made in 1931, when the star

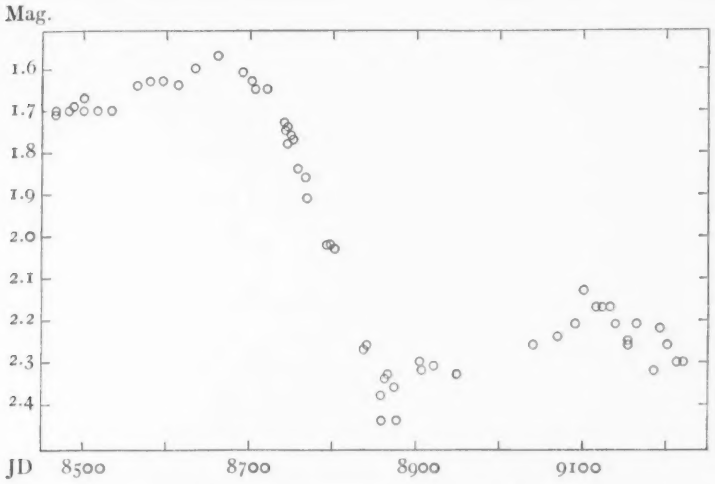

FIG. 1.—Light-curve of γ Cassiopeiae

was observed in a program of color determinations. The magnitudes were deduced from comparison with other stars of class B in the region.

C. M. HUFFER

WASHBURN OBSERVATORY
December 1938

REVIEWS

Astronomy, Vol. II: *Astrophysics and Stellar Astronomy*. By H. N. Russell, R. S. Dugan, and J. Q. Stewart. Boston: Ginn & Co., 1938. Pp. xii+489+xxx. $2.80.

The second volume of the textbook by Russell, Dugan, and Stewart is probably better known to astronomers than any other book. Since 1927, when the first edition appeared, it has served as an inspiring and reliable guide in astronomy, not only for undergraduate and graduate students but for professional astronomers as well. The authors' brilliant summary of the physical conditions in gaseous nebulae, written in 1926, provided the stimulus for Bowen's remarkable discovery,[1] in 1927, of the identity of the two strongest nebulium lines with forbidden transitions of *O* III. The earliest copies of the first edition contained, of course, no mention of Bowen's work. But the later copies were corrected; and the original section 906, "The Problem of 'Nebulium,'" was replaced by a new section, "Identification of 'Nebulium.'" Although this case of an immediate response to a stimulating textbook summary is probably unique in the history of astronomy, there can be no doubt that Russell, Dugan, and Stewart's second volume has, directly and indirectly, stimulated important research in almost all branches of astrophysics. In a sense, its very success has hastened the need for a new edition.

Astronomers all over the world will be grateful to the authors for having prepared a thorough revision of the last chapter (xxvi), "The Evolution of the Stars," and a 31-page supplement, which brings the information up to date. Other revisions have been made in the sections dealing with the solar spectrum and with the sources of stellar energies.

The supplement is rather condensed and perhaps does not do full justice to the newest results. However, it should suffice for several years and should, in the meantime, increase the value of the book.

O. Struve

[1] *Ap. J.*, **61**, 2, 1928.

WILLIAM WALLACE CAMPBELL

1862–1938